NASA CR-134610
SRD-74-034

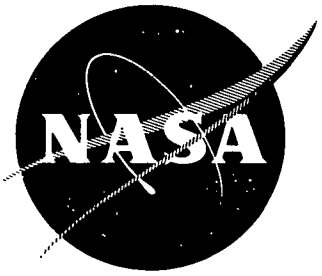

STUDY, SELECTION, AND PREPARTION OF SOLID CATIONIC CONDUCTORS

by

W. L. Roth and O. Muller

GENERAL ELECTRIC COMPANY

prepared for

NATIONAL AERONAUTICS AND SPACE ADMINISTRATION

NASA Lewis Research Center
Contract NAS 3-17339

1. Report No.	2. Government Accession No.	3. Recipient's Catalog No.
NASA CR-134610		

4. Title and Subtitle	5. Report Date
STUDY, SELECTION, AND PREPARATION OF SOLID CATIONIC CONDUCTORS	April 1974
	6. Performing Organization Code
7. Author(s)	8. Performing Organization Report No.
W. L. Roth and O. Muller	SRD-74-034
	10. Work Unit No.
9. Performing Organization Name and Address	
General Electric Company P. O. Box 8 Schenectady, New York 12301	11. Contract or Grant No. NAS3-17339
	13. Type of Report and Period Covered Final Report 11/13/72 - 11/12/73
12. Sponsoring Agency Name and Address National Aeronautics and Space Administration Washington, D.C. 20546	14. Sponsoring Agency Code

15. Supplementary Notes Project Managers: J. B. Bush, General Electric Corporate Research and Development, P. O. Box 8, Schenectady, N. Y. 12301; Albert C. Antoine, Energy Conversion and Material Science Division, NASA Lewis Research Center, Cleveland, Ohio

16. Abstract

Crystal chemical principles and transport theory have been used to predict structures and specific compounds which might find application as solid electrolytes in rechargeable high energy and high power density batteries operating at temperatures less than 200°C. Structures with 1-, 2-, and 3-dimensional channels were synthesized and screened by nuclear magnetic resonance, dielectric loss, and conductivity. There is significant conductivity at room temperature in some of the materials but none attain a level that is comparable to beta-alumina. Microwave and fast pulse methods were developed to measure conductivity in powders and in small crystals.

17. Key Words (Suggested by Author(s))	18. Distribution Statement
Ionic conductors Solid electrolytes Batteries Nuclear Magnetic Resonance Transport numbers	Unclassified, Unlimited

19. Security Classif. (of this report)	20. Security Classif. (of this page)	21. No. of Pages	22. Price*
Unclassified	Unclassified	69	

* For sale by the National Technical Information Service, Springfield, Virginia 22151

TABLE OF CONTENTS

STUDY, SELECTION, AND PREPARATION OF SOLID CATIONIC CONDUCTORS

W. L. Roth and O. Muller

I. SUMMARY

A proposal entitled " Study, Selection, and Preparation of Solid Cationic Conductors" was submitted to NASA in May 1971, in response to RFP No. 416187. It described a research program aimed at the identification and preparation of materials for use as nonporous solid ionic conductors in rechargeable high-energy and power density batteries operating at temperatures less than 200°C. The only materials capable of meeting the required objectives that are now identified are members of the beta-alumina family. A preliminary search for such solid electrolytes was carried out between July 1971 and June 1972 under NASA Contract NAS3-15692. The work was summarized in Report No. CR-120964, dated September 1972. More than twenty compounds were screened, and encouraging results were obtained for nine materials. None were proved to be good ionic conductors at low temperature, in large part because dense single-phase ceramics were not available for measurement of ion transport and conductivity.

This report summarizes a continuation of the search which was carried out between December 1972 and November 1973 under NASA Contract NAS3-17339. The structural criteria for predicting materials with high ion mobility at ambient temperature had been validated in the first phase of the study. These criteria were used to predict new candidates with particular emphasis on materials which could be fabricated in practical systems. The major modification in the technical approach was in the area of evaluation of materials. Two new techniques for measuring ionic conductivity and transport were developed and validated. By use of these methods it now is possible to evaluate candidate materials in the form of powders, small crystals, or fragments of ceramics or glasses. More than twenty-eight materials distributed among eight structure types were synthesized and evaluated. At least nine of these had conductivities of order 10^{-6} ohm^{-1} cm^{-1} at room temperature, but additional work would be required to establish the level of ion transport.

The principal conclusions of the study are as follows:

1. Satisfactory crystal chemical and measurement tools for the prediction and the evaluation of solid ionic conductors have been developed and validated,

2. It is unlikely that the required high levels of ion transport can be sustained in one-dimensional tunnel structures, and

3. There are reasonable prospects for developing high ionic conductivity at moderate temperature in three- and two-dimensional interconnected channel structures. Specific recommendations are made for future work on a broad family of compounds which appear to satisfy the principal requirements for use in a low-temperature, high-energy and power density battery.

II. INTRODUCTION

A. Background

The objective of this research program is the identification and preparation of materials for use as nonporous solid ionic conductors in rechargeable high-energy and power density battery systems operating at temperatures less than 200°C. The primary requirements for the electrolyte are that:

1. The ionic conductivity at operating temperature must be sufficiently high to allow high power density. In practice this means the conductivity should be at least 10^{-3} ohm^{-1} cm^{-1} at 200°C.

2. The cation transport number should be unity, i.e., the current carried by anions and electrons must be negligible.

3. The electrolyte must conduct ions of reactants with high oxidizing and reducing power to achieve high-power density. This requirement eliminates silver conductors and focuses attention on cations in the first and second columns of the periodic table.

4. It must be chemically stable with respect to the cell reactants and products.

5. It must be possible to fabricate the material into thin separators which are mechanically rigid and of low porosity to prevent mixing of the cell reactants.

The only solids known to satisfy these requirements are the beta-alumina sodium ion conductors.

The work to be described in this report is a continuation of a one-year program carried out under National Aeronautics and Space Administration Contract NAS3-15692[2] with the objective to conceive, synthesize, and characterize new solid ionic conductors. In that program a large number of materials were selected on the basis of thermodynamic and crystal-chemical criteria and were subjected to preliminary synthesis and evaluation of their potential as solid ionic conductors. A novel technique, nuclear magnetic resonance (NMR), was employed for the preliminary evaluation. This technique permits the rapid screening of loose powders, thus eliminating the need for the time-consuming preparation of dense, sintered compacts of a large number of materials. Among the materials subjected to NMR analysis, many showed encouraging evidence for ionic motion. These materials are Li_3AlN_2, Li_3BN_2, $Li_xTa_2O_5$, $Li_xV_2O_5$, $NaPrF_4$, $NaYbF_4$, $LiNb_6O_{15}F$, and $LiNO_3 \cdot Z$

which is $LiNO_3$ occluded in the pores of zeolite 4A. Dense samples of the vanadates and tantalates were prepared and ionic conductivity measurements were carried out. The vanadates were shown to be partially ionic and partially electronic conductors with the level of electronic conductivity strongly dependent on the stoichiometry.

B. Technical Approach and Experimental Methods

The search for new low-temperature cation conductors consists of several interrelated tasks. These are: the application of crystal chemical criteria to predict the structures of materials in which high cation mobility at low temperature is theoretically possible, the synthesis and fabrication of selected candidates, and the characterization of conductivity and transport in synthesized candidates. Several conclusions that were reached as a result of the work under Contract NAS3-15692 led to refinements and modifications in the technical approach followed for the work under this contract. One was a decision to reduce the time-consuming work which is required to fabricate dense ceramics until there is evidence the material is a good conductor of ions. A second was to prepare candidates as pure single-phase specimens in order to avoid the ambiguities inherent in the interpretation of conductivity and transport measurements on impure materials. A third was to find methods to measure conductivity and transport in powders or in small crystals.

1. Structure Selection

The basis of the structural approach[2a] is to concentrate the search on Type II and Type III ionic conductors since it is unlikely that Type I conductors can sustain the level of conductivity required for high energy density batteries. Type I conductors are solids in which the concentration of defects is small, generally less than 10^{19} cm^{-3}; Type II are highly nonstoichiometric compounds which usually have a broad solid solution composition range; and Type III are compounds which have structures with many vacant sites of equal or nearly equal energy which mobile cations can occupy. This approach was well validated in the first year's program since many of the solids which satisfied these structural requirements gave evidence for some ion mobility at ambient temperature.

As a result of the first year's work it was possible this year to make the structural criteria more restrictive. Nonstoichiometric compounds frequently contain ions in more than one valence state. A typical example are the lithiumvanadates which were studied in the first year's program. Multiple valence states resulted in considerable electronic conduction which made it difficult to assess the amount of charge transported by ions. In the materials prepared for this study the electronic conduction was reduced by incorporating charge compensating ions without destroying the desired structure. Last year, several open framework, low density compounds were studied which were relatively stoichiometric and contained only a small concentration of defects. Such solids were tested with the hope that they would exhibit some

motional narrowing of the NMR spectrum, thus indicating ionic motion, and that the level of mobility could later be enhanced by substituting foreign ions which would introduce the necessary defects. Examples for such compounds are $NaBO_2$ and Na_2BeF_4. However, since none of these compounds gave evidence for potential ion motion, screening this time was limited to compounds which were known to contain defects.

In selecting structures for a more detailed study, use was made of three sources.

(1) The list of structures for which a preliminary study had already been made in the first year of the contract. Here the objective was to pick the most promising candidates of the previous year -- those which had successfully passed preliminary NMR screening -- and to synthesize them in a purer and/or nonstoichiometric form.

(2) A large list of promising structures that had been compiled some years ago. From this list a small number had been selected for study during the first year of the contract. Some structures from the larger original list were reconsidered during this contract period, even though they had been passed over during the first year.

(3) New promising structures obtained from a search of the recent literature.

In selecting a final group of candidates from these lists, the following crystal-chemical criteria have been applied:

(1) The candidate structures must have either (a) one-dimensional tunnels, (b) two-dimensional sheets of interconnected tunnels, or (c) a three-dimensional framework of interconnected channels. Such channels should be wide enough to allow for the motion of monovalent ions such as Li^{1+}, Na^{1+}, or K^{1+}.

(2) If a one-, two- or three-dimensional path of ionic motion is available in a particular structure, a search was made for other clues which might indicate " looseness" of the monovalent ion, or empty sites in the structure toward which an ion could migrate. Such clues include:

(a) Abnormally large cation-anion distances for the migrating cation.

(b) Abnormally large x-ray temperature factors, meaning larger than normal thermal vibrations for the diffusing cations.

(c) Availability of vacant sites or structural holes toward which the cation could move.

(d) Potential of creating nonstoichiometric solid solutions or vacant sites in compounds where the path of easy ionic motion is "plugged up" with interfering cations.

(3) The physical and chemical properties of the candidate compounds should be of such a nature that practical applications are possible. This requirement eliminates from consideration large groups of compounds:

(a) The solid electrolyte should be chemically resistant toward attack by liquid alkali metals. Many transition metal ions would be reduced under such conditions and are therefore unsuitable.

(b) The candidate compounds should be electronic insulators. This requirement eliminates from consideration many transition metal ions with partly filled d-shells, e.g., tungsten or vanadium bronzes.

(c) Potential solid electrolytes should be chemically stable under ambient conditions; for example, they should not be too hygroscopic. This requirement makes poor candidates out of many lithium- or sodium-rich oxide phases which might otherwise be attractive candidates.

(d) Potential candidates should be capable of being fabricated into dense compacts.

The structures and compounds that were finally selected for experimental investigation were determined by the following procedure. A list of candidates with supporting documentation was generated from a survey of the literature and then submitted to NASA-Lewis Research Center for selection of specific compositions to synthesize and evaluate. Some candidates were unacceptable because there were reasons to believe difficulties would be encountered in their utilization in practical battery systems. One reason was ease of fabrication. Although Li_3AlN_2, Li_3BN_2, and salt-impregnated zeolites had given strong evidence for large ionic motion at ambient temperature, they were rejected because they are hygroscopic and would be difficult to fabricate. Compounds which contained iron, cobalt, vanadium, and similar ions were excluded because they probably would be unstable toward oxidation-reduction reactions. The fluorite arrangements of $NaPrF_4$ and $NaYbF_4$ are probably good fluoride ion conductors but they were not investigated further because cation conductors are specifically desired. The encouraging result obtained for lithium tantalate was not followed up because a study of the tantalate system was to be undertaken at the National Bureau of Standards.

2. Synthesis and Fabrication of Materials

One of the objectives of the preliminary search was to screen a large number of compounds which were to be selected from as many different structure types as possible. For this reason it was not possible to devote much time to refining the synthesis, and many of the measurements were made on impure multiphase materials. The results showed that impure powders could be screened for ion motion by NMR but that pure single-phase material was essential for the evaluation of conductivity and transport.

Particular emphasis was placed on attempts to make nonstoichiometric defect solid solutions. Many structures have potentially conducting channels

or planes which are filled to capacity with alkali metal ions. If vacancies could be introduced into such tunnels or planes, it could provide a passage for the migration of alkali metal ions.

The synthesis of the various compounds was normally done by established methods suggested in the literature. Frequently these methods had to be modified to obtain higher phase purity or to make nonstoichiometric solid solutions.

The phase purity of the various compounds was checked primarily by x-ray diffraction, supplemented by microscopic observation, especially for the glassy phases. An effort was made to identify all phases, including the impurities.

3. NMR Screening

The screening of solids for ionic motion by observing motional narrowing of nuclear magnetic resonance spectra was accomplished with the same techniques described previously.[2] The measurements were made by I. Chung and H. S. Story in the Physics Laboratories of the State University of New York in Albany. Compounds in which the charge carrier was predicted to be a lithium or sodium ion were screened by measuring the NMR spectra at two or more temperatures. Line narrowing with increasing temperature was evidence for ionic motion and was a necessary but not sufficient criterion for ionic transport. The spectra were measured with a Varian Associates wide-line NMR spectrometer with signal averaging.

4. Conductivity and Transport Measurements

The significant properties for the evaluation of solid electrolytes are ionic conductivity and transport number. These measurements usually require either large single crystals or polycrystalline compacts which are dense and single phase. Since the growth of large crystals and the development of fabrication procedures for densifying new materials are difficult and time-consuming processes, the search for new electrolytes would be expedited by procedures which can be applied either to powders or to small crystals. A number of methods which were tested for achieving this objective are described below.

(a) Two-phase measurement of conductivity

Professor Charles W. Tobias suggested it might be possible to determine the conductivity of a powder by suspending it in a solution which contained the same conducting ion from measurements on the total conductivity of the two-phase system. Two experiments were performed by S. P. Mitoff and R. N. King to test the feasibility of this idea. The experiments showed that the two-phase method could not be used in its present form to obtain reliable conductivities of suspended powders.

The tests were carried out by measuring the conductivity of a solution of NaI in propylene carbonate containing a suspension of 60 mesh Monofrax beta-alumina powder. The measurements were compared with similar measurements on a suspension of Pyrex glass with the same particle size. The same results were obtained from two experiments. The second experiment was made with particular care to insure the solids were wet by the liquid by heating the suspension to 95°C under a vacuum of 30 inches of Hg. Both experiments showed the Pyrex glass and beta-alumina increased the resistance of the liquid electrolyte by the same amount (e.g., from 1320 ohms to 3350 ohms, four-probe AC measurements).

The measurements showed that both the Pyrex glass and beta-alumina behaved as insulators and the increase in resistance was due to the volume of the suspended solid. It was concluded that the conducting properties of the two-phase system are determined by the solid-liquid interface and cannot easily be used to obtain information about the suspended solid. No further work was done on this method as it seemed unlikely that it could be used in its present form to measure the conductivity of an unknown powder.

(b) Microwave measurement of conductivity of powders

The bulk conductivity of powders can be measured at microwave frequencies because at very high frequency the individual crystallites are capacitively coupled and the results are determined by the intrinsic properties of the solid. Microwave techniques are frequently used to measure semiconductor and dielectric materials, but to our knowledge they have not been used for the study of ionic conductivity in loose powders. The validity of the method was established by measuring the conductivity of beta-alumina. In addition a few preliminary measurements were made on two candidates synthesized in this study (W-doped $LiNb_6O_{15}F$ and $Li_2Ge_7O_{15}$). At the request of NASA-Lewis Research Center, the microwave screening studies were discontinued and the candidate materials were sent to their laboratories for dielectric loss measurements.[2b] Since both were high-frequency measurements, this was done to avoid duplication of effort and allow the General Electric study to concentrate on the measurement of micro-specimens. A brief description of the microwave equipment and validation measurements is given below.

The conductivity and dielectric constant of powders was measured in the range of centimeter waves by the " hollow-pipe" method introduced by S. Roberts and A. von Hippel[2c] [J. Appl. Phys., 17, 610-616 (1946)] for dielectric measurements. The specimen is contained in a cavity attached to a coaxial line. A transmitter radiates waves of a given frequency which are reflected by a metallic short which terminates the cavity. Standing waves are set up and measured by a probe traveling along a slot in the pipe parallel to its axis. The conductivity and dielectric constant are calculated from the standing wave ratio (SWR) in air and the distance of the first node from the surface of the specimen. The conductivity and permittivity are related by

a transcendental equation which cannot be solved explicitly in terms of the measured parameters. The desired quantities were obtained by using a program written by G. H. Glover of our Laboratory in which a computer inverts the transcendental equations by successive interpolation. The specimen chambers were made of brass and the measurements were made over the frequency range 2 to 4 GHz.

The microwave method was tested by measurements on loosely packed powders (approximately < 100 mesh) of Monofrax H beta-alumina. The resistivity and dielectric constant of beta-alumina are given in Tables I and II. The results show powder conductivities were obtained which are close to accepted values measured on single crystals and dense ceramic specimens. The larger resistivity of the specimen that had not been dried agrees with the well known effects of water vapor absorbed in beta alumina. The frequency dependence indicates some dispersion but the method appears satisfactory for screening purposes.

More work would be required to establish the uniqueness of the parameters deduced by the inversion procedures. The hyperbolic functions are multivalued and measurements with a single thickness of specimen may give ambiguous results. The problem can be solved by measurements on specimens of different thickness. If the conductivity is calculated from two different thicknesses of material, only one pair of values will satisfy both sets of experimental results.

TABLE I

Microwave Conductivity and Dielectric Constant of Beta-Alumina Powder at Room Temperature

Frequency (GHz)	Not dried ρ (ohm-cm)	ϵ_r	Dried ρ (ohm-cm)	ϵ_r
4.00	756	12.1	810	3.00
3.75	1620	8.8	1388	2.59
3.50	1390	10.4	1732	2.94
3.25	2420	11.3	2052	3.31
3.00	2088	12.6	2027	3.83
2.75	7917	2.73	1942	4.03
2.50	5694	3.72	1605	5.31
2.25	5744	4.25	1424	6.43
2.00	--	--	1170	7.83

TABLE II

Temperature Dependence of Microwave Conductivity of Dry Beta-Alumina Powder

Temp (°C)	ρ (ohm-cm)	ϵ_r
24	810	3.007
52	614	3.012
60	560	2.960
70	497	2.976
80	473	2.828
90	438	2.810
100	413	2.830

(c) Conductivity, transport, and pulse measurements on micro-specimens

The following methods were developed to determine the ionic transport in small specimens. They can be used on glasses or polycrystalline ceramics, coarse grained powders, and single crystals. The techniques are still being improved but the methods have already given useful information that could not have been obtained with conventional methods. Key contributions to the success of these methods were made by Dr. G. C. Farrington for the techniques of measuring conductivity in nonaqueous solvents and with fast pulses, and by Mrs. Ethel Fontanella for developing methods for potting solid electrolytes and assembling conductivity cells. The first apparatus was a Teflon polymer cell in which specimens 2 to 4 mm in diameter and about 1 mm thick were measured successfully. The method next was applied to specimens with dimensions between 0.5 and 1 mm by potting the specimen in an epoxy cell (microcell). Some measurements were made with conventional four-probe DC and AC bridge methods, and particular success was obtained with fast pulse measurements.

i. Teflon polymer conductivity cell. The first conductivity cell is shown in Fig. 1. Above is an overall view of the assembled cell and below a disassembled cell. The cell is made of two Teflon polymer blocks, 1 1/4 x 1 1/4 x 1 inch and 1 1/4 x 1 1/4 x 7/8 inch, which are drilled with cavities and clamped together to form compartments into which platinum or silver electrodes are inserted. The compartments are separated by an epoxy disk which contains the solid to be measured. The epoxy disk is sealed into the cell with a pair of Viton or silicone rubber " O" -rings. Each electrolyte compartment contains about 2 ml electrolyte solution and a variety of solvents and electrode systems were used to study different ions and for potentiometric measurements.

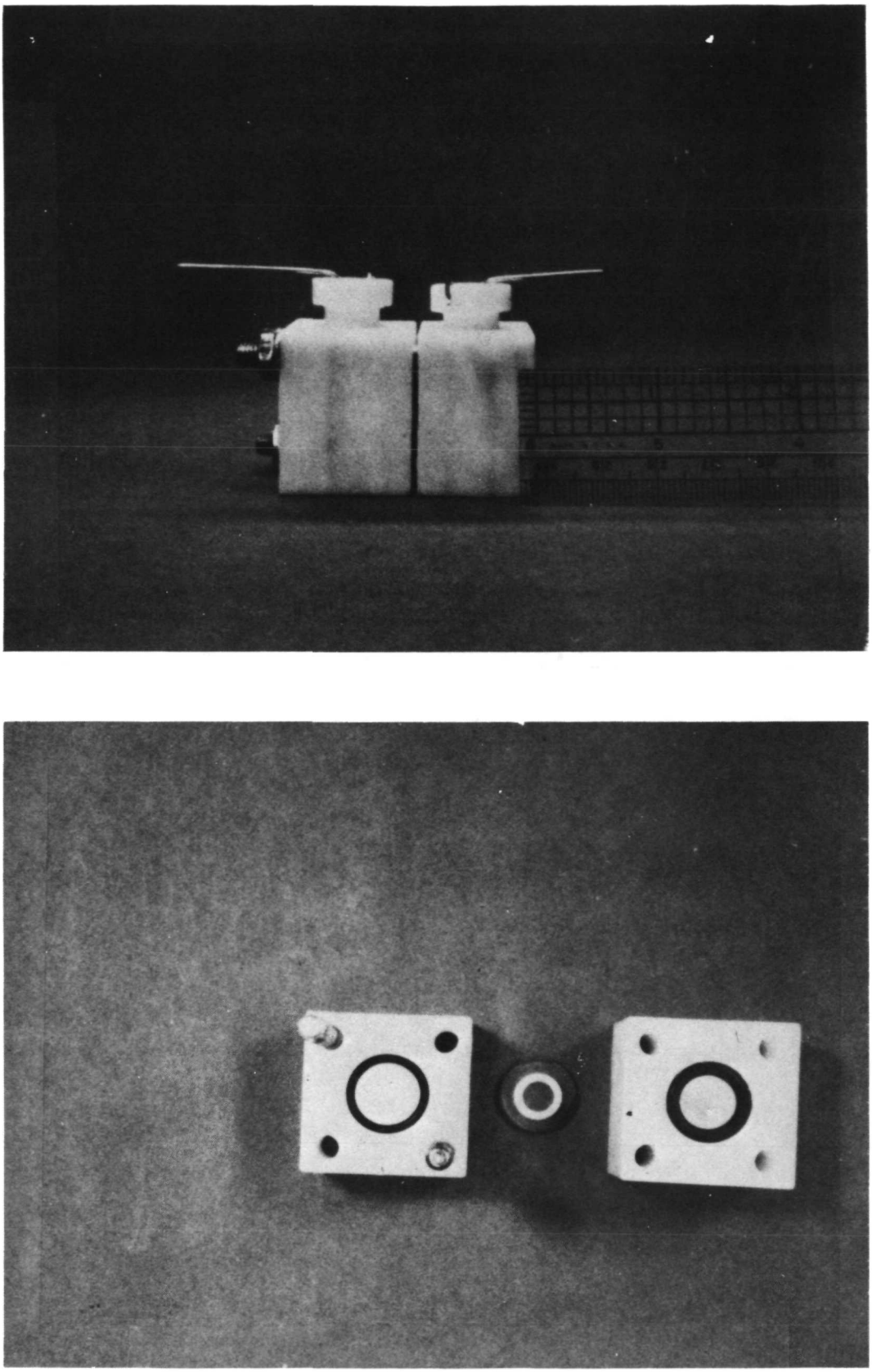

Fig. 1 Conductivity cell. Overall and disassembled views are shown. The specimen is a cross section of a beta-alumina tube tested to validate the pulse method for conductivity measurement.

The sample to be tested is potted in a specially formulated epoxy resin in the form of a disk, 16 mm diameter and usually about 0.5 mm thick. The disk is cast in a silicone rubber mold and curing techniques have been developed which produce disks without gas pockets. The final step in specimen preparation is to grind the disk until the solid electrolyte is exposed on both sides. The potted specimens are helium leak tested before assembling in the cell. Two methods are used to avoid leaks between the specimen and the epoxy potting matrix. Such leaks frequently develop during polishing to expose the surfaces of the solid electrolyte. The solid electrolyte surface may be protected by clamping the specimen between silicone rubber disks before submerging in epoxy. Alternatively, opposed small areas of the specimen are coated with RTV-112, a pourable silicone rubber sealant, cured for 24 hours, then imbedded in epoxy contained in a silicone mold. The cured RTV can be stripped off the surface after the epoxy resin has hardened. The latter procedure can be done under the microscope and is particularly useful for small samples.

The disk is clamped between the " O" -rings in the cell and the complete assembly tested for helium leaks. The cell then is placed in a dry box, the electrolyte solutions are added, and the electrodes are inserted. Electrolyes of lithium perchlorate or sodium trifluoromethane sulfonate dissolved in propylene carbonate and acetyl nitrite are stable and do not react with the components of the cell.

The cell was tested by preparing potted disks of ceramic beta-alumina and single-crystal beta-alumina. Disks were hand lapped to about 0.5 mm and to less than 0.2 mm with a jewelers lathe. This thickness sets the lower limit of crystal size that can be tested by this method.

ii. Microcell. The assembly shown in Fig. 1 was not satisfactory when specimens smaller than 0.5 mm were measured with the pulse technique that will be described later. This was due to the fact the epoxy matrix has a small but finite conductivity and capacitive and polarization effects at the liquid electrolyte-solid interface dominated the response of the samples with small dimensions. The problem was solved by constructing microcells of the type shown in Fig. 2 in which the liquid electrolyte-solid interface is reduced to the sample size. In essence, a cell is built around each sample by casting epoxy bubbles on both sides of the potted specimen, then tunnels are drilled to contain the liquid electrolyte and platinum leads. The liquid electrolyte is introduced into the cell with a hypodermic needle.

iii. Pulse technique for conductivity measurement. The procedure developed to measure ionic conductivity is to observe the structure of a square wave constant pulse in order to separate the IR drop in the solid electrolyte from interfacial polarization.

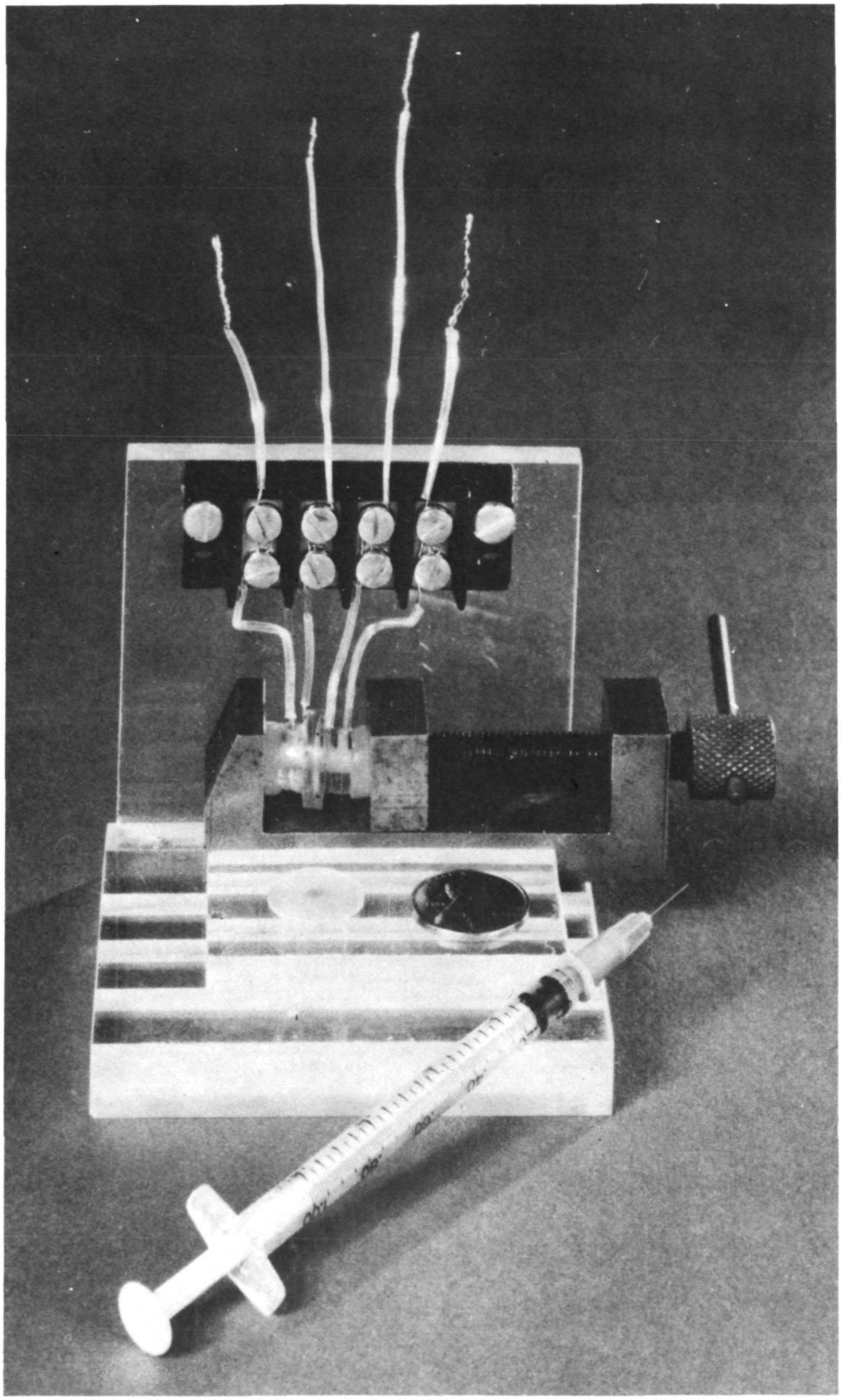

Fig. 2 Microcell for small specimens. Also shown is a potted sample before cell assembly. The liquid electrolyte is introduced with a hypodermic needle.

The experimental apparatus consists of a 2N3904 transistor acting as a fast response switch in series with a ca 20 Kohm resistance and a 22 1/2 volt battery. Switching is effected by driving the transistor base with a 0 to +4v square wave pulse train supplied by a PAR Model 175 universal programmer. The programmer also triggers a Model 7B52 delayed sweep time base in a Tektronic Model 7704A oscilloscope. Vertical oscilloscope input is provided by a dual trace Model 7A12 amplifier which permits simultaneous monitoring of the potentials of the two sensing electrodes in the Teflon polymer electrolysis cell.

The interface polarization was displayed by observing the rise and decay of a 3×10^{-4} amp current pulse introduced as a 0.05 sec square wave. The voltage drop due to polarization was manifested by approximately exponential slow components superimposed on the leading and trailing edges of the square wave. The resistivity of the beta-alumina calculated from the initial rapid decay was found to be 1550 ohm-cm.

With this apparatus it is possible to apply constant current pulses of varying amplitudes to the two working electrodes in the Teflon polymer electrolysis cells while simultaneously monitoring either the total pulse shape or magnified pulse structure at initiation or termination. Pulses of 200 msec to 1 msec duration have generally been used. These have had rise and fall times into a 2000 ohm dummy resistance of less than 0.4 μsec.

In an actual measurement, a series of current pulses is applied to the electrolysis cell which is connected in series with a precise 2000 ohm General Radio resistor. Voltage drops across the sensing electrodes and the standard resistance are recorded. Typical currents are in the range of 15 to 50 μamp. As has been described previously, the pulse measurement technique relies on the concept that the portion of the total applied cell voltage which arises from electrolyte iR drop decays almost instantaneously upon cessation of current flow while that portion of cell voltage which arises from interfacial polarization decays at a much slower rate, typically over a period of 10 to 50 msec. If a sharp enough current pulse can be applied to a cell and sensitive enough equipment is used to carefully examine the resulting shape of the total applied voltage, absolute magnitudes of iR drop and interfacial polarization can be determined. A four-electrode technique was used in these experiments to separate any electrochemical polarizations at the electrodes where current is applied from the polarizations at the solid electrolyte/liquid electrolyte interface.

III. VALIDATING EXPERIMENTS

A. Bridge Measurements

The reliability of the conductivity techniques was tested by measurements on beta-alumina ceramic specimens of known conductivity. The room temperature resistivity of freshly prepared ceramic beta-alumina, measured by the four probe technique, was 2490 ohm-cm at 10 Hz and 66 ohm-cm at 300 kHz. Experience has shown these values may increase slightly (25%) due to absorption of water from the atmosphere. The beta-alumina was cut and ground to a regular parallelopiped with area equal to $0.8 \times 0.6 = 0.48$ cm^2 and thickness of 0.075 cm and potted in epoxy resin.

Measurements were made in a Teflon polymer cell with coiled Pt electrodes and 1M $NaClO_4$ in propylene carbonate. Initial values were obtained at 1000 Hz with an AC bridge. The resistance of the cell with no separator was 496 ohms and that of the blank epoxy disk without beta-alumina about 10^6 ohms. The apparent resistance of the beta-alumina membrane, after subtracting that of the liquid electrolyte, was then found to be 2700-496 = 2204 ohms, corresponding to a resistivity of

$$2204 \times \frac{0.48}{0.075} = 15,000 \text{ ohm-cm.}$$

The large resistivity calculated from the cell measurement, approximately seven-fold greater than the four-probe DC value, is evidence of significant polarization at the solid-liquid electrolyte interface.

B. Applications of Pulse Technique to Beta Alumina

The pulse technique was validated by measuring the ionic conductivity in a well-characterized sample of beta-alumina. The beta-alumina ceramic was cut and polished to expose a disk 2 mm in diameter and 0.474 mm thick.

Figure 3 shows the overall structure of the cell voltage response to a constant current pulse through beta-alumina separating two-cell compartments filled with 0.1M $NaClO_4$ in propylene carbonate. The numbers in the upper- and lower-left corners are the vertical scale factors in mV/cm for the upper and lower traces, respectively. Sweep time in μsec/cm is recorded in the upper or lower right-hand corners. Total cell voltage between the two sensing electrodes is the difference between both traces.

Note in Fig. 3 the sharp rise upon onset of pulse and sharp fall upon termination. The termination region is magnified in the lower photograph. A sharp drop occurring within a fraction of a microsecond occurs in the voltage of each electrode. Only the electrode response recorded in the upper trace includes the effects of the beta-alumina; the lower trace arises from the sensing electrode separated from ground solely by propylene carbonate

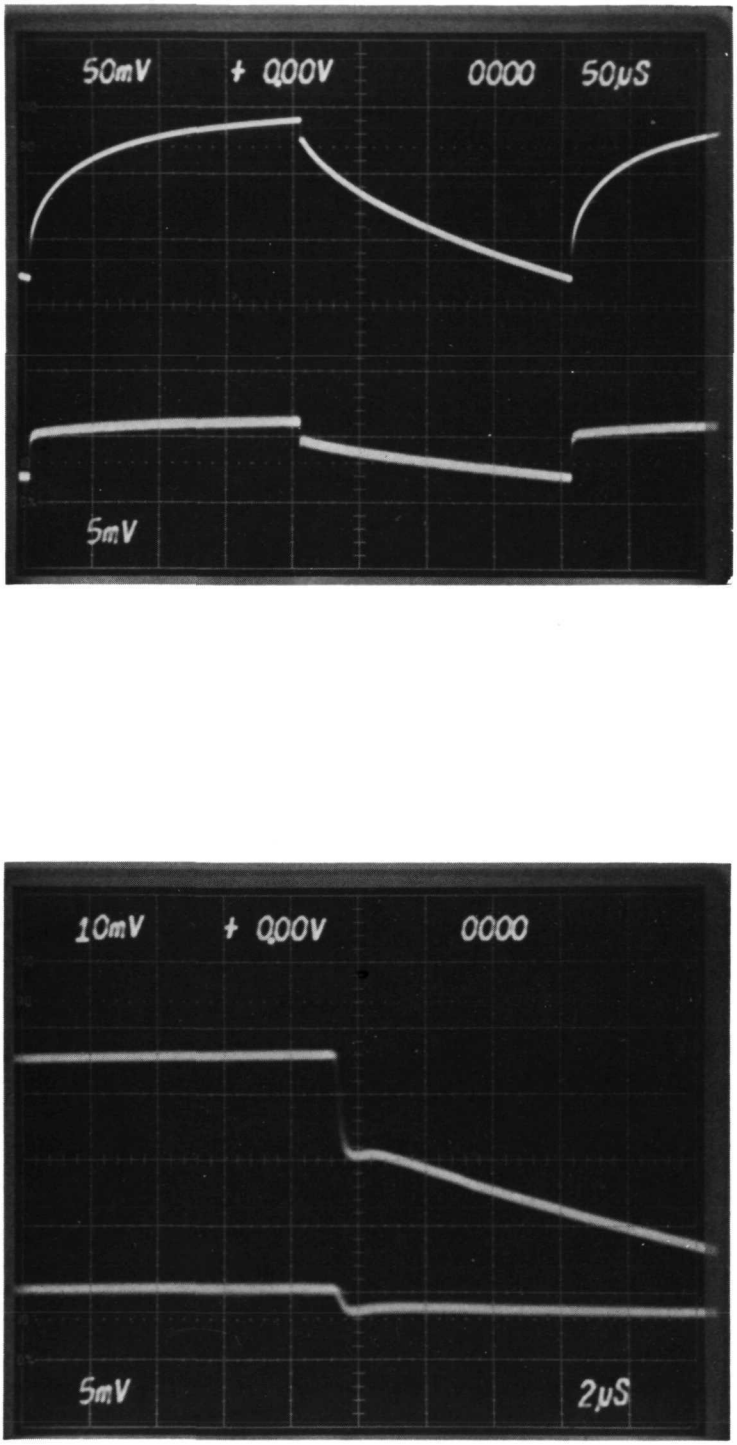

Fig. 3 Cell voltage response to constant current pulse through beta-alumina. Lower trace is expansion of termination region.

solution. The sharp voltage drops are interpreted as measurements of iR loss whereas the slower potential decay of the upper trace reflects decay of interfacial polarization at the beta-alumina surface. An ionic conductivity of 1100 ohm-cm is calculated from these data after correction for the resistance of the propylene carbonate solution. Since the conductivity and area of the candidate conductors frequently are much smaller than that measured above, experiments were undertaken to validate the method with a smaller specimen of beta-alumina.

An attempt was made to determine the resistance of a sample of polycrystalline beta-alumina having an area exposed of 0.0020 cm^2, or about 1% of that of any sample previously measured. The cell response was the same as that exhibited by a pure epoxy disk under similar conditions.

The sensitivity of the pulse technique for small specimens was increased by maximizing the ratio of sample area to disk area. With a minute sample of beta-alumina pulse measurements with the microcell described in the preceding section gave $\rho \simeq 1000$ ohm cm, in agreement with accepted values.

An additional complication stems from the fact that the epoxy disk between two conducting liquids acts as a capacitor. When the conductivity between the cells is high, this has little effect on these measurements. However, when the conductivity is low, the entire cell responds as a capacitor. The constant current source then ceases to function properly and the pulse technique becomes useless. The microcell, in which the nonconductive area is minimized, solved this problem as well.

The possibility was explored of using a potentiometric method to establish ionic conductivity in specimens which are extremely small or resistive. The liquid electrolyte was replaced by solutions which were 0.2M $AgClO_4$ + 0.1M $NaClO_4$ and 0.002M $AgClO_4$ + 0.1M $NaClO_4$ on opposite sides of the beta alumina sample. The potential developed between Ag electrodes was 0.131V, in reasonable agreement with the theoretical value

$$0.059 \log \frac{0.2}{0.002} = 0.118\text{V}.$$

Unfortunately, the same result was obtained when the blank epoxy disk was substituted for that containing beta-alumina, and we conclude the epoxy resin or Viton rubber are too conducting for this to be a practicable method.

IV. RESULTS AND DISCUSSION OF RESULTS

A. $LiNb_6O_{15}F$-Type Compounds

1. Structure and transport model

The tunnel structure found for $LiNb_6O_{15}F$[1] is illustrated in Fig. 4. The building blocks are made up of pentagonal NbX_7 bipyramids, sharing edges with five NbX_6 octahedra. These building blocks are joined together at the corners in three dimensions, leaving hollow tunnels in which the Li^{1+} ions are presumed to occupy two possible sites. * Either site would yield six to eight Li-O

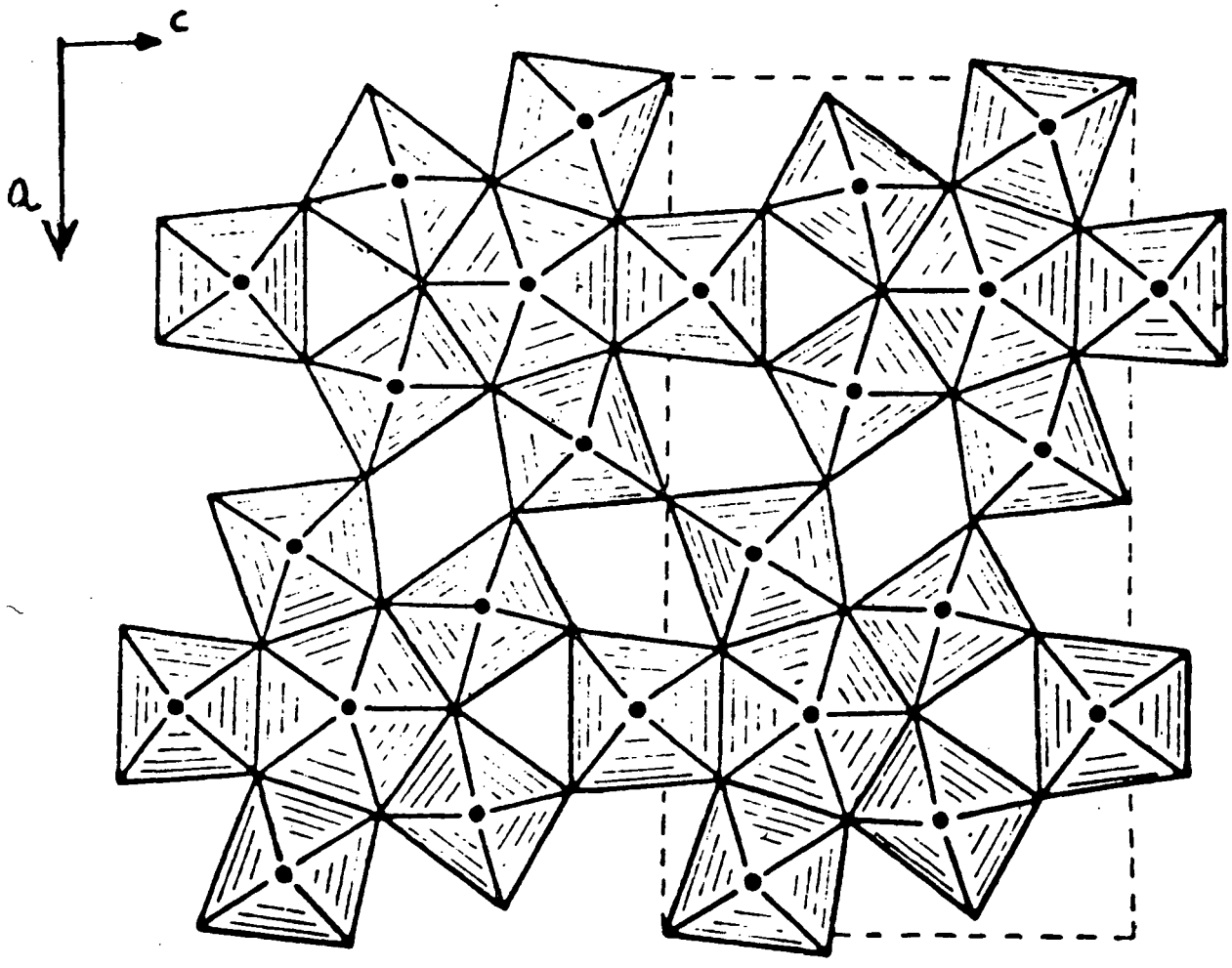

Fig. 4 The structure of $LiNb_6O_{15}F$. (Li^{1+} ions are not shown.) Taken from Ref. 1.

*Due to their low scattering power, the Li atoms cannot be located easily by x-ray methods. The Li-sites have been inferred from the knowledge of the rest of the structure.

distances between 2.5Å and 3.0Å. These distances are considerably larger than conventional Li-O bonds which are of the order 1.95Å to 2.30Å. It would appear, therefore, that these tunnels are wide enough for migration of Li^{1+} ions along the tunnels or b-direction of Fig. 1. In preliminary NMR screening[2] motional narrowing at -26°C was observed for ^7Li in $LiNb_6O_{15}F$, indicating at least local ionic motion of the Li^{1+} ions.

If the Li ions occupied fully one of the two Li sites, with the other type of channels completely empty, ionic conductivity would not be expected in stoichiometric $LiNb_6O_{15}F$. However, one could image nonstoichiometric variants (listed below) with either lower or higher Li content, made by substituting ions such as Ti^{4+}, Mo^{6+}, or W^{6+} and adjusting the O/F ratio. It is quite possible that both Li sites are partly occupied by Li^{1+} ions. In this case high ionic mobility might be expected even for stoichiometric $LiNb_6O_{15}F$.

2. Synthesis

(a) $LiNb_6O_{15}F$ and $Li_{0.8}Nb_{5.6}W_{0.4}O_{15.2}F_{0.8}$

$LiNb_6O_{15}F$ and $Li_{0.8}Nb_{5.6}W_{0.4}O_{15.2}F_{0.8}$ can be prepared by heating the appropriate mixtures of LiF, Nb_2O_5 and WO_3 in sealed platinum tubing (as a loose powder) or a sealed platinum crucible (in the form of compressed pellets). For one set of samples the heat treatment was 2 days at 1200°C in a muffle furnace. A second set of samples was heated for 1 day at 950°C. The resulting products for both temperatures and compositions were single phase and of the $LiNb_6O_{15}F$ type. No impurity peaks could be identified by x-ray diffraction. The crystals tend to be blade-like and up to 2 mm in length.

(b) $Li_{0.9}Nb_{5.8}Mo_{0.2}O_{15.1}F_{0.9}$ and $Li_{0.86}Nb_{5.72}Mo_{0.28}O_{15.14}F_{0.86}$

Mo-substituted phases of the above compositions could be prepared in the same manner as described above for $LiNb_6O_{15}F$, except that here the samples are heat treated at lower temperatures: 1 day at 950°C. X-ray diffraction data showed that these phases were of the $LiNb_6O_{15}F$ type. No impurity peaks could be detected.

(c) Attempted Synthesis of $Li_{0.8}Nb_{5.6}Mo_{0.4}O_{15.2}F_{0.8}$ and $Li_{0.7}Nb_{5.4}Mo_{0.6}O_{15.3}F_{0.7}$

Attempts were also made to synthesize $LiNb_6O_{15}F$-type compounds of compositions $Li_{0.8}Nb_{5.6}Mo_{0.4}O_{15.2}F_{0.8}$ and $Li_{0.7}Nb_{5.4}Mo_{0.6}O_{15.3}F_{0.7}$. However, these two compositions gave a two-phase mixture: (a) a coarsely crystalline $LiNb_6O_{15}F$-type phase with blade-like crystals up to 2 mm, (b) a fine needlelike phase of a darker color.

(d) Ti-Substituted Phases

Attempts were made to prepare a $LiNb_6O_{15}F$-type phase of composition $Li_{1.2}Nb_{5.6}Ti_{0.4}O_{14.8}F_{1.2}$. The synthesis proceeded as described for $LiNb_6O_{15}F$. A compound of the desired $LiNb_6O_{15}F$ structure type could not be obtained, and it is tentatively concluded that Ti^{4+} cannot be substituted into the $LiNb_6O_{15}F$ structure in significant amounts.

3. Evaluation

Strong motional narrowing of ^7Li in stoichiometric $LiNb_6O_{15}F$ was previously reported.(2) The dependence of line width on temperature indicated the lithium motion was probably localized or short range. NMR spectra of $LiNb_6O_{15}F$ doped with molybdenum and tungsten are shown in Figs. 5(a), (b), (c), and (d). The ^7Li spectrum, measured at room temperature and 186°C, shows strong motional narrowing. The line widths of the doped compounds are more narrow than in stoichiometric $LiNb_6O_{15}F$ (Table III), showing that substitution of Nb by Mo and W increases the lithium mobility, probably because more vacancies and disorder were introduced in the tunnels. No motional narrowing of the fluorine NMR spectrum was detected over the same temperature range. The absence of a Knight shift in the stoichiometric compound was previously reported to show the absence of electronic conductivity. It is believed the same is true for the doped compounds because the composition of the phases was adjusted to maintain the niobium in the pentavalent state.

TABLE III

NMR Spectra of $LiNb_6O_{15}F$ Compounds

Sample	Compound	Nucleus	Temp (°C)	Width, Gauss
C-5a	$Li_{0.9}Nb_{5.8}Mo_{0.2}O_{15.1}F_{0.9}$	^7Li	22	1.8 ± 0.5
			186	0.17 ± 1.0
		^{19}F	22	4.0 ± 1.0
			186	4.0 ± 1.0
C-9a	$Li_{0.9}Nb_{5.8}W_{0.2}O_{15.1}F_{0.9}$	^7Li	22	2.0 ± 0.4
			186	0.18 ± 0.04
		^{19}F	22	4.0 ± 1.0
			186	Not measured
	$LiNb_6O_{15}F$	^7Li	22	3.0 ± 0.2
			183	0.6 ± 0.1

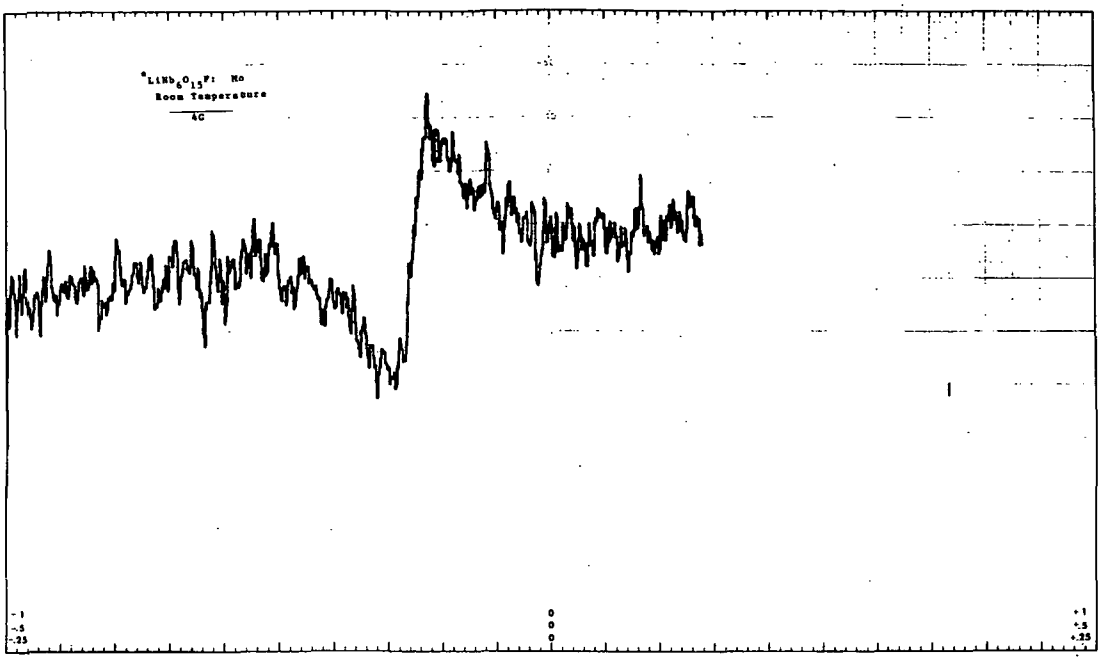

Fig. 5(a) NMR spectrum of ^{7}Li in $Li_{0.9}Nb_{5.8}Mo_{0.2}O_{15.1}F_{0.9}$ at room temperature. The peak width is 1.8 gauss.

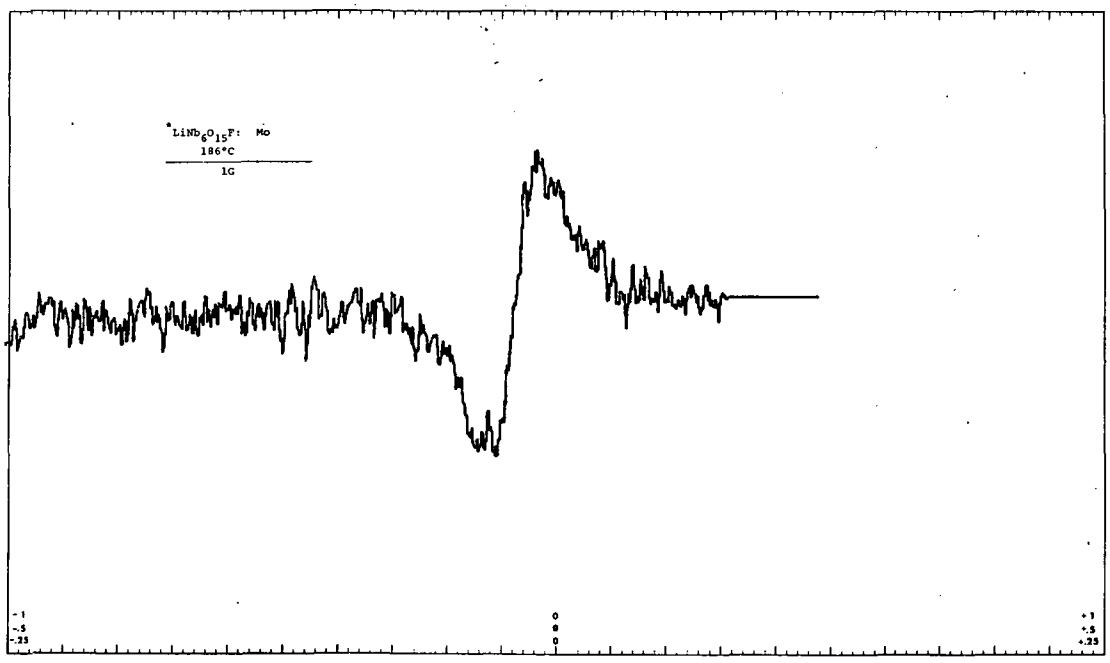

Fig. 5(b) Above at 186°C. The peak width is motionally narrowed to 0.17 gauss.

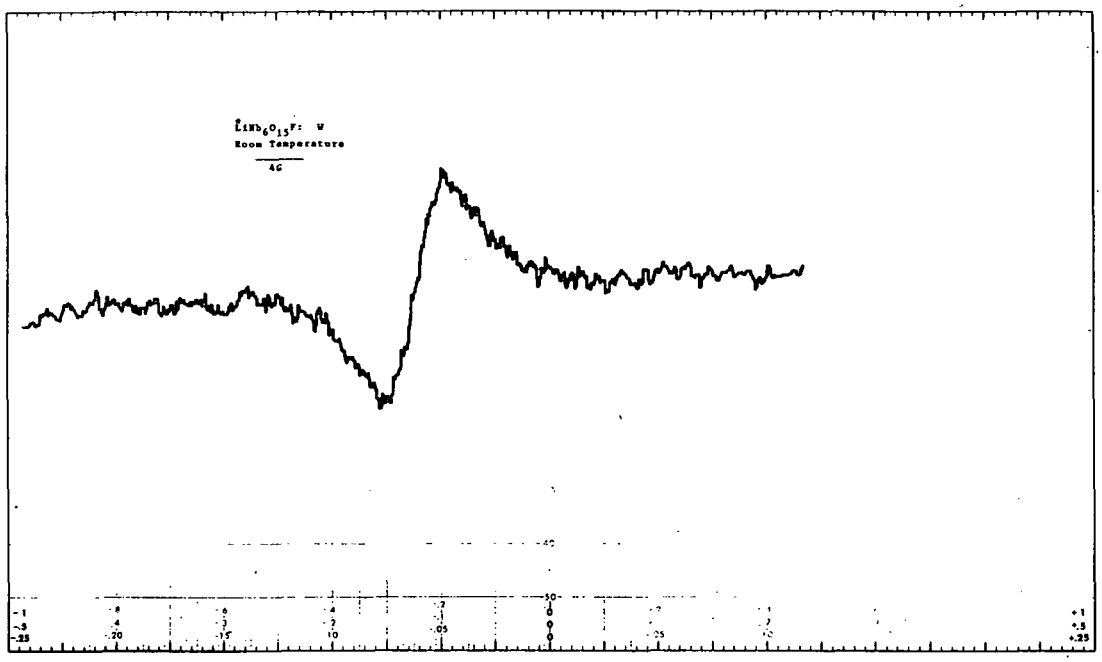

Fig. 5(c) NMR spectrum of ^{7}Li in $Li_{0.8}Nb_{5.6}W_{0.4}O_{15.2}F_{0.8}$ at room temperature. The peak width is 2.0 gauss.

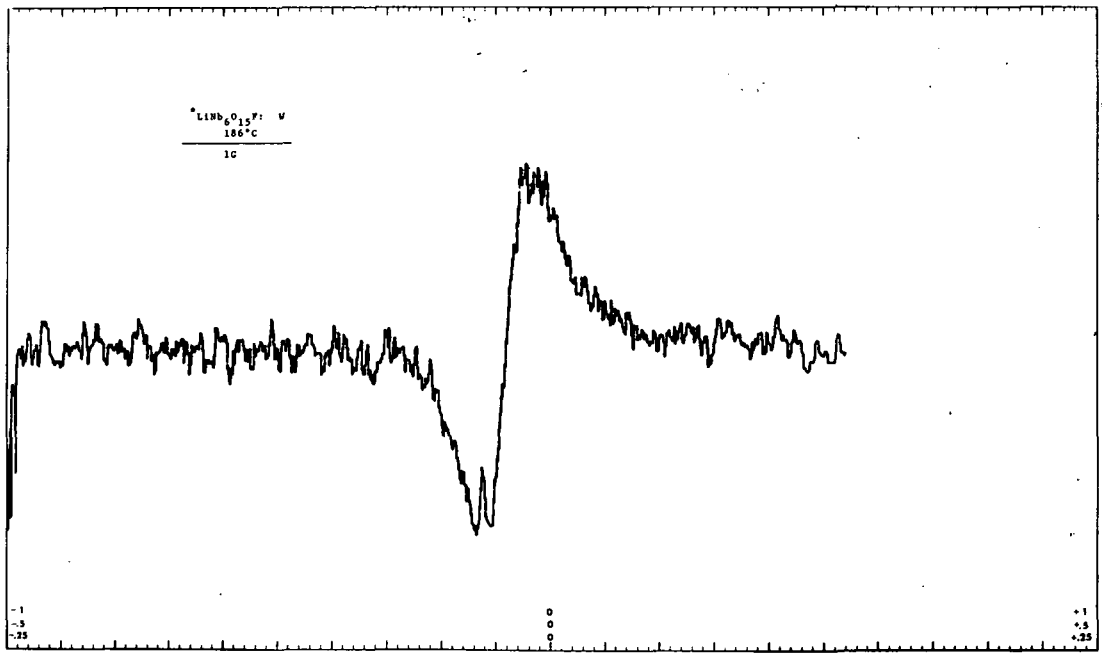

Fig. 5(d) Above at 186°C. The peak width is reduced to 0.18 gauss.

The crystals that were available were too small for reliable transport measurements at the present stage of development of our microcell method. Attempts were made to measure the conductivity in molybdenum-doped single crystals ($Li_{1-x}Nb_{6-2x}Mo_{2x}O_{15+x}F_{1-x}$ with $x < 0.2$). In order to prevent leaks about the edges, it was necessary to pot the crystal completely and expose a circular area only 0.25 mm in diameter for measurement. The growth habit is not known so individual crystals were potted with their major face parallel and perpendicular to the applied potential. The first set of measurements, which were made in the Teflon polymer cell, gave responses that were the same as expected for the epoxy disk. The measurements were repeated with similar results in a microcell to reduce interface effects (Fig. 6). It is estimated that the conductivity is probably less than 10^{-5} ohm^{-1} cm^{-1} at room temperature.

Dielectric loss measurements were made at NASA-Lewis Research Center on three of the lithium niobate compositions (Table IV). Neither the stoichiometric compound (C-1) nor the tungsten-doped material (C-3) gave indication of resonance peaks over the temperature range of 100° to 500°K. Titanium-doped lithium niobate (C-4) exhibited resonance peaks which were taken as strong evidence that the relaxation responsible for the resonances is that of mobile ions. The AC conductivity measured at 10^6 Hz was as follows:

TABLE IV

Sample	Composition	AC Conductivity (ohm^{-1} cm^{-1}) Room Temp	500°K
C-1	$LiNb_6O_{15}F$	2×10^{-7}	2×10^{-6}
C-3	$Li_{0.8}Nb_{5.6}W_{0.4}O_{15.2}F_{0.8}$	5×10^{-7}	6×10^{-6}
C-4	$Li_{1.2}Nb_{5.6}Ti_{0.4}O_{14.8}F_{1.2}$	8×10^{-6}	6×10^{-4}

In summary, lithium niobium oxyfluoride appears to be a moderate to poor conductor of lithium ions at low temperature, and the conductivity is improved by doping.

B. Hollandite-Type Compounds

1. Structure and Transport Model

Hollandite is a tunnel structure which takes its name from the mineral hollandite, approximately $BaFeMn_7O_{16}$. K^{1+}, Na^{1+} and Pb^{2+} can substitute for Ba^{2+} and Al^{3+} for manganese or iron. The structure was first described by Byström and Byström[3] and is illustrated in Fig. 7. In the structure, MnO_6 octahedra and FeO_6 octahedra randomly form an open framework which leaves empty channels. Approximately half of the available sites in the channels are occupied by Ba^{2+} ions. It has been postulated[3] that these Ba^{2+} ions are strung out along these tunnels in a regular manner, such that each

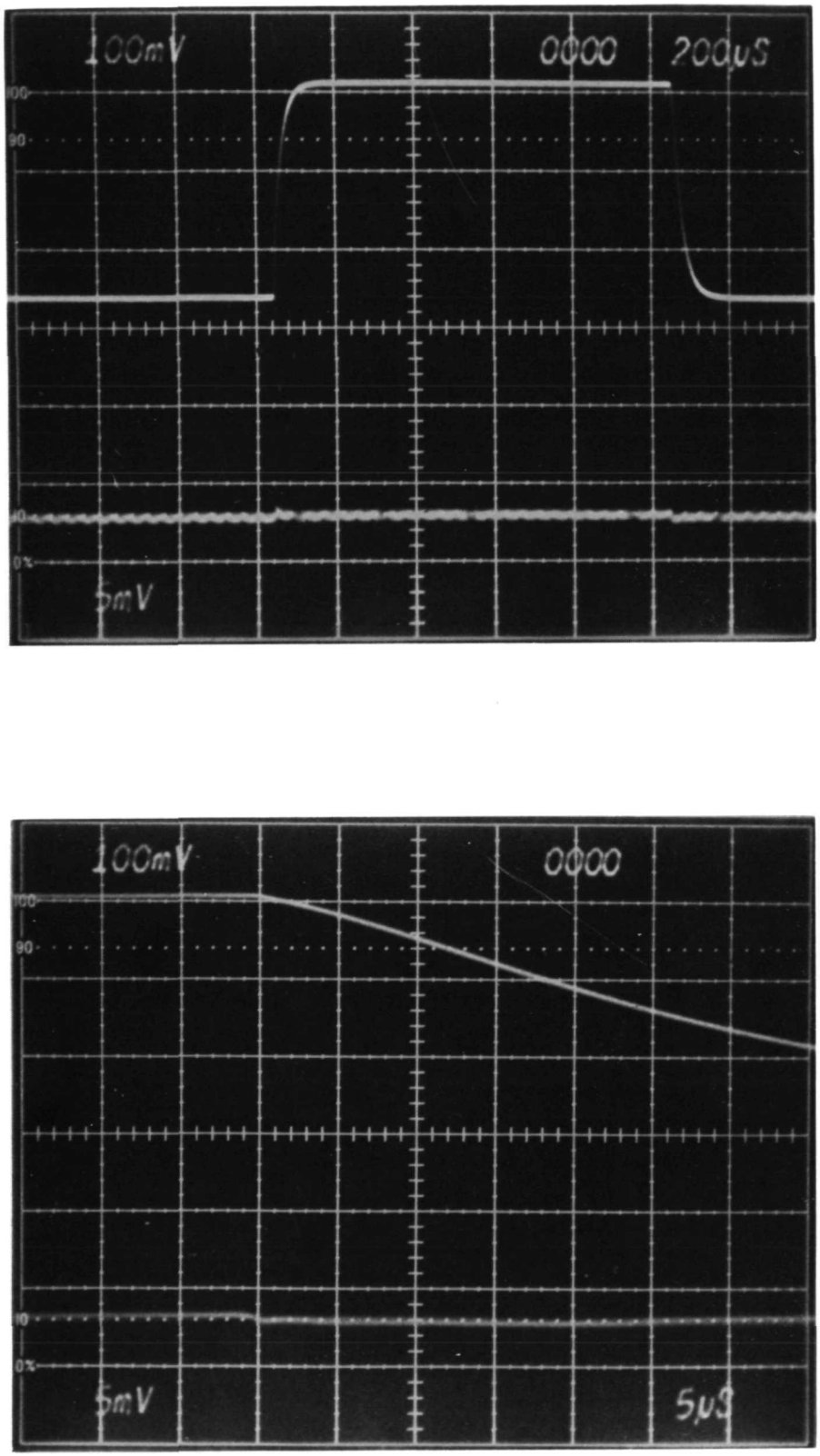

Fig. 6 Response of Mo-substituted $LiNb_6O_{15}F$ crystal in microcell. The lower trace is an expansion of the termination region.

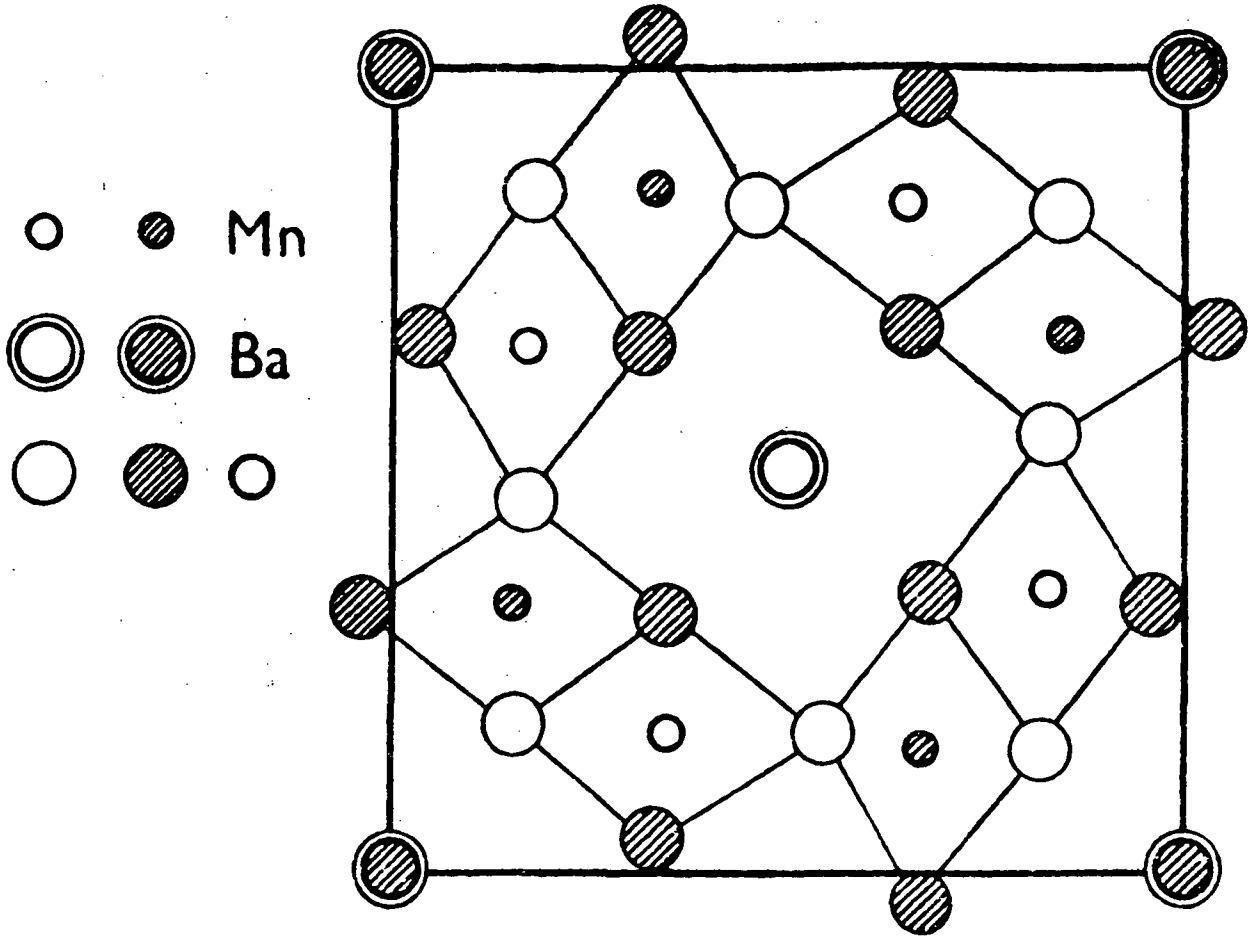

Fig. 7 The structure of hollandite projected on the (001) plane. After Ref. 3.

Ba^{2+} ion is followed by a vacant site and each vacant site by a Ba^{2+} ion. These Ba^{2+}-□-Ba^{2+}- .... chains are randomly arranged in the structure, so that there is only a one-dimensional order in the tunnels. It has also been postulated that the vacant sites between Ba^{2+} ions can be partly occupied by water molecules which are always present in the mineral. [3]

In recent years a large number of new hollandite-type compounds have been reported[4, 5] in which alkali metal ions (especially K^{1+} and Rb^{1+}) completely replace the Ba^{2+} ions inside the tunnels. Such K^{1+} or Rb^{1+}-hollandites can be completely stoichiometric so that all sites within the channels are occupied, and no vacancies exist, e.g., $K_2ZnTi_7O_{16}$, $K_2Ga_2Ti_6O_{16}$, $Rb_2MgTi_7O_{16}$, $Rb_2Al_2Ge_6O_{16}$, etc. For some systems, both stoichiometric and non-stoichiometric phases can be prepared. For example, in the K_2O-TiO_2-Al_2O_3 system, stoichiometric $K_2Al_2Ti_6O_{16}$ and nonstoichiometric $K_{1.6}\square_{0.4}$ $(Al_{1.6}Ti_{6.4})$ O_{16} can be prepared, both with the hollandite structure. [4]

Stoichiometric hollandites have also been made with Ag^{1+}, Tl^{1+} or Na^{1+} in the tunnels; [5] however, Cs^{1+}-hollandites can only be made non-stoichiometric. [4] Apparently the large size of the Cs^{1+} and Ba^{2+} ions does

not permit complete filling of the hollandite channels. For Ba^{2+}-hollandites, the repulsion between two adjacent Ba^{2+} ions is probably another reason why attempts to synthesize stoichiometric Ba-hollandites (such as $Ba_2Mg_2Ti_6O_{16}$) have so far been unsuccessful.

2. Synthesis

The hollandite samples were of composition $K_{1.6}Mg_{0.8}Ti_{7.2}O_{16}$ and were obtained from the NASA-Lewis Research Center.

3. Evaluation

The hollandite boule was described as polycrystalline with preferred orientation of crystallites with tetragonal c-axes parallel to the boule axis. The resistivity at room temperature measured by dielectric loss on similar material was 80 ohm-cm. On the other hand, the room-temperature resistivity measured with four-probe DC was 10^4 to 10^5 ohm-cm.

No attempt was made to determine motional narrowing of the potassium NMR spectrum because the nuclear moment is very small and the potassium peak probably would not have been seen above background.

Four hollandite specimens were cut from the boule for conductivity and transport measurements. Each had a cross-sectional area of about 0.12 cm^2 and was 0.10 cm thick. Two were cut parallel and two were cut perpendicular to the boule axis. Identical results were obtained with the two pairs of duplicate specimens.

The conductivity of hollandite was measured in the Teflon polymer cell. The top trace of Fig. 8 shows the voltage response to an 18 μamp, 200 msec pulse through a solution of 0.05M tetrabutyl ammonium tetrafluoborate, 0.02M $KClO_4$ in propylene carbonate, without an epoxy disk or sample present. The center trace shows the response to the same current pulse with the cell containing the sample of hollandite cut with the conducting tunnels (c-axis) parallel to the pulse direction. Note the well-defined iR drop upon pulse termination. We have calculated a hollandite ionic conductivity of 200 ohm-cm from these plots after correction was made for the resistance of the propylene carbonate solution.

In contrast, the bottom trace of Fig. 8 shows the cell response when the same current pulse was applied to a hollandite sample in a direction perpendicular to the conducting tunnels. The cell impedance is so high that less than 1 μamp current flows. No sharp iR drop is seen in the magnified trace because the total cell impedance is so high that the cell responds like a capacitor shunted by a large resistance. Sample resistance perpendicular to the tunnels is estimated to be greater than 10^5 ohm-cm from these traces.

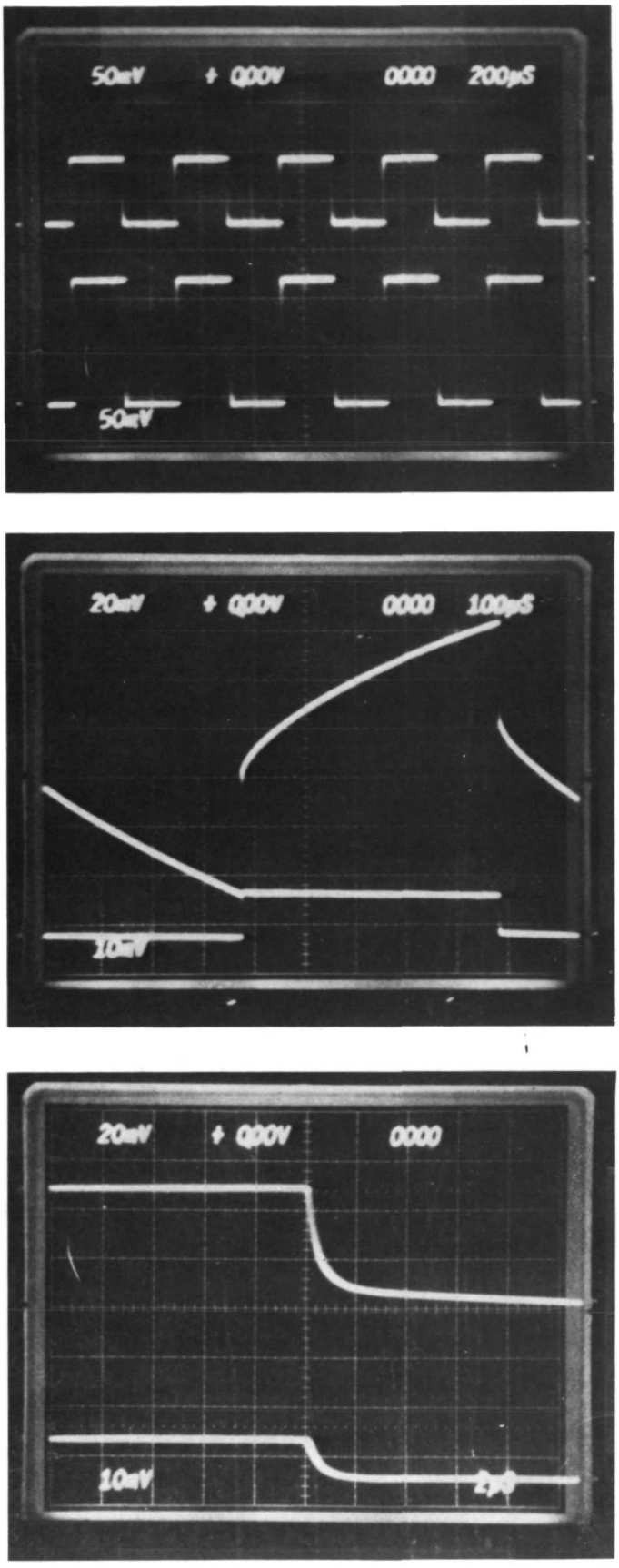

Fig. 8 Hollandite. The upper trace is voltage response with no specimen present: 18 μamp - 200 μ sec pulse through 0.02 M $KClO_4$. Middle trace is response to hollandite oriented with tunnels parallel to field. Lower trace is response when tunnels are perpendicular to the field.

The pulse measurements having shown that there is large ionic conductivity in a direction parallel to the tunnels in hollandite, an attempt next was made to determine the potassium transport down the tunnels.

The hollandite slab was placed between two propylene carbonate solutions, both 0.1 M in tetrabutyl ammonium tetrafluoroborate one saturated with $KClO_4$. The propylene carbonate was dried over activated alumina. The cell was filled in a dry box, then closed tightly to prevent contamination by water before removing for measurement.

The hollandite specimen was polarized between two platinum electrodes maintained at 5V potential difference. The cell developed an initial current greater than 1 μamp which decayed to 0.09 μamp in 5 minutes after transporting a total of 2.7×10^{-5} coulombs. After 20 minutes the current was 0.05 μamp and 7.4×10^{-5} coulombs had been passed. The current continued to decay with time and the experiment was discontinued after one hour 52 minutes when i = 0.03 μamp and Q = 2.3×10^{-4} coulombs. Pulse measurements were made in both directions throughout the experiment and we continued to observe the same responses as previously reported. No attempt was made to measure the transport number by analyzing for potassium since the maximum potassium that could have been transferred was only 2×10^{-9} eq.

There are about 10^{15} tunnels per cm^2 of the c-face of hollandite. The large current that was observed at the beginning of the experiment corresponded to a transport of about 2×10^{-14} coulombs/cm^2, approximately equal to that calculated if a few potassium ions entered or left each tunnel. The current then decayed to the relatively small value of 0.2 μamp/cm^2 which may represent migration down the tunnel.

We conclude there is high short-range conductivity in potassium hollandite and this property is measured by both the DC pulse method and by dielectric loss. However, the transport and DC measurements show that long-range conductivity at room temperature is small and probably is determined by the slow migration of potassium ions down the tunnels.

C. Cordierite-Type Compounds

1. Structure and Transport Model

The structure of the mineral cordierite (essentially $Mg_2Al_4Si_5O_{18}.xH_2O$) is another tunnel structure which is of interest as a potential solid electrolyte. The structure was first studied by Byström[6] and later by Gibbs,[7] Smith and Schreyer.[8] It is made up of a three-dimensional tetrahedral network of the composition $Al_4Si_5O_{18}$. The Mg^{2+} ions occupy octahedral sites, and varying amounts of water are located in the wide channels running parallel to the c-axis. The structure is illustrated in Figs. 9 and 10 giving a good view of the channels which are lined with oxygen ions and have a radius of

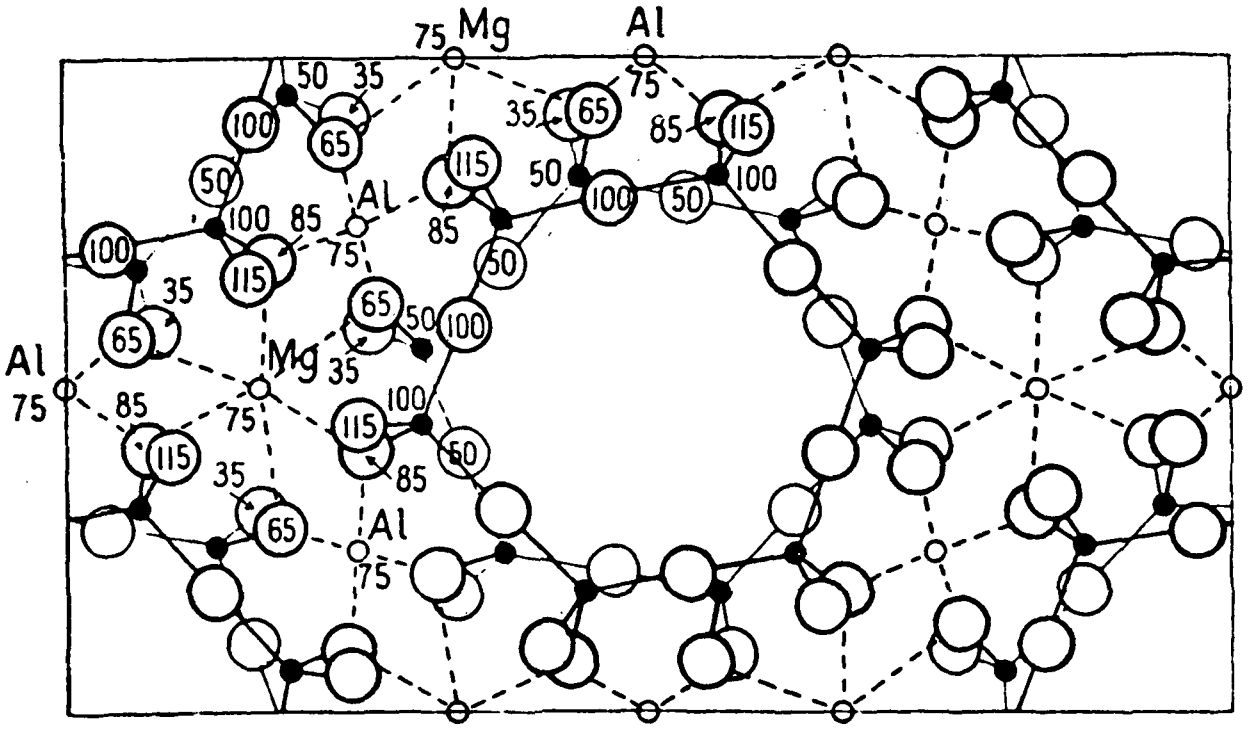

Fig. 9 The structure of cordierite, viewed down the c-axis. After Ref. 6.

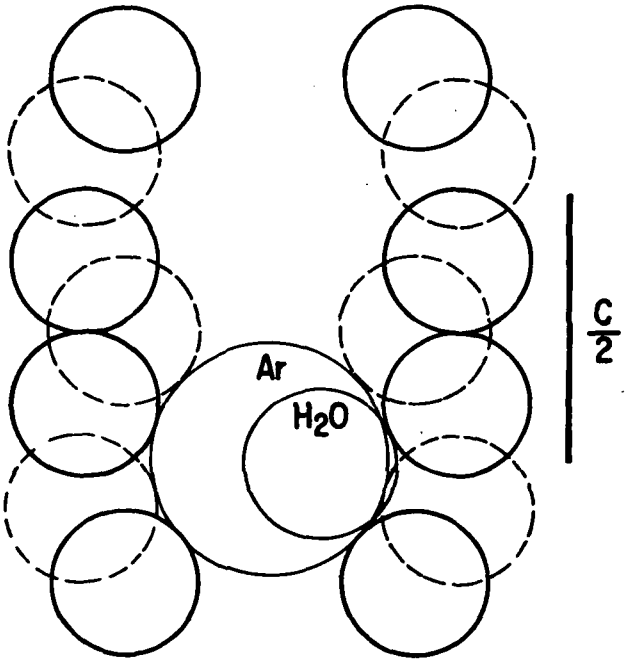

Fig. 10 Cross-sectional view of a tunnel in the cordierite structure. After Ref. 8. Note that the tunnels are large enough to accommodate not only water molecules but even the larger argon atoms with a radius of 1.92Å.

1.4Å at the narrowest neck and 2.2Å at the widest. The channels can be completely free from any water, and in fact, the compound $Mg_2Al_4Si_5O_{18}$ exists as a stable phase in the ternary system $MgO-Al_2O_3-SiO_2$. See W. Schreyer and J. F. Schairer.[9] It is known from the analyses of cordierite minerals and from recent crystal chemical studies that alkali ions such as Na^{1+} can occupy to some extent the wide channels. Na^{1+} ions are expected to be too small to occupy the center of the tunnels and would probably be located at the edge of the channels. Larger ions would probably occupy a more central position in the tunnels. It is possible ionic conductivity may result if alkali ions are introduced into these channels. The situation is expected to be especially favorable for K^{1+} and Rb^{1+} ions.

Recently cordierites of the compositions $Na_xMg_2(Al_{4-x}Be_xSi_5O_{18})$ have been synthesized where x can be up to 0.55. Here the substitution $Al^{3+} = Be^{2+}+Na^{1+}$ was used to introduce substantial amounts of Na^{1+} into the empty channels. See Provondra and Langer.[10]

2. Synthesis

To synthesize alkali-rich cordierites, it was felt best to avoid systems involving the toxic element beryllium, such as the $Na_xMg_2(Al_{4-x}Be_xSi_5O_{18})$ solid solution series.[10]

We have therefore tried to modify cordierite ($Mg_2Al_4Si_5O_{18}$) by making other substitutions, namely: $Si^{4+}=Al^{3+}+K^{1+}$, $Si^{4+}=Al^{3+}+Na^{1+}$, $Mg^{2+}=Li^{1+}+K^{1+}$ and $Mg^{2+}=Li^{1+}+Na^{1+}$. In the last two cases, the Li^{1+} ion substitutes for Mg^{2+} and the larger alkali ions go into the channels. The following cordierite-type compositions were chosen for synthesis: $Na_{0.2}Mg_2Al_{4.2}Si_{4.8}O_{18}$, $K_{0.2}Mg_2Al_{4.2}Si_{4.8}O_{18}$, $Na_{0.4}Mg_2Al_{4.4}Si_{4.6}O_{18}$, $K_{0.4}Mg_2Al_{4.4}Si_{4.6}O_{18}$, $Rb_{0.4}Mg_2Al_{4.4}Si_{4.6}O_{18}$, $Na_{0.2}Mg_{1.8}Li_{0.2}Al_4Si_5O_{18}$ and $K_{0.2}Mg_{1.8}Li_{0.2}Al_4Si_5O_{18}$. The starting materials were $NH_4Al(SO_4)_2 \cdot 12H_2O$, $MgSO_4$ and the appropriate alkali sulfates. Ammonium stabilized Ludox colloidal silica suspension was used as a source of silica. The sulfates were first dissolved in hot water; then the appropriate amount of Ludox colloidal silica was added. The suspension was heated to dryness (at ~200°C) in a drying oven and then transferred to a platinum crucible and heated gradually from 300° to 1200°C in a furnace in air. The samples were kept at 1200°C for about 20 minutes and then withdrawn from the furnace. At this stage the samples are fine, white powders which x-ray diffraction indicated is made up of three phases: mullite ($3Al_2O_3 \cdot SiO_2$), sapphirine ($Mg_7Al_{18}Si_3O_{40}$) and cristobalite-related (or carnegieite-like) alkali silicate phases. At this stage no trace of a cordierite phase was detected.

The powders were now heated at 1560°C for 20 minutes in air and cooled. In this way glasses were formed which were devitrified for two days at 1000°C.

The products were then x-rayed with the following results:

Nominal Composition	X-ray Results	
$Na_{0.2}Mg_2Al_{4.2}Si_{4.8}O_{18}$	100% cordierite.	No detectable impurities.
$K_{0.2}Mg_2Al_{4.2}Si_{4.8}O_{18}$	98% cordierite.	Possible trace (2%) of spinel.
$Na_{0.2}Mg_{1.8}Li_{0.2}Al_4Si_5O_{18}$	~90% cordierite.	Some spinel and possibly β-spodumene.
$K_{0.2}Mg_{1.8}Li_{0.2}Al_4Si_5O_{18}$	~90% cordierite.	Some spinel and possibly β-spodumene.
$Na_{0.4}Mg_2Al_{4.4}Si_{4.6}O_{18}$	~97% cordierite.	Possible trace of α-Al_2O_3.
$K_{0.4}Mg_2Al_{4.4}Si_{4.6}O_{18}$	~95% cordierite.	~5% α-Al_2O_3.

The excess α-Al_2O_3 may indicate that the real composition of the solid solution is somewhat below the nominal composition in sodium or potassium. Some sodium or potassium may be lost through volatilization during the firing of the samples, and a chemical analysis will be necessary to determine the real alkali content. Refractive index measurements of both the crystalline and glassy cordierite samples indicate that the alkali substituted cordierites have significantly lower indices than pure crystalline or glassy $Mg_2Al_4Si_5O_{18}$.

For the Rb analogue, significant amounts of a pure, homogeneous glass could not be obtained. In attempting to make such glasses, the reaction was so vigorous that a foamy, porous material was obtained instead of pure glass. The major components of the porous material were glass and crystalline spinel-type $MgAl_2O_4$. The same type of foaming also occurred in several runs with the Na and K-cordierites, but here such foaming could be avoided by the use of smaller samples.

Our results for the Na^{1+} and K^{1+} substituted cordierites are encouraging, and indicate that limited substitution of the types: $Si^{4+}=Al^{3+}+K^{1+}$ or $Si^{4+}=Al^{3+}+Na^{1+}$ can take place. The possible presence of β-spodumene ($LiAlSi_2O_6$) in the Li^{1+}-substituted samples, raises some doubt as to whether the substitution $Mg^{2+}=Li^{1+}+Na^{1+}$ really occurs. The identification of small amounts β-spodumene in these samples must be considered as tentative, since only the most intense β-spodumene-type x-ray peak could be detected.

3. Evaluation

Several attempts were made to observe the sodium NMR spectrum in sodium cordierite. The spectra were averaged for 30 to 40 hours and measured at high r-f to increase the sensitivity. In no case was the sodium peak detected above the background. A typical NMR spectrum of Na-cordierite obtained by sweeping through the region expected for the sodium peak is shown in Fig. 11. The failure to detect any sodium could be due to many

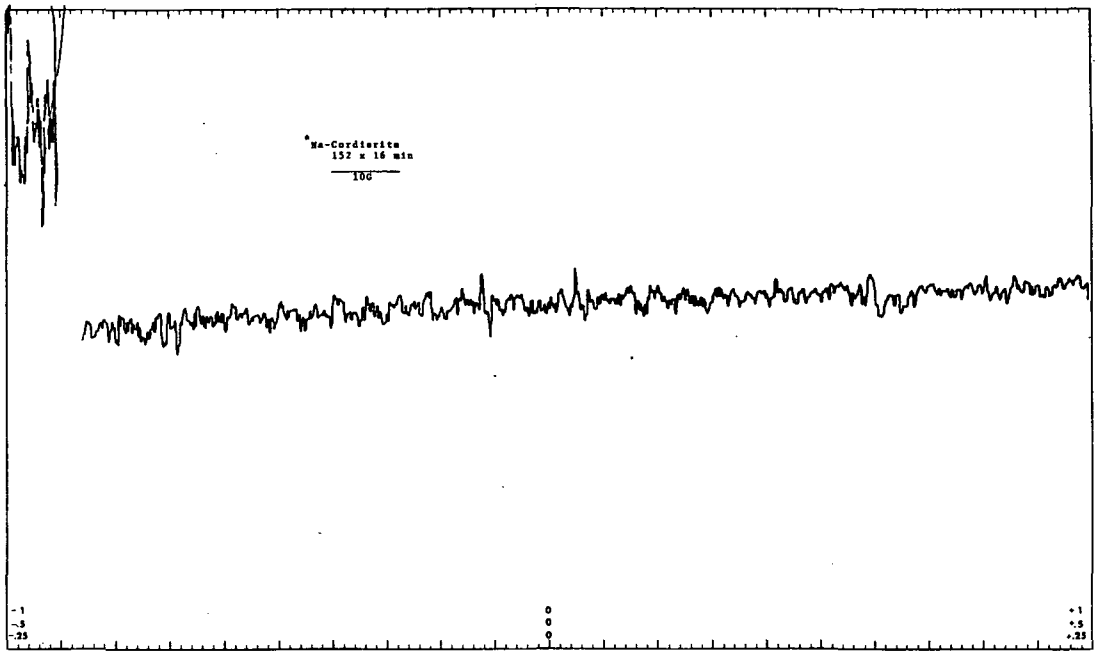

Fig. 11 NMR spectrum of sodium cordierite ($Na_{0.4}Mg_2Al_{4.4}Si_{4.6}O_{18}$) at room temperature. The ^{23}Na spectrum was accumulated for 40 hours.

reasons: low sodium concentration, large quadrupole interactions, and/or the distribution of sodium ions in two or more crystallographic sites.

The response of potassium cordierite ($K_{0.2}Mg_2Al_{4.2}Si_{4.8}O_{18}$) was tested in a microcell. The exposed specimen area was a disk with diameter 1.5 mm thickness about 1.5 mm. The shape of the complete pulse and the trailing edge at high resolution is shown in Fig. 12. The small rapid iR drop and the current flow indicates that potassium cordierite is probably a potassium ion conductor. The room-temperature conductivity is small, probably less than potassium hollandite.

The results of the dielectric loss measurements on the cordierite samples are in Table V. None of the materials gave indication of resonance peaks over the temperature range of 100° to 500°K.

D. $NaNbO_2F_2$-Type Compounds

1. Structure and Transport Model

The structure of monoclinic $NaNbO_2F_2$ can be described as a layer structure made up of $(NbO_2F_2)_n^{n-}$ sheets which are held together by Na^{1+} ions only. (There are no anion bridges connecting these sheets.)[11] The sheets are apparently made up of NbO_4F_2 octahedra, linked to each other at the four oxygen corners. The structure is illustrated in Fig. 13. The eight nearest Na-X distances in the irregular NaF_6O_2 polyhedron range from

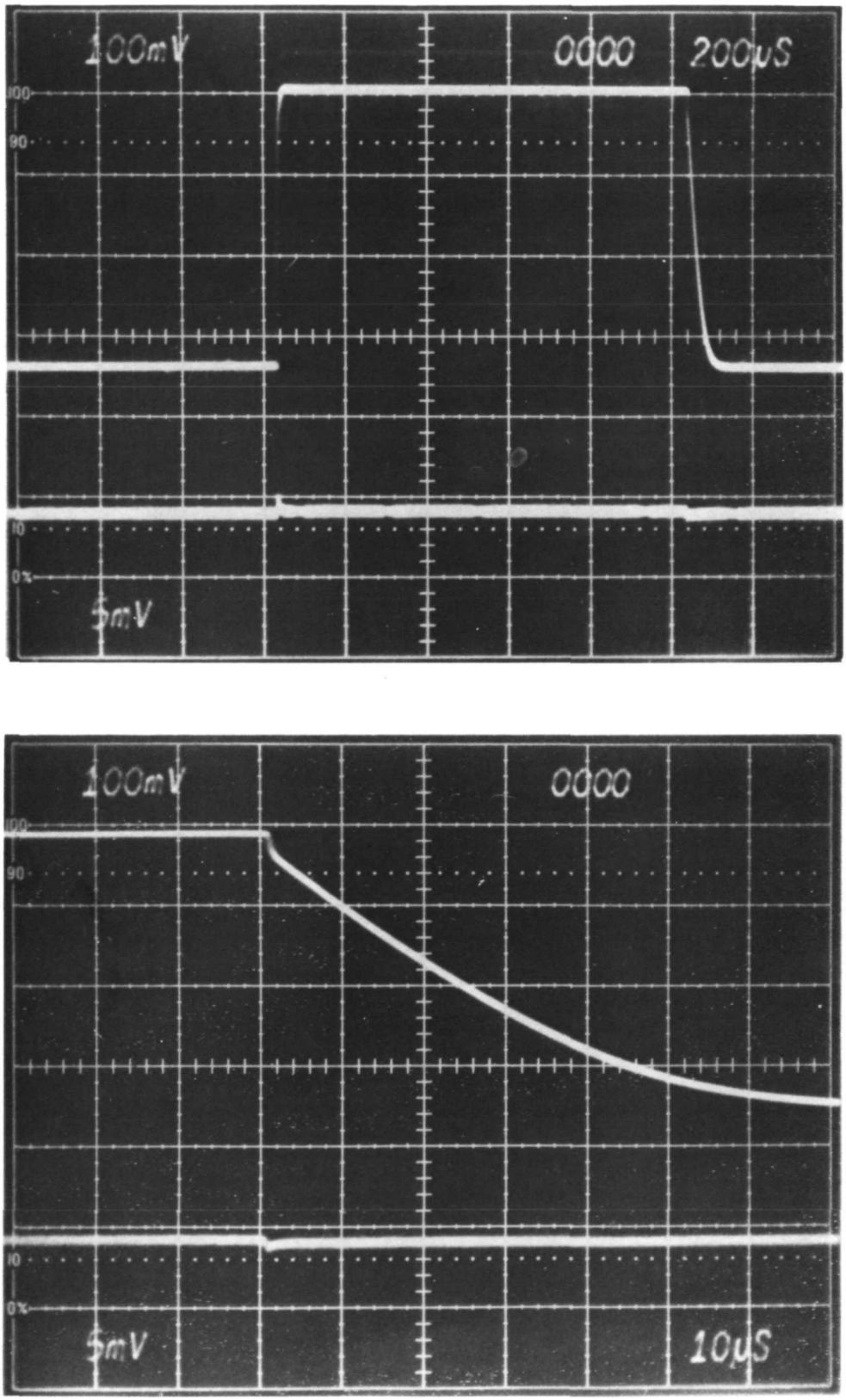

Fig. 12 Voltage response of potassium cordierite in microcell. The trailing edge of the pulse is shown below.

TABLE V

Sample and Composition			Room Temperature Conductivity Frequency (Hz)	ohm^{-1} cm^{-1}
B42as	$K_{0.2}Mg_2Al_{4.2}Si_{4.8}O_{18}$	100% cordierite	10^3	4.9×10^{-10}
			10^4	3×10^{-9}
			10^5	1.8×10^{-8}
			10^6	1.1×10^{-7}
B49as	$K_{0.4}Mg_2Al_{4.4}Si_{4.6}O_{18}$	95% cordierite; 5% Al_2O_3	10^3	1.3×10^{-9}
			10^4	9×10^{-9}
			10^5	7×10^{-8}
			10^6	4×10^{-7}
B41as	$Na_{0.2}Mg_2Al_{4.2}Si_{4.8}O_{18}$	100% cordierite	10^3	3×10^{-10}
			10^4	2×10^{-9}
			10^5	9×10^{-9}
			10^6	1.2×10^{-9}
B48as	$Na_{0.4}Mg_2Al_{4.4}Si_{4.6}O_{18}$	97% cordierite; 3% Al_2O_3	10^3	6×10^{-10}
			10^4	4×10^{-9}
			10^5	1.5×10^{-8}

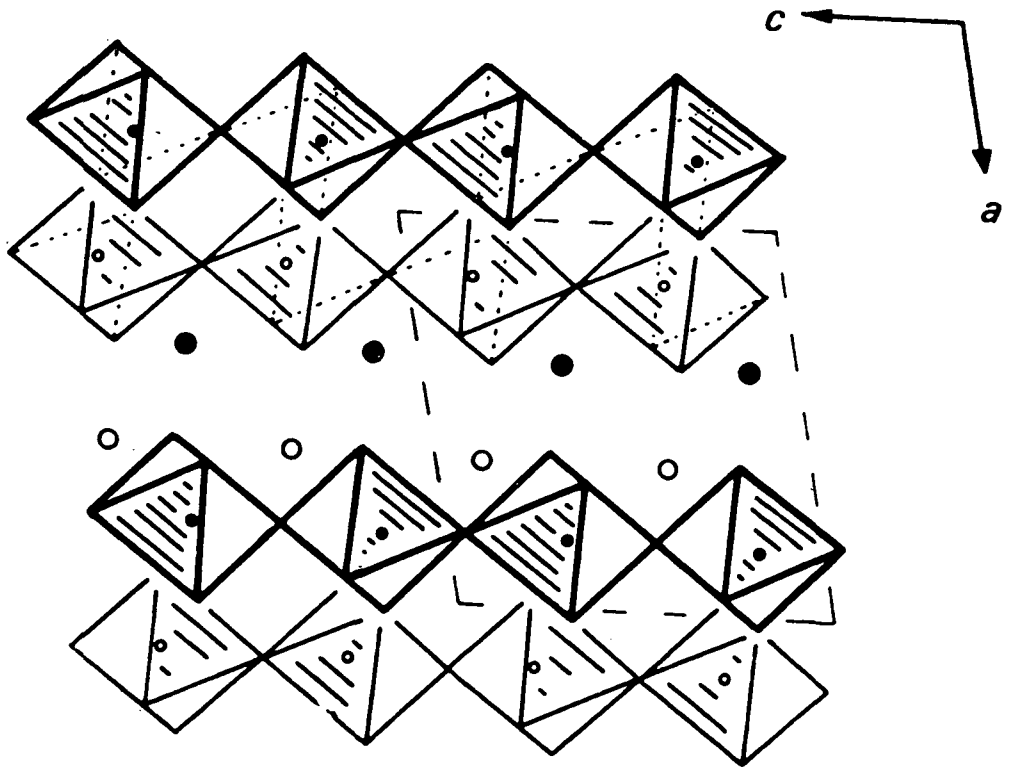

Fig. 13 The structure of $NaNbO_2F_2$ projected on the (010) plane. After Ref. 11.

2.22Å to 3.13Å). The isotropic temperature coefficient for Na^{1+} (B = 2.42) indicates larger than normal thermal vibrations.[11]

We believe that there is a chance of high Na^{1+} ion mobility in this structure if vacancies can be introduced into the Na^{1+} sites. For this purpose, the composition of $NaNbO_2F_2$ could be modified by changing the O/F ratio or introducing hexavalent ions into the octahedral site, e.g., Mo^{6+} or W^{6+}. One could similarly try to modify the composition of $NaNbO_2F_2$ by substituting Ca^{2+}, Sr^{2+}, Pb^{2+}, Y^{3+} or Nd^{3+} ions for Na^{1+}.

2. Synthesis

There is probably little chance of Na^{1+} ion conduction in stoichiometric $NaNbO_2F_2$. With a view of making sodium-deficient $NaNbO_2F_2$ phases, the following reactions were tried:

$$0.9NaF + NbO_2F = Na_{0.9}NbO_2F_{1.9}$$

$$0.9NaF + 0.9NbO_2F + 0.1MoO_3 = Na_{0.9}Nb_{0.9}Mo_{0.1}F_{1.8}O_{2.1}$$

$$0.9NaF + 0.9NbO_2F + 0.1WO_3 = Na_{0.9}Nb_{0.9}W_{0.1}F_{1.8}O_{2.1}$$

$$0.7NaF + 0.1YF_3 + NbO_2F = Na_{0.7}Y_{0.1}NbO_2F_2$$

$$0.7NaF + 0.1NdF_3 + NbO_2F = Na_{0.7}Nd_{0.1}NbO_2F_2$$

$$0.8NaF + 0.1CaF_2 + NbO_2F = Na_{0.8}Ca_{0.1}NbO_2F_2$$

$$0.8NaF + 0.1SrF_2 + NbO_2F = Na_{0.8}Sr_{0.1}NbO_2F_2$$

$$0.8NaF + 0.1PbF_2 + NbO_2F = Na_{0.8}Pb_{0.1}NbO_2F_2$$

For most chemicals, reagent grade starting materials were used, but NbO_2F had to be prepared according to the following procedure:

Optical grade Nb_2O_5 (99.95%) was dissolved in concentrated hydrofluoric acid in a platinum crucible. The resulting solution was filtered and the clear solution was evaporated to dryness. The powder was heated for one day under vacuum at 220°C. The resulting dry powder was pure NbO_2F, with no impurity peaks detectable in the x-ray pattern.

The starting materials were dried under vacuum at 220°C, weighed out in the appropriate ratio, mixed, and pressed into pellets. The pellets were loaded into platinum crucibles, heated at 400°C under vacuum for 1 hour and then sealed. The crucibles were then heated at 600°C for 2 hours to 1 day. Some mixtures were also heat-treated at 700°C for 1/2 day.

Although stoichiometric $NaNbO_2F_2$ could be made in reasonably pure form, there was no evidence for the existence of the defect solid solutions, no matter what heat treatment was used. It appears that the hoped-for solid solutions do not form, and instead new phases appear. Efforts were made to

identify these new phases and for some compositions a tentative interpretation is given below.

X-ray patterns for the Mo and W-substituted phases give a two-phase mixture of $NaNbO_2F_2$ and substantial amounts of an unknown phase. The x-ray patterns for $Na_{0.7}Y_{0.1}NbO_2F_2$, $Na_{0.7}Nd_{0.1}NbO_2F_2$ and $Na_{0.8}Ca_{0.1}NbO_2F_2$ bear a strong resemblance to each other and may belong to the same structure type. These patterns could not be identified with any known Na-Nb compounds. However, a study of various sodium tantalum oxyfluorides has been published recently[12] and from the given cell constants for these tantalum oxyfluorides we calculated x-ray powder patterns. We found that the major x-ray peaks of $Na_{0.7}Y_{0.1}NbO_2F_2$, $Na_{0.7}Nd_{0.1}NbO_2F_2$ and $Na_{0.8}Ca_{0.1}NbO_2F_2$ can be indexed on the basis of the $Na_2Ta_3O_6F_5$-type unit cell. Similarly, the patterns of $Na_{0.8}Sr_{0.1}NbO_2F_2$ and $Na_{0.9}NbO_2F_{1.9}$ can be indexed for the most part on the basis of the $Na_4Ta_5O_{10}F_9$-type unit cell. These two structure types are unknown and their x-ray patterns have not been published; therefore, the tentative identifications made above are speculative. The x-ray pattern for $Na_{0.8}Pb_{0.1}NbO_2F_2$ is different from the others but bears some resemblance to that of $Na_{0.8}Sr_{0.1}NbO_2F_2$. It seems that the $NaNbO_2F_2$ structure does not tolerate defect solid solutions and that new structure types appear if the Na/Nb ratio is lowered.

3. Evaluation

The sodium and fluorine NMR spectrum in $Na_{0.8}Sr_{0.1}NbO_2F_2$ were measured at room temperature and 186°C (Figs. 14a, b). The peak-to-peak line widths were broad (about 8 gauss) and no motional narrowing was observed over this temperature range.

The ionic conductivity of the pure and doped $NaNbO_2F_2$ specimens could not be measured because they were too porous. The dielectric loss and AC conductivity results are given in Table VI.

E. Phases with a Defect Perovskite Structure

1. Structure and Transport Model

The well-known perovskite structure is illustrated in Fig. 15 for the idealized cubic form.

Normally the perovskite structure would not be considered as a good candidate for high cationic conductivity. In this ABX_3 structure, the large A-cations are 12-coordinated and form together with the X-anions cubic close-packed layers perpendicular to the cubic [111] directions. In this close-packed array, the B-cations occupy octahedral interstices. In stoichiometric ABX_3 perovskites, such as $SrTiO_3$ or $KNbO_3$, the high packing efficiency and lack of open channels would rule out any high cationic

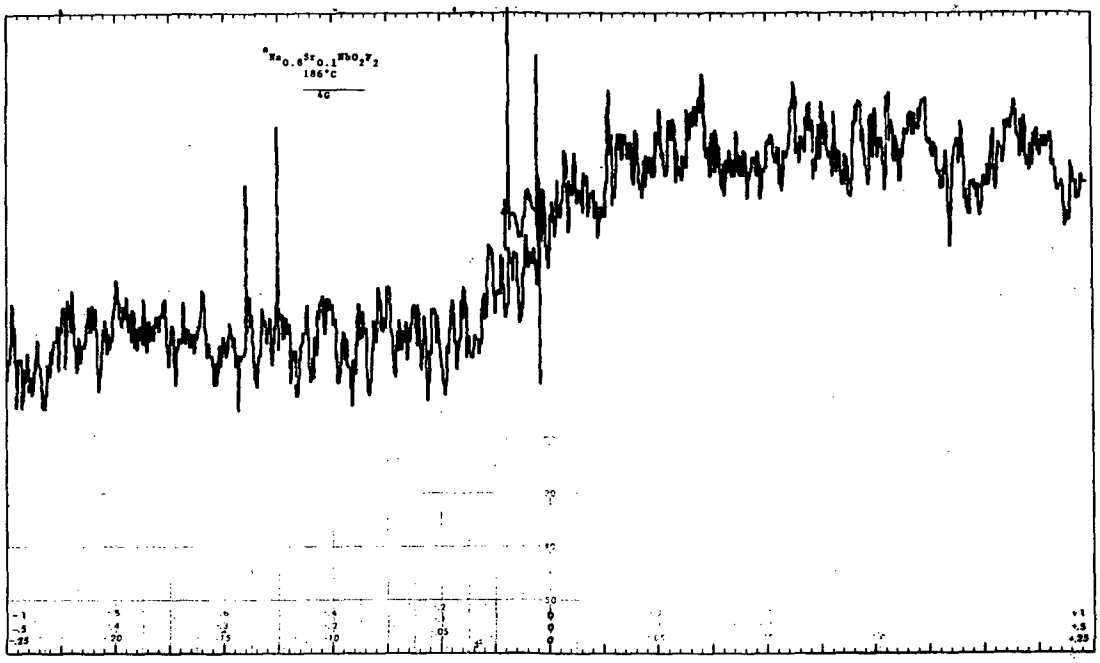

(a)

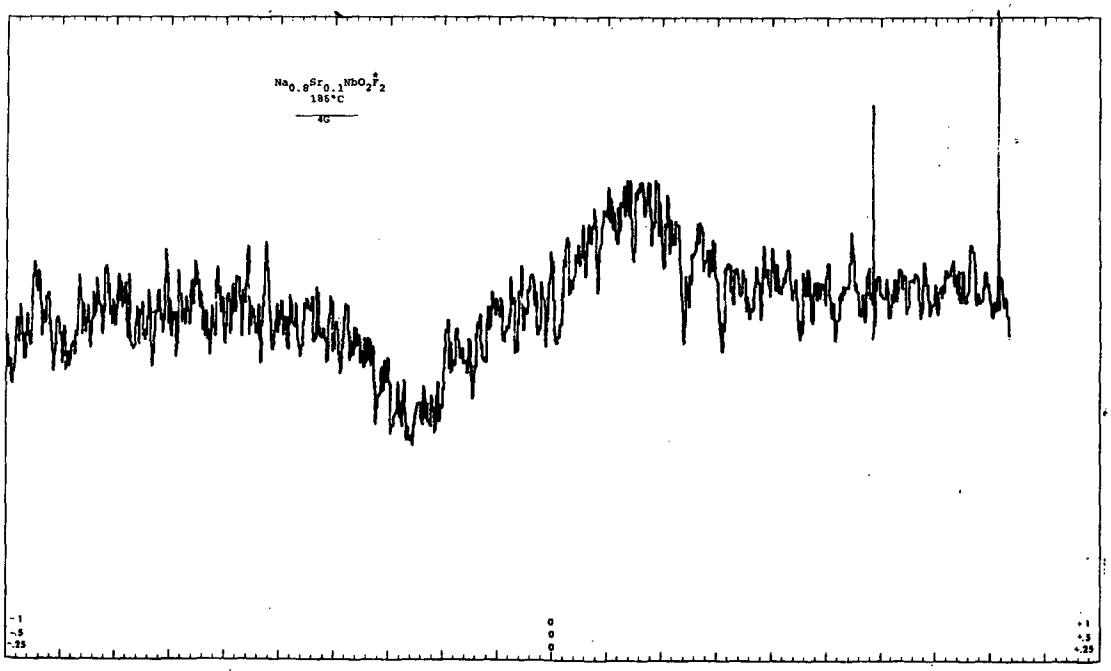

(b)

Fig. 14 (a) NMR spectrum of ^{23}Na in $Na_{0.8}Sr_{0.1}NbO_2F_2$ at 186°C.
(b) Spectrum of ^{19}F.

TABLE VI

Sample	Additive	Resonance Peak	AC Conductivity at Room Temp. ($ohm^{-1}\,cm^{-1}$)	
C-12 b		Yes	10^3Hz	2×10^{-9}
		$\Delta E < 1$ kcal (must be	10^4	1×10^{-8}
		electron blocking with	10^5	4×10^{-8}
		ρ elect $\geqslant 108$)	10^6	1×10^{-7}
C-18	Y	No	10^3	1.9×10^{-10}
			10^4	1.5×10^{-9}
			10^5	2×10^{-8}
			10^6	3×10^{-7}
C-19	Nd	No	10^3	2×10^{-9}
			10^4	1.4×10^{-8}
			10^5	9×10^{-8}
			10^6	4×10^{-7}
C-20	Ca	No	10^3	8×10^{-10}
			10^4	3×10^{-9}
			10^5	3×10^{-8}
			10^6	3×10^{-7}
C-21	Sr	Yes	10^3	1.3×10^{-8}
		$\Delta E \sim 8.1$ kcal mol^{-1}	10^4	9×10^{-8}
		ρ 25° $\sim 6 \times 10^6$ ohm-cm	10^5	3×10^{-7}
			10^6	8×10^{-7}
C-22	Pb	No	10^3	5.7×10^{-10}
			10^4	2.5×10^{-9}
			10^5	1.5×10^{-8}
			10^6	4×10^{-8}

mobility. Even if the structure is made nonstoichiometric by creating vacancies in the A-site, one would not normally expect these large A-cations to move easily to the vacant sites because the constrictions which separate the A-sites are too narrow.

However, these objections can be partly overcome when we consider non-stoichiometric variants of the known cubic perovskite $La_{0.5}Li_{0.5}TiO_3$ (a_0 = 3.861Å)(13). Here Li^{1+} apparently occupies (randomly with La^{3+}) the 12-coordinated A-site with twelve very large Li-O distances of 2.73Å. It is very unusual for an intermediate size cation such Li^{1+} to occupy a 12-coordinated site with such very large Li-O separations. More typical Li-O distances are of the order 1.95Å to 2.30Å.

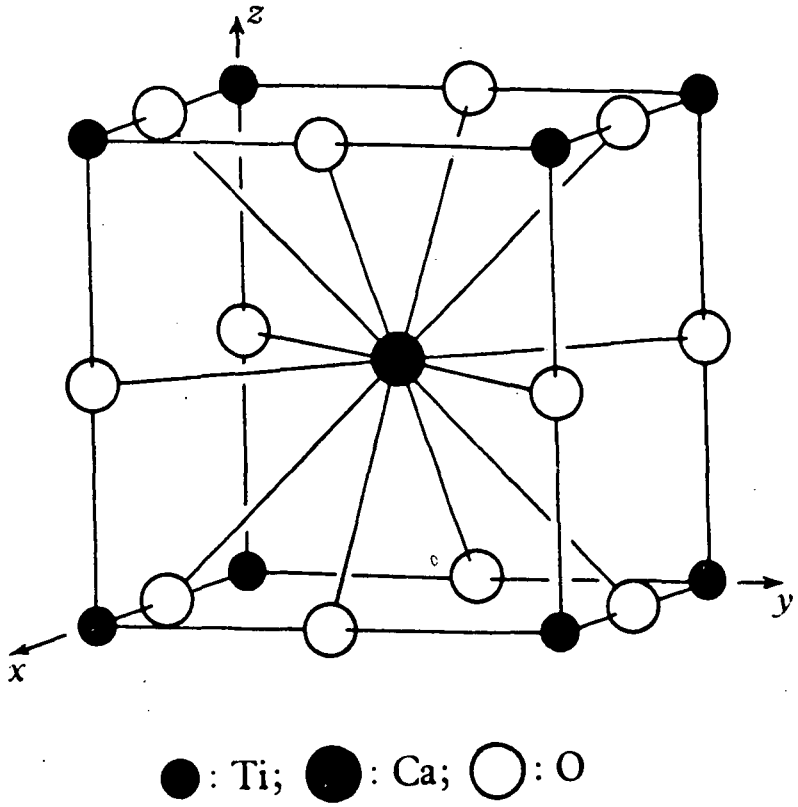

Fig. 15 The ideal or cubic perovskite structure.

It was hoped that vacancies can be induced in this perovskite to provide for cation motion. This could be done by substituting a stable pentavalent ion such as Nb^{5+} or Ta^{5+} for tetravalent Ti. We could thus envision a cubic perovskite of composition $(La_{0.5}Li_{0.3}\square_{0.2})^{XII}(Ti_{0.8}Ta_{0.2})^{VI}O_3$, where the introduction of 20% vacancies into the A-site could result in high lithium ion mobility. For this study it is especially significant that a cubic perovskite of composition $(La_{2/3}\square_{1/3})TiO_3$ can be very closely approached, [13-17] and that here density measurements definitely indicate vacancies in the A-site. [16]

The greatest stumbling block toward high Li^{1+} mobility in a perovskite such as $(La_{0.5}Li_{0.3}\square_{0.2})^{XII}(Ti_{0.8}Ta_{0.2})^{VI}O_3$ is perhaps the narrow constriction through which the Li^{1+} ion must move to go from one A-site to one of the six neighboring A-sites. (On the average, about one of these six A-sites would be vacant.) At its closest approach to the other ions, Li^{1+} will be surrounded by four square planar oxygens at a distance of 1.93Å and four square planar Ti^{4+} (or Ta^{5+}) ions at a distance of 2.73Å. However, this short Li-O bond is still within the range of typical 4-coordinated Li-O distances: 1.86Å to 2.05Å according to the International Tables for X-ray Crystallography. The motion of Li^{1+} ions through this constriction would therefore be possible, but not easy.

The phase diagram for the ternary system Li_2O-La_2O_3-TiO_2 has not been established and of the binaries, only the system La_2O_3-TiO_2 has been studied over the entire range.[18] However, fragmentary data are available on the other two binary systems.

Recently cubic perovskites were found in the system $Y_x(Ta_{3x}W_{1-3x})O_3$[19] over a narrow composition range $0.20 < x < 0.24$. We have investigated the possibility of using such a cubic perovskite--e.g., $\square_{0.78}Y_{0.22}(Ta_{0.66}W_{0.34})O_3$--as a base for introducing small amounts of Li and Na in the 12-coordinated site.

2. Synthesis

For the titanium-perovskites, the following compositions were attempted:

$(La_{0.5}Li_{0.3}\square_{0.2})(Ti_{0.8}Ta_{0.2})O_3$, $(La_{0.5}Na_{0.3}\square_{0.2})(Ti_{0.8}Ta_{0.2})O_3$,

$(Nd_{0.5}Li_{0.3}\square_{0.2})(Ti_{0.8}Ta_{0.2})O_3$, $(Nd_{0.5}Na_{0.3}\square_{0.2})(Ti_{0.8}Ta_{0.2})O_3$.

Li_2CO_3, Na_2CO_3, Ta_2O_5, TiO_2, La_2O_3, and Nd_2O_3 were intimately mixed in the appropriate ratios. In the attempted synthesis, two approaches were used:

1. The mixes were loaded into platinum boats and heated at 1200°C for 2 hours. Then the samples were withdrawn from the furnace and cooled in air.

2. The mixtures were dissolved in concentrated nitric acid. The resulting solution was heated to dryness in platinum crucibles. The crucibles were then transferred to a muffle furnace and heated very gradually from 300° to 1200°C. The temperature was maintained at 1200°C for 2 hours and the crucibles were subsequently quenched by quickly immersing them in cold water.

Neither of the two methods of synthesis resulted in the hoped for cubic defect perovskite. Instead, a birefringent product was obtained in all cases.

The complex x-ray patterns of the products have not yet been interpreted completely, but the more intense x-ray peaks are near the peak positions expected for a cubic perovskite. It appears that the products may be ordered, distorted perovskites.

For the tantalum-tungsten perovskites, the oxides were mixed as shown in the equation below:

$$0.05\ Li_2WO_4 + 0.099\ Y_2O_3 + 0.347\ Ta_2O_5 + 0.256\ WO_3 = Li_{0.10}Y_{0.198}(Ta_{0.694}W_{0.306})O_3.$$

To make the Na-analogue, $Na_2WO_4 \cdot 2H_2O$ was substituted for Li_2WO_4. These two mixtures were pressed into pellets and reacted for one-half hour at 1200°C. In a modification of the above procedure, the samples were sealed into platinum tubing, heated at 1400°C for about one hour, and then quickly withdrawn and quenched in cold water.

None of the resulting products appeared to be of the cubic perovskite type. All samples were birefringent with a more complex perovskite-related x-ray pattern.

It appears that for all the attempted perovskites, the undistorted cubic structure could not be obtained. The distorted (and ordered) perovskites which were apparently formed would not be considered good candidates for cationic conductivity since the structural perovskite-like framework has probably collapsed around the small Li^{1+} or Na^{1+} sites, making ionic mobility of these ions less likely.

3. Evaluation

The two Ta-W perovskite-type samples were evaluated by dielectric loss. No loss peaks were observed and it is unlikely that these materials are good ionic conductors at low temperature. As pointed out in Section 2, we attribute the absence of conductivity to the collapse of the perovskite-like framework around the small monovalent cations.

F. Sodium Tungsten Bronze-type Compounds

1. Structure and Transport Model

A considerable effort was made last year in attempts to determine the ionic transport in nonstoichiometric lithium vanadates which are mixed electronic-ionic conductors. Since the differentiation of electron and ion charge carriers is a problem requiring investigation in all solid conductors, it was desirable to observe the nature of the response of our newly developed fast-pulse technique to materials of that kind. Sodium tungsten bronze was chosen for the test instead of lithium vanadate because large single crystals were available.

The $Na_{0.9}WO_3$ structure is essentially a slightly distorted version of the ideal (cubic) perovskite structure shown in Fig. 15. 10% of the Na sites are vacant, and some degree of ionic motion might therefore be possible. Such ionic motion would be difficult to detect by conventional conductivity measurements, due to the very high electronic conduction.

2. Sample Preparation

An electrolytically grown single crystal of $Na_{0.9}WO_3$ was obtained from Dr. R. C. DeVries of the General Electric Company. From a larger single

crystal, a smaller piece was cut for the cell measurements described below.

3. Evaluation

The sodium tungsten bronze crystal was cut parallel to one of the pseudo-cubic crystal axes and mounted in a microcell. The conducting surface was a circular area 1.0 mm in diameter and the crystal was 1.2 mm thick. The response of the cell to pulses of long and short duration is shown in Fig. 16. A large current flow is observed, and in addition, a slow, capacitive-like charge and decay extending for approximately 20 μsec. The capacitive-like behavior was not observed when platinum was substituted for the sodium tungsten bronze and, therefore, it is unlikely the slow processes are due to polarization at the interface. The observations suggest there may be a threshold for current flow, possibly related to the displacement of sodium ions in the tunnels.

G. $NaLiGe_4O_9$-Type Compounds

1. Structure and Transport Model

The structure of the orthorhombic $NaLiGe_4O_9$[20] is illustrated in Fig. 17 and consists of $(GeO_3)_n^{2n-}$ chains made up of GeO_4 tetrahedra sharing corners. These chains are connected by GeO_6 octahedra to form a three-dimensional framework. This framework gives rise to interwoven tunnels which are occupied by Na^+ and Li^+ ions. The tunnels might be sufficiently wide to permit some alkali ion motion in three dimensions. The most promising ionic conductors are perhaps the nonstoichiometric variants where vacancies in the alkali ion positions are created by substituting pentavalent ions for Ge^{4+}, either in the octahedral site (Nb^{5+}, Ta^{5+}, Sb^{5+}) or tetrahedral site (V^{5+}). However, some ionic motion may take place even in the stoichiometric $Li_2Ge_4O_9$ along interstitial sites.

In their regular sites, Li^{1+} ions are 5-coordinated with Li-O bonds at 1.827Å to 2.397Å at the corners of a square pyramid. Actually this Li^{1+} ion is distributed randomly over two equivalent sites 0.6Å apart, and there is a good chance that dynamic exchange between these two places may occur, which would enhance the likelihood of Li^{1+} ion mobility along the channels.

Na^{1+} ions occupy six-coordinated sites in different channels than the Li^{1+} ions, with Na-O distances ranging from 2.326Å to 2.900Å. This Na^{1+} ion can be completely replaced with Li^{1+} to form the end member $Li_2Ge_4O_9$. If the Li^+ ions were to occupy exactly the same site as Na^{1+} ions, there would be six very large Li-O distances (2.55Å on the average). It has been postulated[20] (but not proved) that Li^{1+} would prefer a different site (removed by $1/2\, b_0 = 2.31$Å) along the same channel which would yield six shorter Li-O distances (2.26Å), on the average. Since Li^{1+} ions have a low scattering

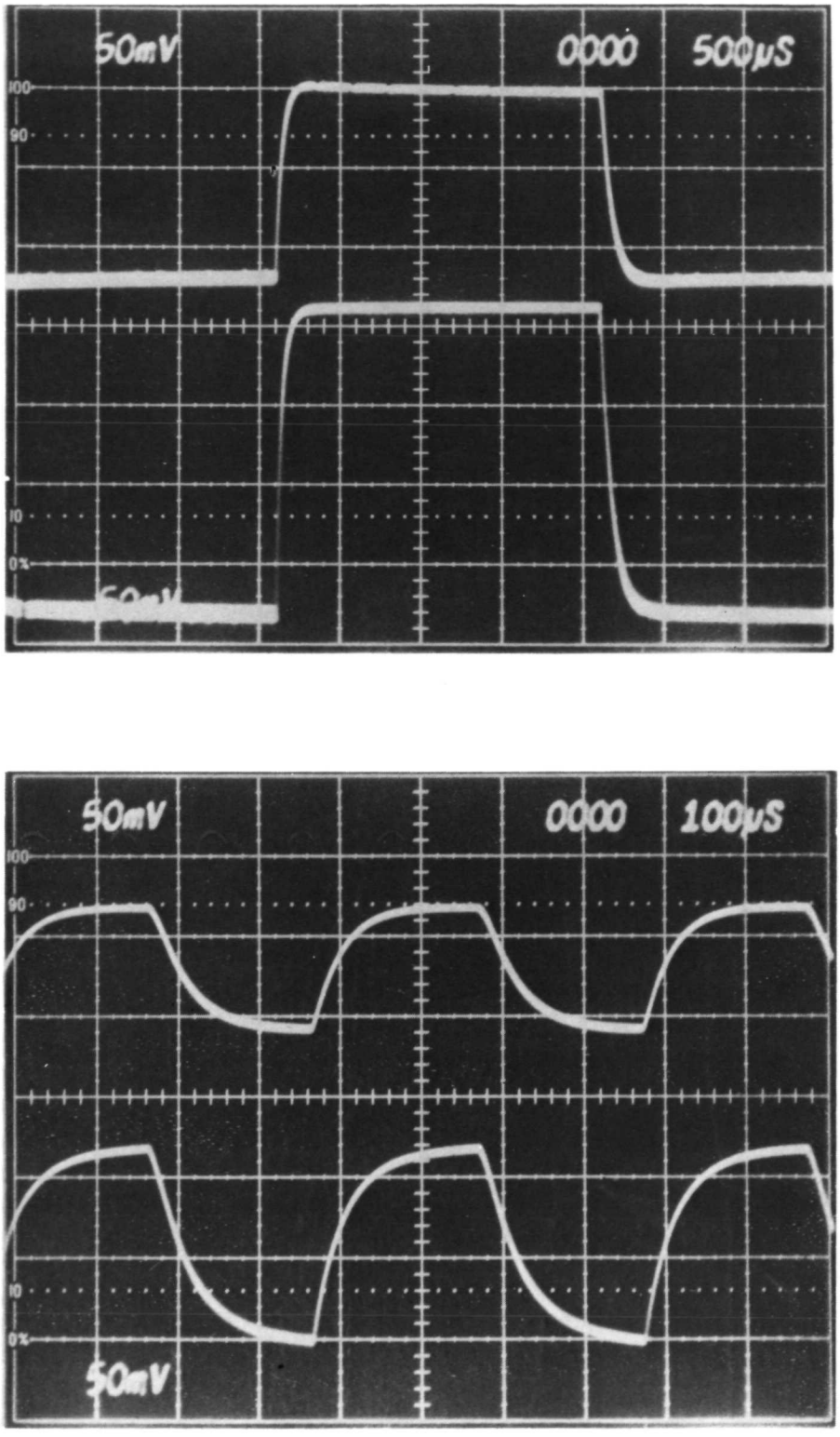

Fig. 16 Voltage response of sodium tungsten bronze crystal to constant current pulse. Above, 250 μsec pulse; below, 20 μsec pulse.

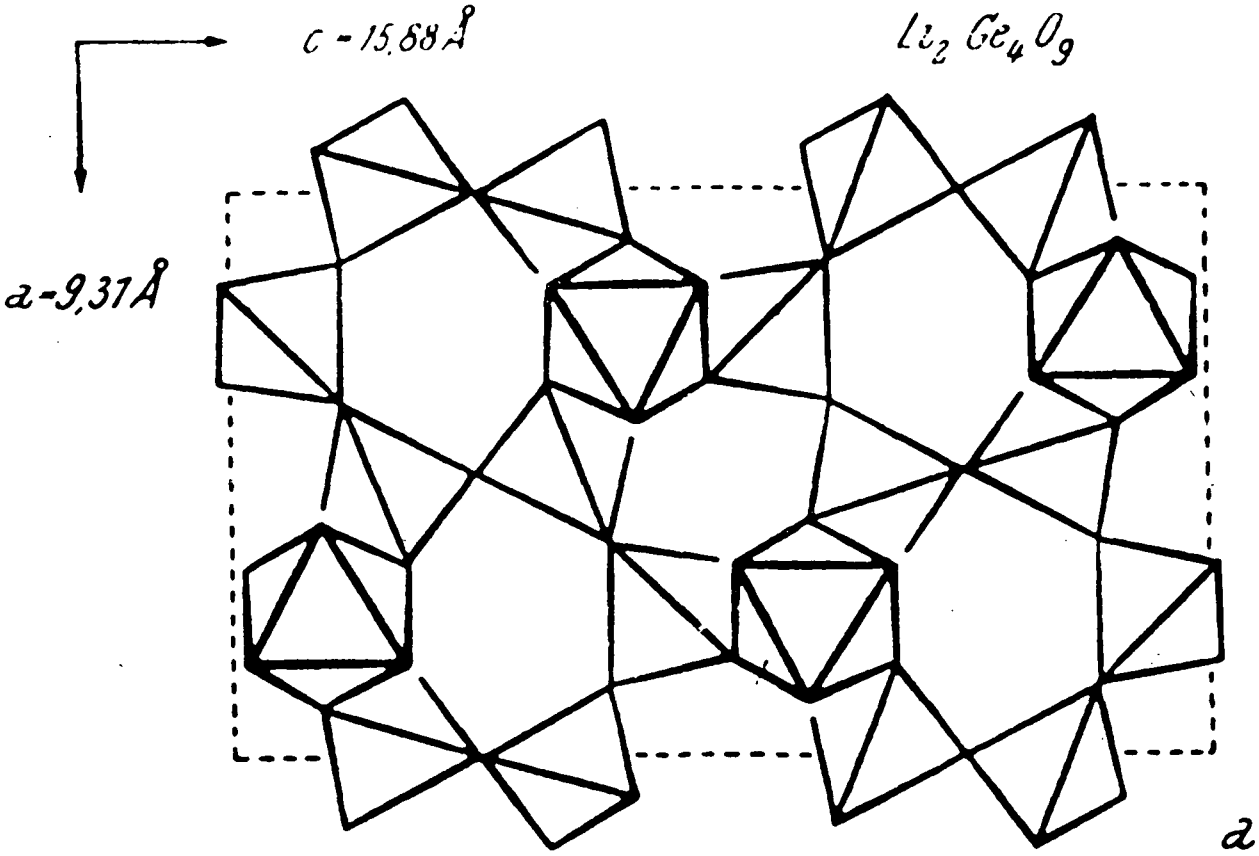

Fig. 17 The framework of interlinked GeO_4 tetrahedra and GeO_6 octahedra in the $NaLiGe_4O_9$ structure. After Ref. 23.

factor and cannot be easily placed by x-ray diffraction study, there is some uncertainty regarding the sites occupied by Li^{1+} ions in $Li_2Ge_4O_9$. However, the intensity agreement is a little better if Li^{1+} ions are placed in the site giving shorter Li-O bonds. It seems possible, however, that both sites could be partially occupied, a factor that might enhance ionic mobility.

2. Synthesis

A phase equilibrium diagram is available for the system Li_2O-GeO_2, [21] however, it is partly incorrect in the region of interest. [22] Since glasses can be quenched from the Li_2O-GeO_2 melt, it was decided to synthesize and examine both glassy and crystalline samples.

Several glasses near the $Li_2Ge_4O_9$ composition have been prepared: $Li_2Ge_4O_9$, $NaLiGe_4O_9$, $Li_{1.7}Ge_{3.7}Nb_{0.3}O_9$, $Li_{1.7}Ge_{3.7}Ta_{0.3}O_9$, $Li_{1.7}Ge_{3.7}Sb_{0.3}O_9$ and $Li_{1.7}Ge_{3.7}V_{0.3}O_9$. To synthesize these glasses, the appropriate amounts of GeO_2 and Li_2CO_3 (or Na_2CO_3) were intimately mixed and heated in air at 900°C in a platinum crucible. The resulting powder was then mixed with appropriate amounts of the other oxides (Nb_2O_5, Ta_2O_5, Sb_2O_5 and V_2O_5).

The powders were loaded into platinum capsules and sealed. The sample capsules were heated at 1200°C for 1/2 hour and then quenched by quickly immersing them into cold water. The quench rate must be quite rapid or partial crystallization occurs. If larger mixtures of powder are heated in a platinum crucible, a clear glass cannot be quenched from 1200°C due to partial crystallization on cooling. In such cases clear glasses could be recovered only as a skin near the platinum wall. The glasses were homogeneous, clear, and colorless, except for the V^{5+}-substituted glass which was amber-colored. The glasses were checked microscopically for homogeneity by observing the refractive index.

Initially some problems were encountered in the attempted synthesis of crystalline $Li_2Ge_4O_9$ and substituted variants. When the starting materials were heated at various temperatures below 1200°C, the resulting $Li_2Ge_4O_9$ phase was impure and x-ray analysis indicated the presence of significant amounts of Li_2GeO_3, $Li_2Ge_7O_{15}$ and GeO_2. Purer crystalline products could be obtained by heating the glasses, described above, in sealed platinum tubes, at 650° to 700°C for several days. The crystalline products thus obtained gave the expected x-ray pattern for stoichiometric $Li_2Ge_4O_9$ free from impurity peaks. For compositions $Li_{1.7}Ge_{3.7}Ta_{0.3}O_9$ and $Li_{1.7}Ge_{3.7}Nb_{0.3}O_9$ impurities of the $Li_2Ge_7O_{15}$ phase (5% to 15%) were detected.

For the composition $NaLiGe_4O_9$ a pure crystalline material could be prepared by either of two methods:

(a) Heating $NaLiGe_4O_9$ glass at 700°C for several days. This results in a very finely crystallized sample.

(b) Heating the appropriate amounts of Na_2CO_3 and GeO_2 slowly in a platinum crucible to 1200°C, and then withdrawing the crucible and letting it cool in air. This gives a coarsely crystallized material.

3. Evaluation

The compositions $Li_2Ge_4O_9$ and $NaLiGe_4O_9$ were prepared as glasses and screened by NMR for cation mobility at room temperature. The glasses were then devitrified and NMR screening repeated on the crystalline phases. The NMR results are summarized in Table VII.

There is strong motional narrowing of the lithium resonance in the glass form of $Li_2Ge_4O_9$. The peak width at room temperature (Fig. 18) is only 1.4 gauss and it narrows further to 0.4 gauss at 153°C. The lithium spectrum in the crystallized compound is nearly the same at room temperature (Fig. 19), but at 115°C the spectrum is resolved into two peaks: one with width 1.5 gauss, the second 0.35 gauss. This agrees with the prediction made on the basis of structural considerations that lithium atoms might occupy two different crystallographic sites. The latter motionally narrowed peak is probably due to lithium ions with large Li-O distances which have replaced the sodium in the 6-fold sites occupied by Na in $NaLiGe_4O_9$.

TABLE VII

NMR Spectra of ^7Li in $Li_2Ge_4O_9$ Compounds

Material	Phase	Temp (°C)	Line Width (Gauss)
$Li_2Ge_4O_9$	Glass	-100	1.9
		22	1.4
		120	0.8
		163	0.4
$Li_2Ge_4O_9$	Polycrystal	22	1.5
		115	0.35 and 1.5
$NaLiGe_4O_9$	Glass	-34	1.6
		22	1.6
		95	1.6
	Polycrystal	22	1.3
		115	1.3

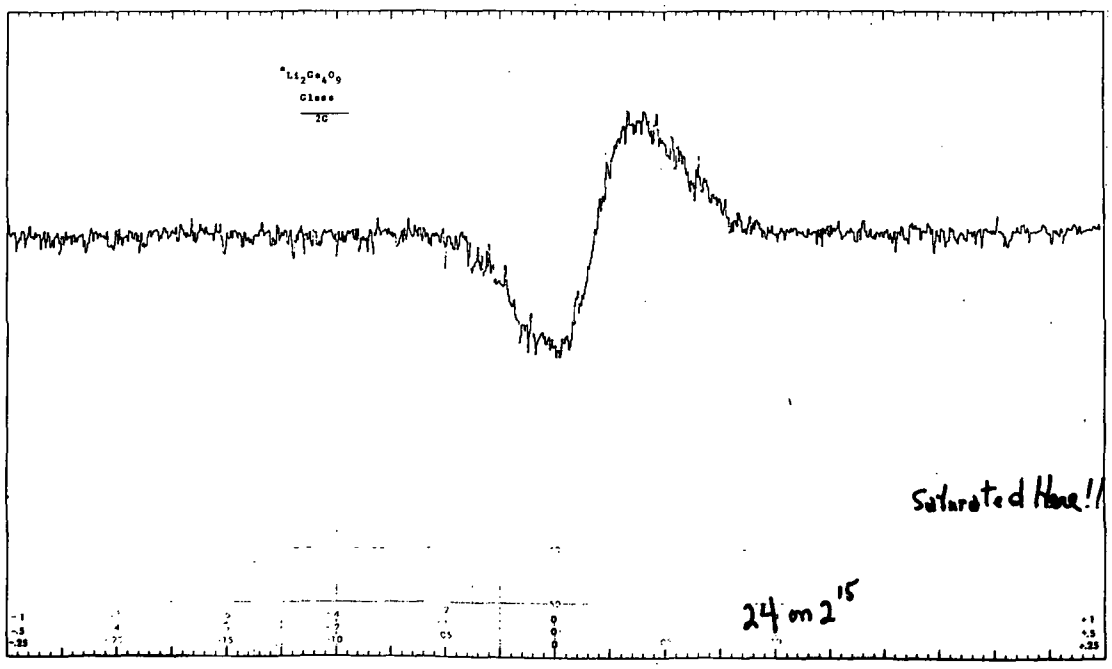

Fig. 18 NMR spectrum of ^7Li in glass with composition $Li_2Ge_4O_9$ at room temperature. The peak width is 1.4 gauss.

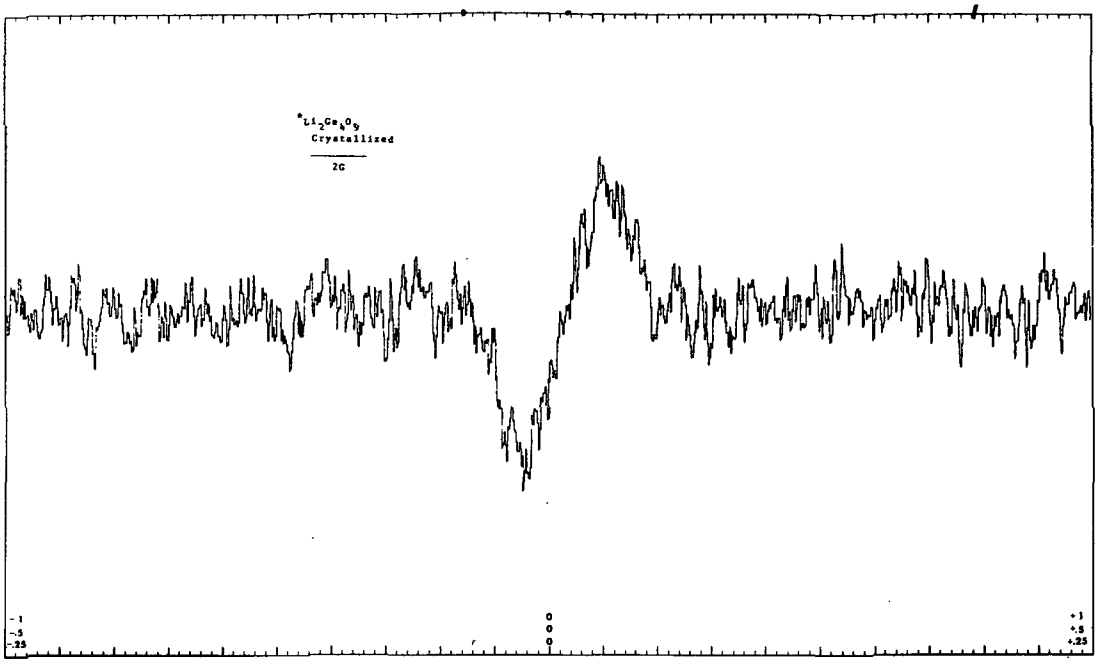

Fig. 19 NMR spectrum of ^{7}Li in crystalline $Li_2Ge_4O_9$ at room temperature. The peak width is 1.5 gauss.

Motional narrowing of the lithium NMR spectrum was not observed either in the glass or in the crystalline phases of $NaLiGe_4O_9$ (Figs. 20 and 21). This is consistent with the structural interpretation suggested to explain the $Li_2Ge_4O_9$ spectra because sodium ions are significantly larger than lithium ions. The sodium spectrum could not be detected despite prolonged signal averaging (25 hours). This indicates the spectrum is broadened by the crystalline fields, and the sodium ions are relatively immobile.

The pulse shape in one specimen of $Li_2Ge_4O_9$ glass was successfully observed in a microcell. Attempts to measure the other compositions failed because the materials cracked and developed leaks when they were helium tested. The glass was 0.24 mm thick with an effective cross section of 2.5 × 3.5 mm. The cell response indicated the conductivity is small, in agreement with dielectric loss measurements made at NASA-Lewis Research Center. No resonance peaks were observed and the room-temperature AC conductivity was 4×10^{-10} at 10^3 Hz and 2×10^{-7} ohm^{-1} cm^{-1} at 10^6 Hz.

H. $Li_2Ge_7O_{15}$-Type Compounds

1. Structure and Transport Model

The structure of $Li_2Ge_7O_{15}$[23] is related to the $NaLiGe_4O_9$ type discussed above. In $Li_2Ge_7O_{15}$, GeO_4 tetrahedra are linked together at the corners to form corrugated layers which are connected by GeO_6 octahedra to form a

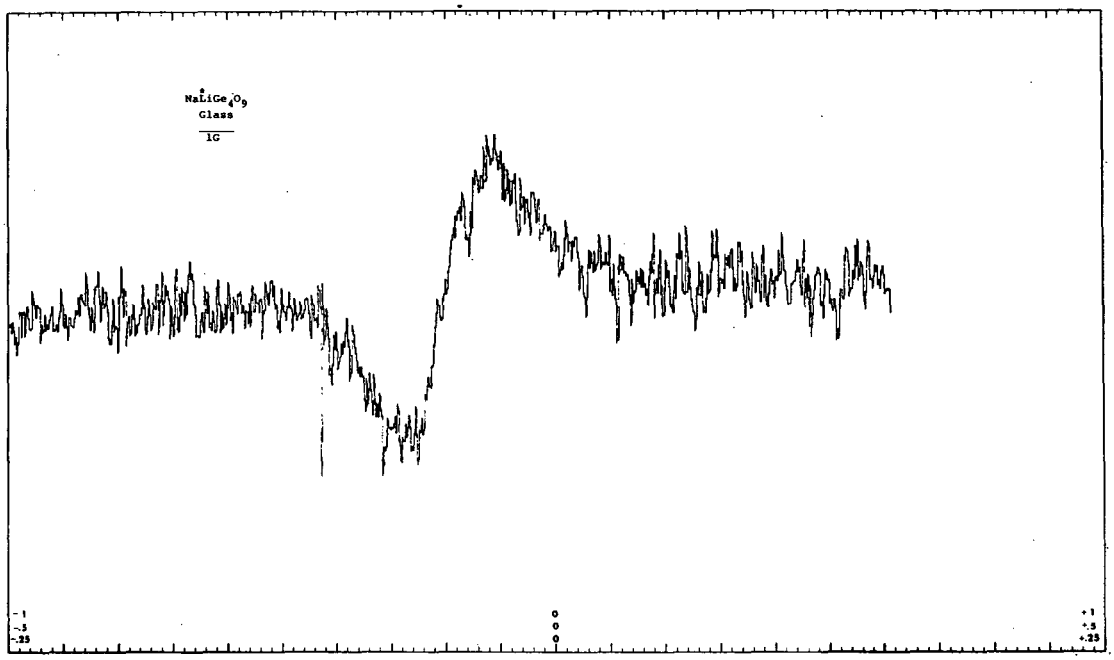

Fig. 20 NMR spectrum of ^{7}Li in glass with composition $NaLiGe_4O_9$ at room temperature. The peak width is 1.6 gauss.

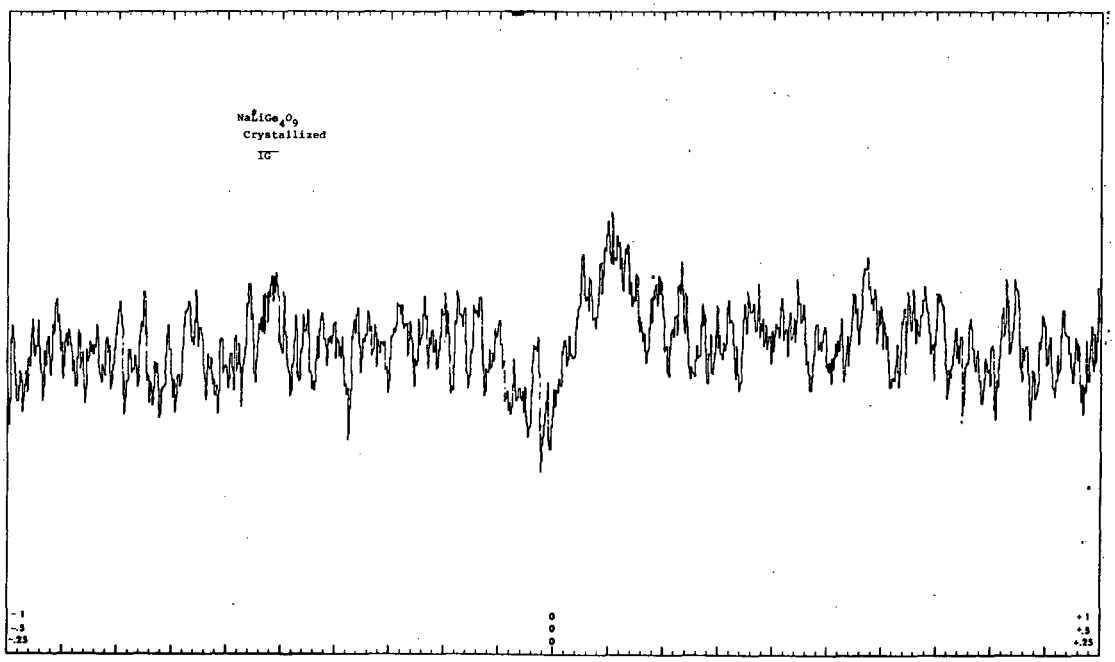

Fig. 21 NMR spectrum of ^{7}Li in crystalline $NaLiGe_4O_9$ at room temperature. The peak width is 1.3 gauss.

loose three-dimensional framework. This can be seen from Fig. 22. Within this framework there are interwoven channels which can accommodate Li^{1+} ions.[23] The two Li^{1+} sites both have 6-coordinated Li^{1+} ions with Li-O distances varying from 1.933Å to 2.367Å. The structure is so loose that it might accommodate larger ions (such as Na^{1+}) in interstitial sites. One such 6-coordinated interstitial site has an average X-O distance of 2.563Å.[23]

Three-dimensional motion of alkali ions is conceivable both for stoichiometric $Li_2Ge_7O_{15}$ and nonstoichiometric variants (described below), since there are interstitial sites and wide enough tunnels in this loose framework structure.

The low density and "looseness" of the $Li_2Ge_7O_{15}$ structure is apparent from the large molecular volume (298.8Å^3) when compared to the molecular volume of 218.2Å^3 derived from the component oxides Li_2O and tetragonal GeO_2.

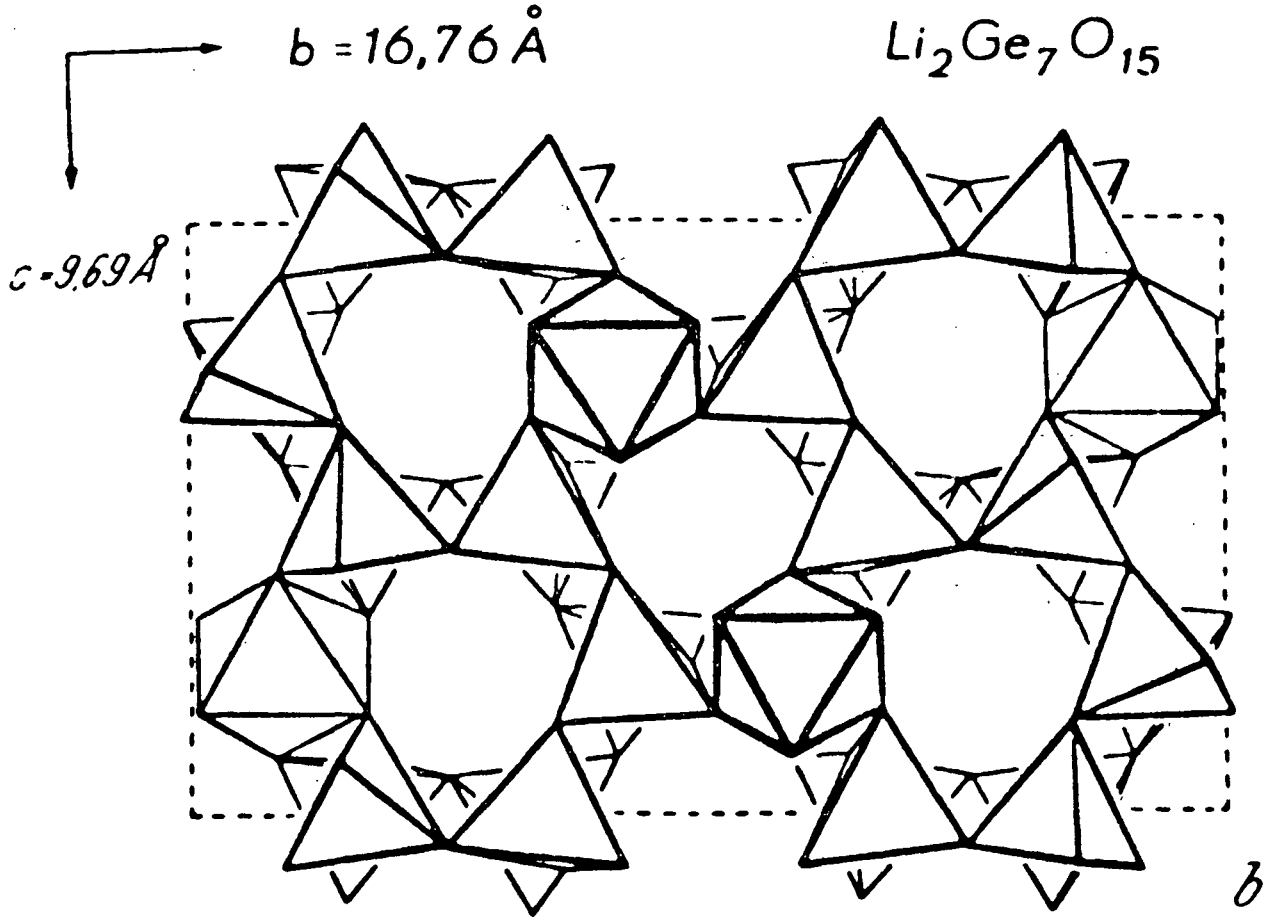

Fig. 22 The structure of $Li_2Ge_7O_{15}$ projected on the (100) plane.

Nonstoichiometric $Li_2Ge_7O_{15}$ type phases can be envisioned by substituting pentavalent ions for Ge^{4+} and creating vacancies in the Li^{1+} sites, e.g., $Li_{2-x}Ge_{7-x}Nb_xO_{15}$. Alternately one could try to force additional alkali ions (like Na^{1+}) into the large interstitial holes by making solid solutions of the type $Li_2Na_xGe_{7-x}Al_xO_{15}$.

2. Synthesis

Both glassy and crystalline phases have been prepared for $Li_2Ge_7O_{15}$ and substituted derivatives.

(a) $Li_2Ge_7O_{15}$

Larger amounts of $Li_2Ge_7O_{15}$ (20 to 50 grams) have been prepared by slowly heating an intimate mixture of the appropriate amounts of Li_2CO_3 and GeO_2 from 450° to 1000°C in a platinum crucible, holding the temperature at 1000°C for one hour, and then withdrawing the crucible from the furnace. The $Li_2Ge_7O_{15}$ product so obtained is a very fine crystalline powder of high purity. X-ray patterns show either no detectable impurity peaks or only traces of GeO_2.

When the above-described synthesis is carried out at significantly higher or lower final heating temperatures, pure $Li_2Ge_7O_{15}$ is not obtained. A synthesis at 1120°C resulted in large amounts of excess GeO_2. A low-temperature preparation (850°C) contained in addition to $Li_2Ge_7O_{15}$ significant amounts of four other phases: GeO_2 (quartz structure), GeO_2 (rutile structure), $Li_2Ge_4O_9$, and Li_2GeO_3.

Glassy $Li_2Ge_7O_{15}$ can be made by heating the appropriate Li_2CO_3-GeO_2 mixture (or crystalline $Li_2Ge_7O_{15}$) slowly up to 1200°C in a platinum tube or crucible. The platinum containers are then quickly withdrawn from the furnace and immersed in cold water. If a slower cooling rate is used, partial crystallization takes place. The $Li_2Ge_7O_{15}$ glass has a refractive index of 1.690.

(b) Substituted glasses near the $Li_2Ge_7O_{15}$ stoichiometry

Homogeneous glasses of the following compositions were made and are listed below with their refractive indices:

Composition of Glass	Refractive Index
$Li_{1.7}Ge_{6.7}Sb_{0.3}O_{15}$	1.692
$Li_{1.7}Ge_{6.7}Ta_{0.3}O_{15}$	1.698
$Li_{1.7}Ge_{6.7}Nb_{0.3}O_{15}$	1.698
$Li_{1.7}Ge_{6.7}V_{0.3}O_{15}$	1.688
$Li_2Na_{0.3}Ge_{6.7}Al_{0.3}O_{15}$	1.676

The glasses can be made by heating the appropriate mixtures of crystalline $Li_2Ge_7O_{15}$, GeO_2, Sb_2O_5, Ta_2O_5, Nb_2O_5, and V_2O_5 in sealed platinum tubes for 1/2 hour at 1200°C, and then rapidly quenching the tubes in cold water.

The $Li_{1.7}Ge_{6.7}Ta_{0.3}O_{15}$ glass has the lowest tendency to crystallize, and this composition can therefore be prepared in larger batches by slowly heating the appropriate mixture of oxides in an open platinum crucible to 1200°C, and then removing the crucible from the furnace.

The $Li_2Na_{0.3}Ge_{6.7}Al_{0.3}O_{15}$ glass can be made by heating the appropriate mixture of Li_2CO_3, Na_2CO_3, GeO_2, and Al_2O_3 at 850°C for two hours. The resulting mixture was then sealed into platinum tubes and heated for 1/2 hour at 1200°C. The tubes were then quenched in cold water.

(c) Crystalline, Nonstoichiometric $Li_2Ge_7O_{15}$-Type Phases

Efforts were made to prepare nonstoichiometric $Li_2Ge_7O_{15}$-type phases by heating the appropriate mixtures of oxides and Li_2CO_3 from 450° to 1000°C. This method, however, yielded pure samples only for stoichiometric $Li_2Ge_7O_{15}$. Even when the heat treatment was modified, nonstoichiometric $Li_2Ge_7O_{15}$ type phases could not be prepared in the pure state.

A successful synthesis of pure crystalline $Li_{1.7}Ge_{6.7}Ta_{0.3}O_{15}$ and $Li_{1.7}Ge_{6.7}Sb_{0.3}O_{15}$ was finally achieved when glasses of the same compositions were used as starting materials. The glasses were annealed at 600°C for about three days. The x-ray patterns of the products showed only peaks belonging to the $Li_2Ge_7O_{15}$ structure, indicating a high phase purity.

Attempts to anneal the $Li_2Na_{0.3}Ge_{6.7}Al_{0.3}O_{15}$ glass at 600°C did not result in a pure crystalline phase. While the major phase was of the $Li_2Ge_7O_{15}$ type, smaller (but significant) amounts of $NaLiGe_4O_9$ and a quartz type phase were also present.

3. Evaluation

Strong motional narrowing of the ^7Li NMR spectrum is seen in both $Li_2Ge_7O_{15}$ and $Li_{1.7}Ge_{6.7}Ta_{0.3}O_{15}$ glasses (Figs. 23, 24, and Table VIII). Devitrifying the glasses resulted in slight line broadening indicating that crystallization tends to immobilize the lithium atoms. The lithium spectrum in the crystalline compounds is still narrow (1.0 gauss) and the critical temperature for motional narrowing may have been displaced to a higher value.

The conductivity in $Li_2Ge_7O_{15}$ glass and in the tantalum doped glass was measured in a microcell. The response is nearly capacitive (Fig. 25), but there was a slight current flow indicating small conductivity.

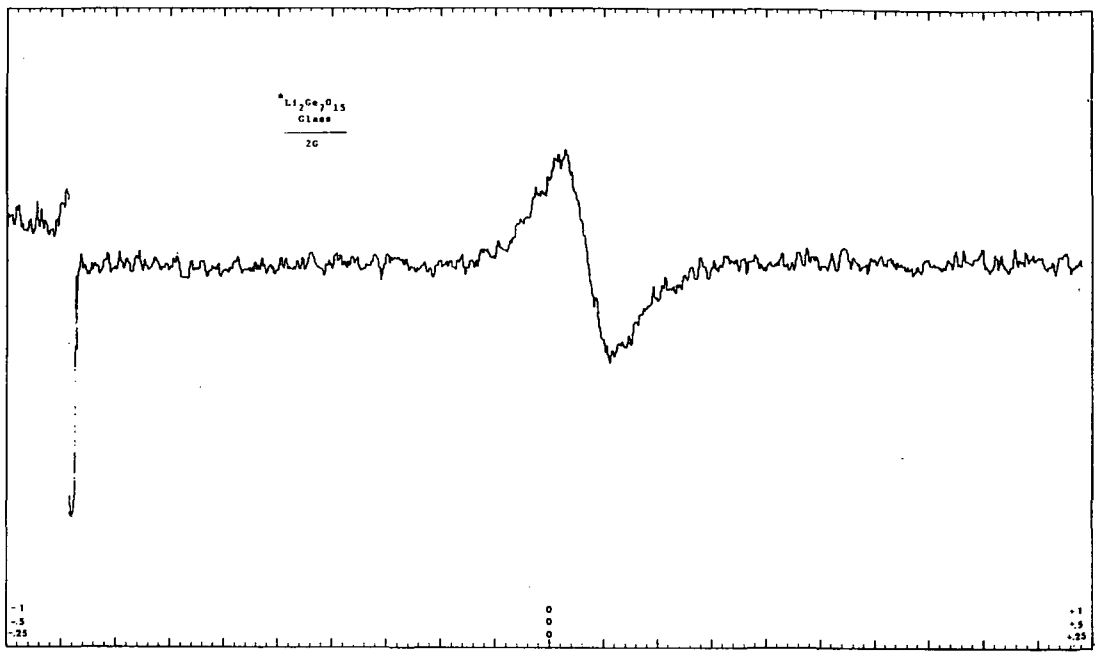

Fig. 23 NMR spectrum of ^{7}Li in glass with composition $Li_2Ge_7O_{15}$ at room temperature. The peak width is 0.9 gauss.

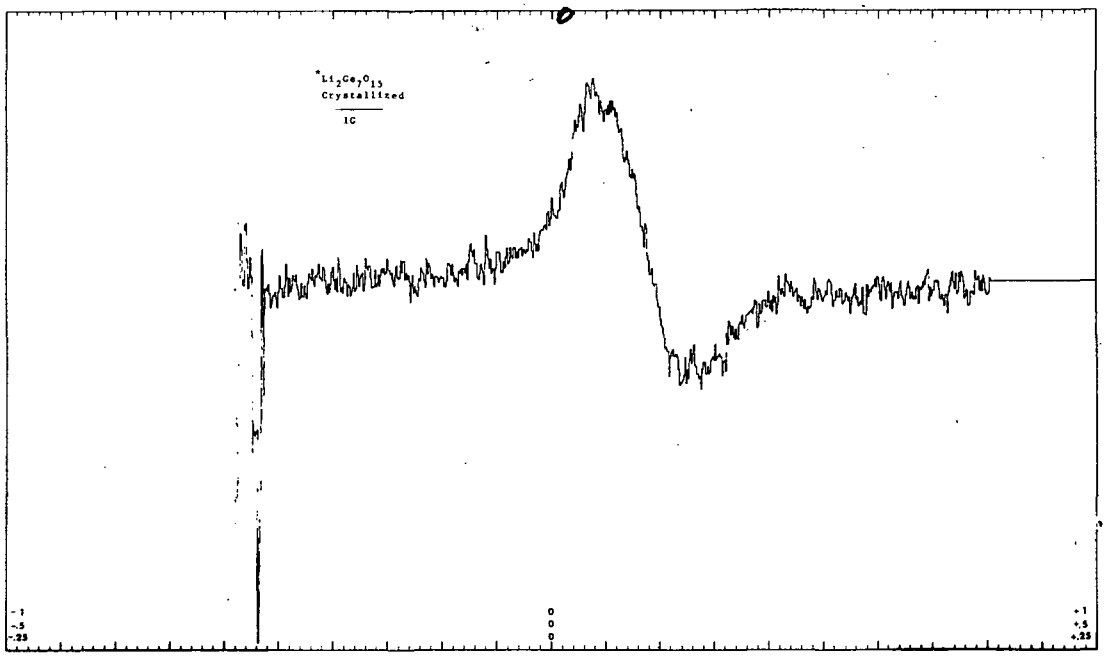

Fig. 24 NMR spectrum of ^{7}Li in crystalline $Li_2Ge_7O_{15}$. The peak width is 1.0 gauss.

TABLE VIII

NMR Spectra of ^{7}Li in $Li_2Ge_7O_{15}$-Type Compounds

Material	Phase	Temp (°C)	Line Width (Gauss)
$Li_2Ge_7O_{15}$	Glass	22	0.9
		165	0.45
	Crystal	22	1.0
		170	1.0
$Li_{1.7}Ge_{6.7}Ta_{0.3}O_{15}$	Glass	-34	1.2
		22	1.0
		96	0.65
	Crystal	22	1.0
		95	1.0

The dielectric loss and room temperature AC conductivity measurements on glassy and crystalline $Li_2Ge_7O_{15}$ compositions are summarized in Table IX.

TABLE IX

Sample	Phase	AC Conductivity at Room Temp (ohm^{-1} cm^{-1})	
$Li_2Ge_7O_{15}$	Glass	10^3 Hz	$\sim 10^{-6}$
		10^5	$\sim 10^{-6}$
	Polycrystal	10^3	$< 5 \times 10^{-12}$
		10^5	$\sim 1.5 \times 10^{-9}$
$Li_{1.7}Ge_{6.7}Ta_{0.3}O_{15}$	Glass	10^3	$\sim 5 \times 10^{-10}$
		10^5	3×10^{-8}
	Polycrystal	10^3	1.5×10^{-10}
		10^4	1.4×10^{-9}
		10^5	1.2×10^{-8}
		10^6	$< 5 \times 10^{-8}$

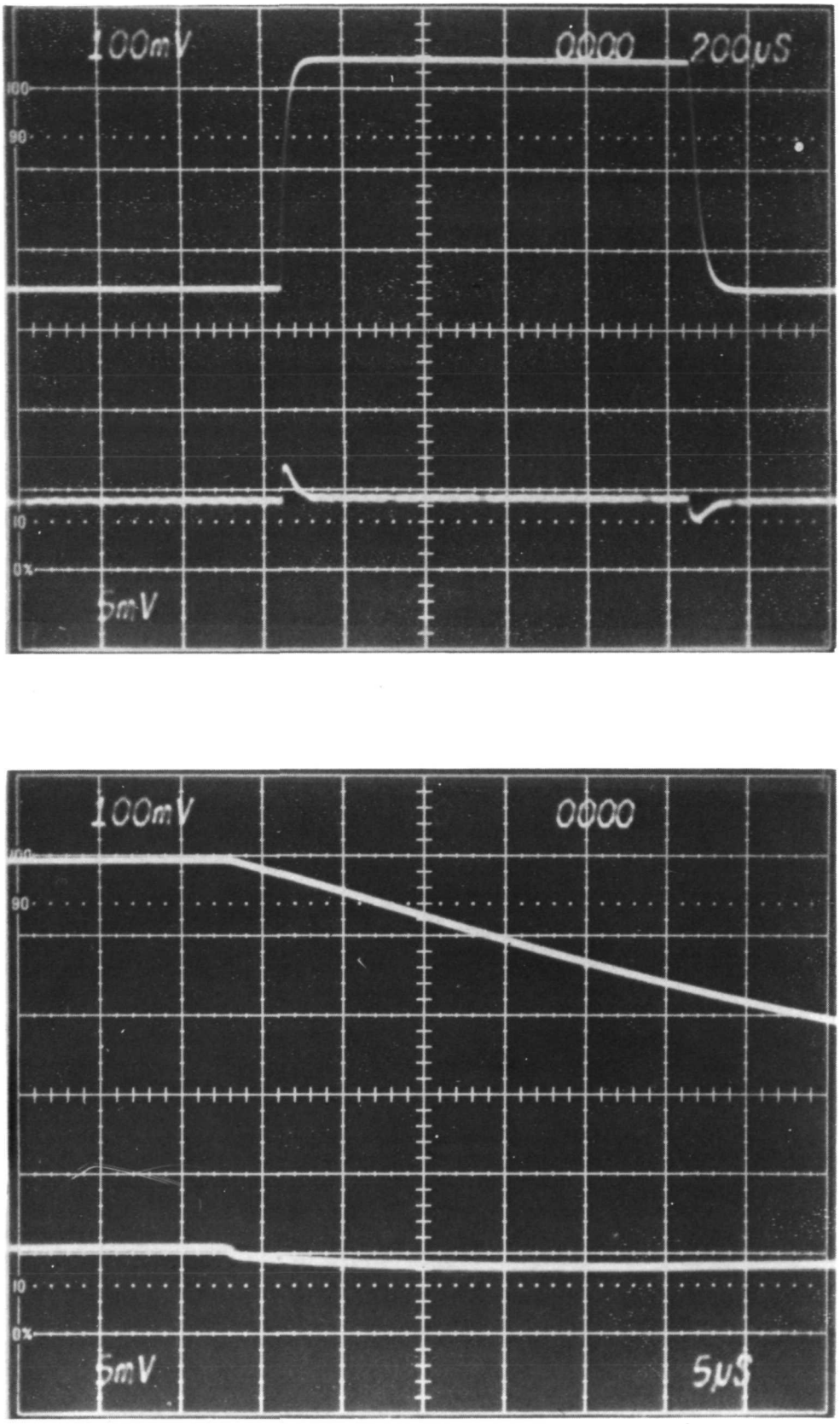

Fig. 25 Voltage response of $Li_2Ge_7O_{15}$ glass to constant current pulse in microcell. A small current flow can be seen in the expanded region of the trailing edge of the pulse.

The dielectric loss showed no peaks, but a small AC conductivity was measured at room temperature in lithium germanate glass. The reason for the smaller AC conductivity in the doped glass is not understood.

In summary, there is strong short-range motion of lithium atoms in pure and doped $Li_2Ge_7O_{15}$ glass, and this motion is decreased when the phase is crystallized. The ionic conductivity due to long-range movement of lithium ions is small but possibly was detected in $Li_2Ge_7O_{15}$ glass.

I. Hexagonal $NaLnF_4$-Type Compounds

1. Structure and Transport Model

The hexagonal $NaNdF_4$ structure is the stable low-temperature form for all $NaLnF_4$ phases (Ln = lanthanon or yttrium). For many $NaLnF_4$ compounds a phase transition takes place at higher temperatures to the well-known cubic fluorite structure.[24-26]

The structure of the hexagonal $NaNdF_4$[24] is shown in Fig. 26. There are three crystallographically independent sites for the cations. One is a 9-coordinated site and occupied only by Nd^{3+} ions. Another 9-coordinated

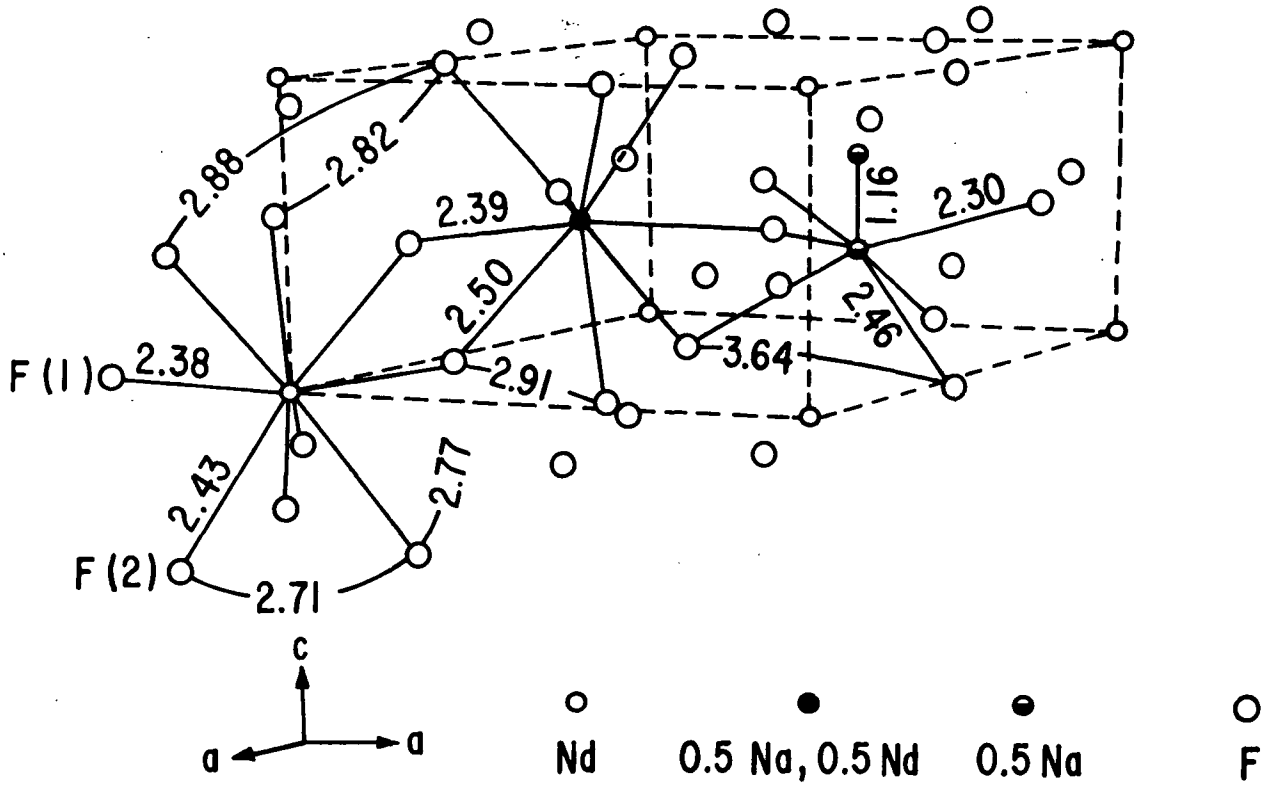

Fig. 26 The structure of hexagonal $NaNdF_4$.

site has 50% Nd^{3+} and 50% Na^{1+} ions distributed at random. A third octahedral site is half empty and half occupied by Na^{1+} ions. The structure study[24] shows that the Na^{1+} ions in these half-empty Na^{1+}-sites have strong anisotropic thermal motion, as do some of the fluoride ions. The thermal parameters of the Na^{1+} ion may reflect the uncertainty of site occupancy rather than true thermal motion.

Our interest in the $NaNdF_4$-compounds was primarily in the high-temperature cubic fluorite type solid solution phases[25, 26] rather than in the low-temperature hexagonal structure.[24] It was recognized, however, that the high-temperature fluorite form was more likely to be a F^- ion conductor than a Na^{1+} ion conductor. Since there was no interest in potential F^- ion conductors (for practical reasons) the earlier preliminary studies on the cubic $NaLnF_4$ phases[2] were dropped. The studies on the hexagonal phases were continued since high ion mobility had been established in the cubic form, and it was possible the Na^{1+} ion in the half-empty site might be mobile.

2. Synthesis of $NaNdF_4$-Type Phases

Hexagonal $NaPrF_4$, $NaNdF_4$, and $NaYF_4$ were prepared as follows: commercially obtained NaF, PrF_3, NdF_3, and YF_3 were dried at 220°C under vacuum for about a day. The starting materials were then mixed in a 1:1 molar ratio and compressed into pellets. The pellets were placed in a platinum crucible and heated at 400°C under high vacuum to eliminate any traces of moisture. The crucible was then sealed and heated at 750°C for 7 hours and subsequently at 600°C for 12 hours. The pellets were analyzed by x-ray diffraction, which showed that the hexagonal $NaYF_4$ and $NaNdF_4$ phases were free from detectable impurities. In the $NaPrF_4$ sample small amounts (~5%) of NaF were detectable.

No attempt was made to prepare nonstoichiometric phases of the hexagonal $NaNdF_4$ type. It is well known from a study of the phase equilibria of the NaF-LnF_3 systems[25, 26] that these hexagonal phases do not form extensive solid solutions, unlike the high-temperature cubic forms.

A sample of $NaYF_4$ was hot pressed for 20 minutes at 7700 psi and 620° to 630°C. The specimen was contained in a graphite die and shown by x-ray diffraction to still be of the hexagonal modification, with no impurity peaks detectable.

3. Evaluation

Three samples of hexagonal $NaLnF_4$ compounds were examined for evidence of motional narrowing using wide-line NMR (Table X). Both the ^{23}Na and ^{19}F spectra were run at different temperatures. The room-temperature spectra of $NaYF_4$, $NaPrF_4$, and $NaNdF_4$ are shown in Figs. 27 through 32. The peak-to-peak line widths measured at various temperatures

TABLE X

NMR Spectra in Hexagonal $NaLnF_4$ Compounds

Material	Nucleus	Temp (°C)	Width (Gauss)
$NaYF_4$	Na	22	6.0
		90	6.0
		186	6.0
	F	22	9.0
		186	10.0
$NaPrF_4$	Na	22	8.0
		90	8.0
		186	8.0
	F	22	7, 30
		186	5, 19
$NaNdF_4$	Na	22	8.0
		90	8.0
		186	8.0
	F	22	7, 34
		186	5, 20

are given in Table X. There is no evidence for motional narrowing of the sodium nuclei in any of the samples. On the other hand, some of the fluorine spectra did show some decline in line width with increasing temperature. The fluorine spectra are complex, apparently having a narrow line superposed on a broad line. The mechanism of the broadening is not understood. ^{19}F has no quadrupole moment and any broadening effects would arise from its dipole moment. The line width of the broad lines is believed too great to be accounted for on the basis of coupling between fluorine neighbors and may arise from coupling between the fluorine and the rare earth ions. This is consistent with the less broad line observed for the yttrium compound.

The absence of motional narrowing of the sodium nuclei is in contrast to what was observed in the cubic $NaLnF_4$ compounds last year. Motional narrowing of both the sodium and fluorine spectra was observed and the results could be interpreted by motion of either or both kinds of nuclei.

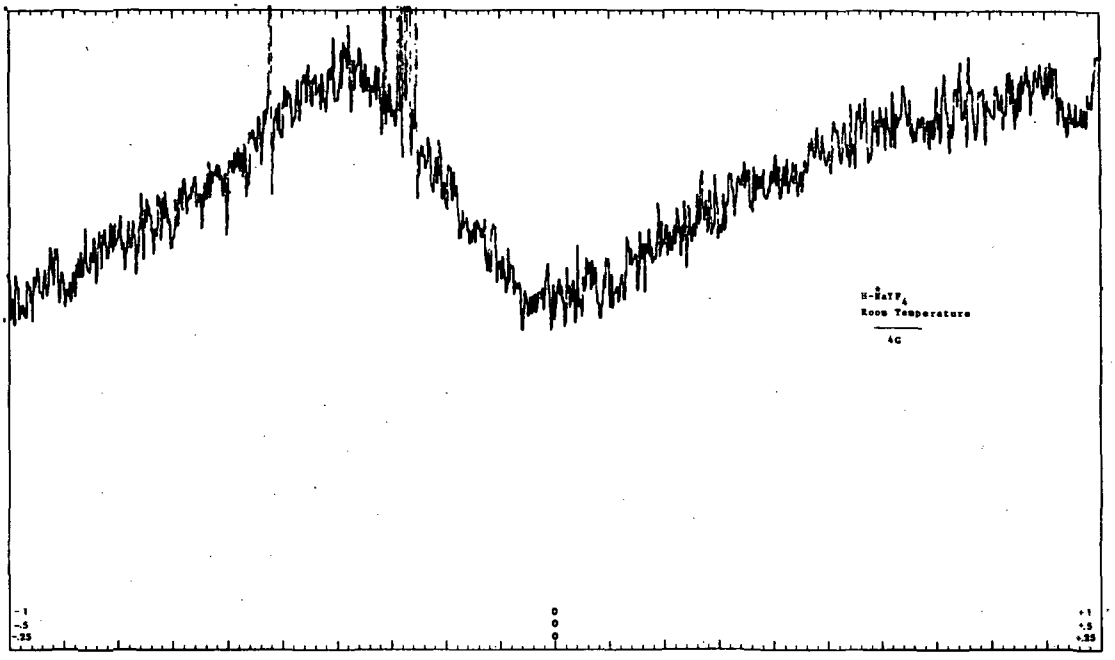

Fig. 27 NMR spectrum of ^{23}Na in hexagonal $NaYF_4$ at room temperature. The peak-to-peak width is 6.0 gauss.

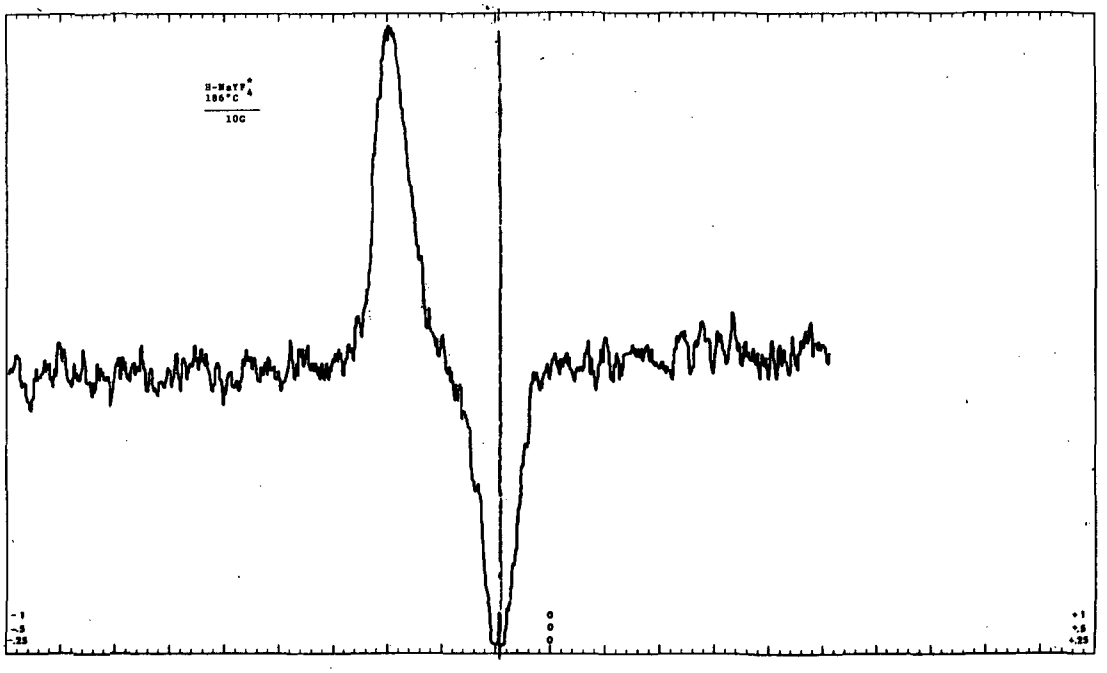

Fig. 28 NMR spectrum of ^{19}F in hexagonal $NaYF_4$ at 186°C. The peak width is 10 gauss, approximately the same as room temperature.

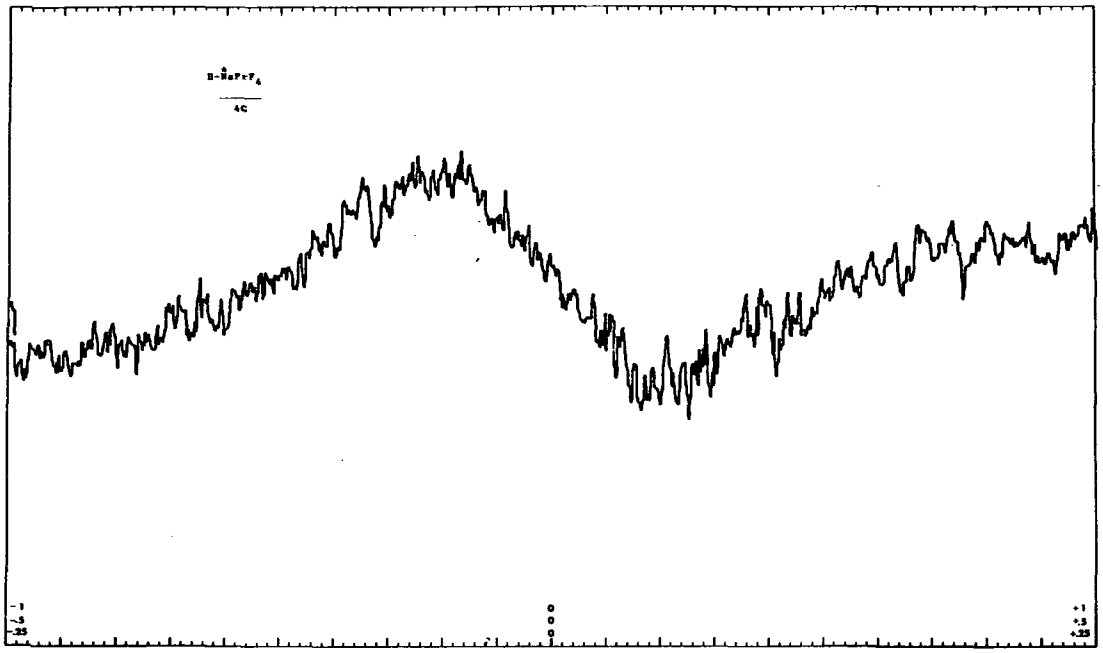

Fig. 29 NMR spectrum of ^{23}Na in hexagonal $NaPrF_4$ at room temperature. The peak width is 8.0 gauss.

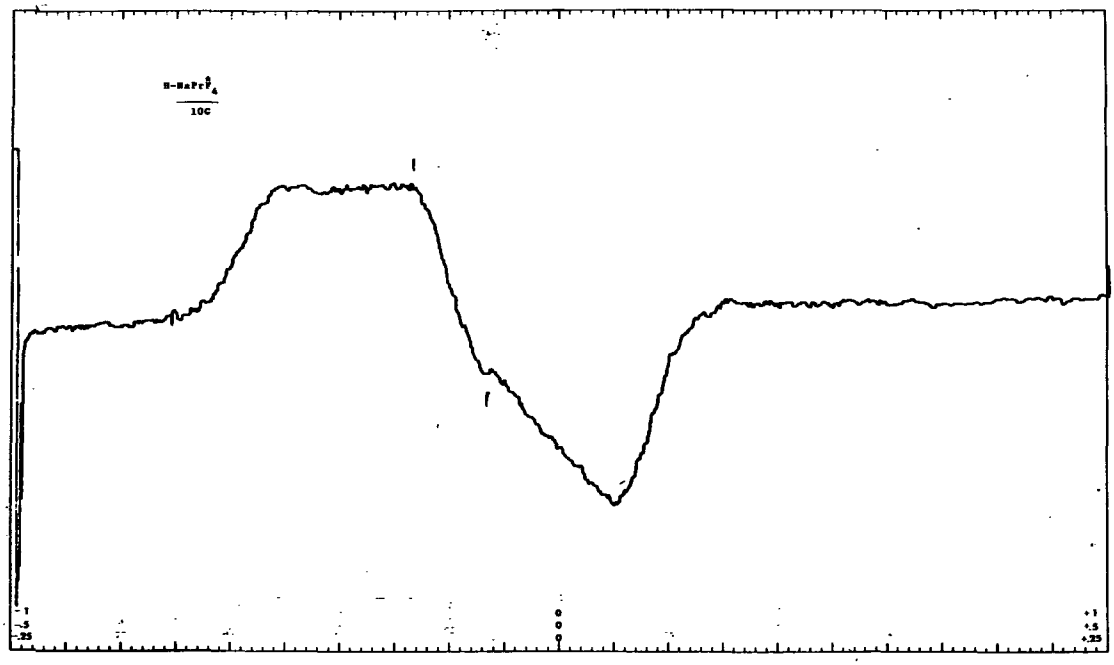

Fig. 30 NMR spectrum of ^{19}F in hexagonal $NaPrF_4$ at room temperature. The spectrum is complex and apparently consists of a narrow peak superposed on a broad peak.

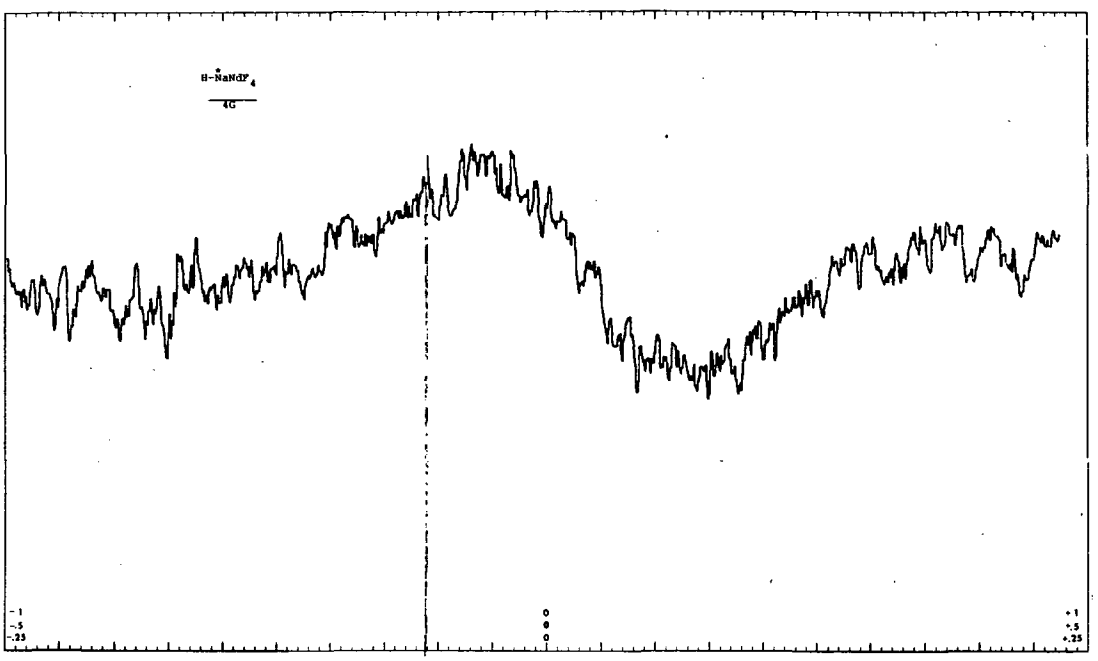

Fig. 31 NMR spectrum of ^{23}Na in hexagonal $NaNdF_4$ at room temperature. The peak width is 8.0 gauss.

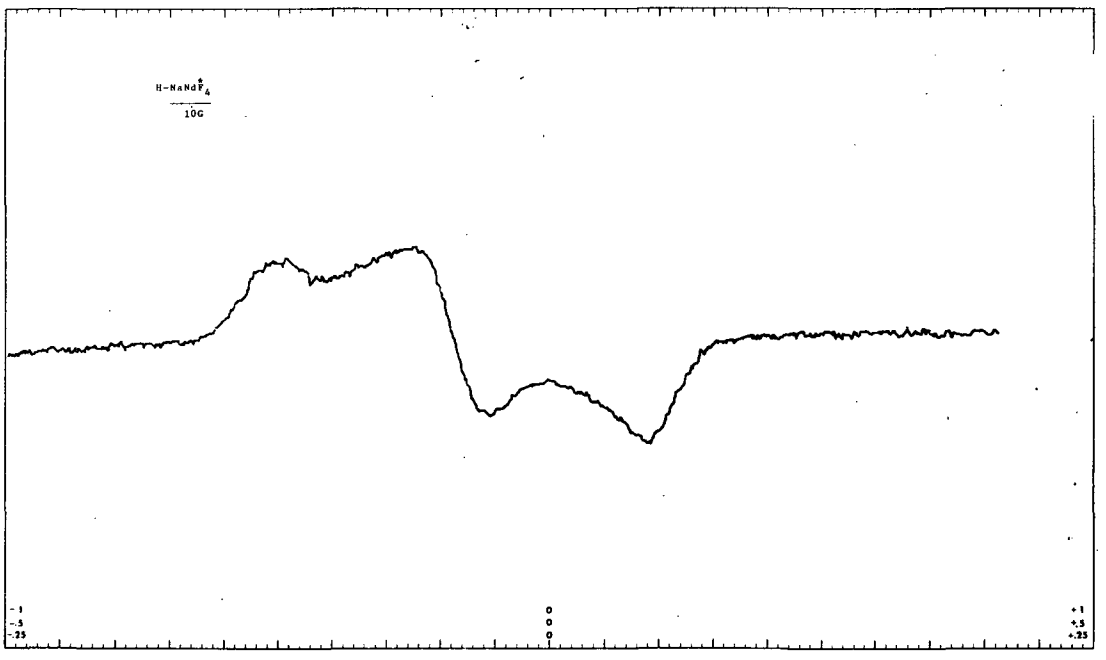

Fig. 32 NMR spectrum of ^{19}F in hexagonal $NaNdF_4$ at room temperature. The two fluorine peaks are resolved.

Since narrowing of the fluorine spectrum alone is seen in the hexagonal compounds, the sharpening of the sodium spectrum in the cubic compounds was probably caused by sodium motion and was not due to motion of the neighboring fluorine nuclei.

Dielectric loss and room temperature AC conductivity measurements made at NASA-Lewis Research Center indicated possible ionic conductivity in hexagonal $NaNdF_4$ and $NaYF_4$. Their results are given in Table XI.

TABLE XI

Sample	Resonance Peak	AC Conductivity at Room Temp (ohm^{-1} cm^{-1})	
C-15a $NaPrF_4$	Yes (two peaks observed: ΔE = 5.4-6.9 kcal from low-temp peak may be Na motion; ρ 25°C ~1 ohm-cm ΔE = 15.9 kcal from high-temp peak may be F motion); ρ 25°C = 5×10^5	10^3 Hz	5×10^{-9}
		10^4	6×10^{-8}
		10^5	5×10^{-7}
		10^6	2×10^{-6}
C-16 $NaNdF_4$	Yes (10^6 Hz, 125°C, Cole-Cole conductivity ~2×10^{-6} ohm^{-1} cm^{-1} at 125°K)	10^3	1.6×10^{-8}
		10^4	$4. \times 10^{-8}$
		10^5	1.6×10^{-7}
		10^6	6.4×10^{-7}
C-17 $NaYF_4$	Yes (10^6 Hz, 125°K, Cole-Cole conductivity ~5×10^{-6} ohm^{-1} cm^{-1} at 125°K)	10^3	2.6×10^{-8}
		10^4	6.9×10^{-8}
		10^5	2.4×10^{-7}
		10^6	1.1×10^{-6}
C-17as $NaYF_4$ hot-pressed	Yes ΔE = 4.3 kcal ρ 25°C ~ 10 ohm-cm	10^3	4.8×10^{-9}
		10^4	2.6×10^{-8}
		10^5	1.4×10^{-7}
		10^6	1.9×10^{-6}

We conclude from the dielectric loss and AC conductivity measurements that the hexagonal $NaLnF_4$ compounds are moderate conductors at low temperature. The conductivity probably could be increased by doping, but the NMR spectra show the phase is an anion conductor and consequently of little interest in the present context.

J. Dalyite-Type Compounds

1. Structure and Transport Model

The structure of the rare mineral dalyite (ideally $K_2ZrSi_6O_{15}$) has recently been determined by Fleet.[27] The structure is illustrated in Figs. 33 and 34, and can be considered as a layer structure of a new type. The layers are

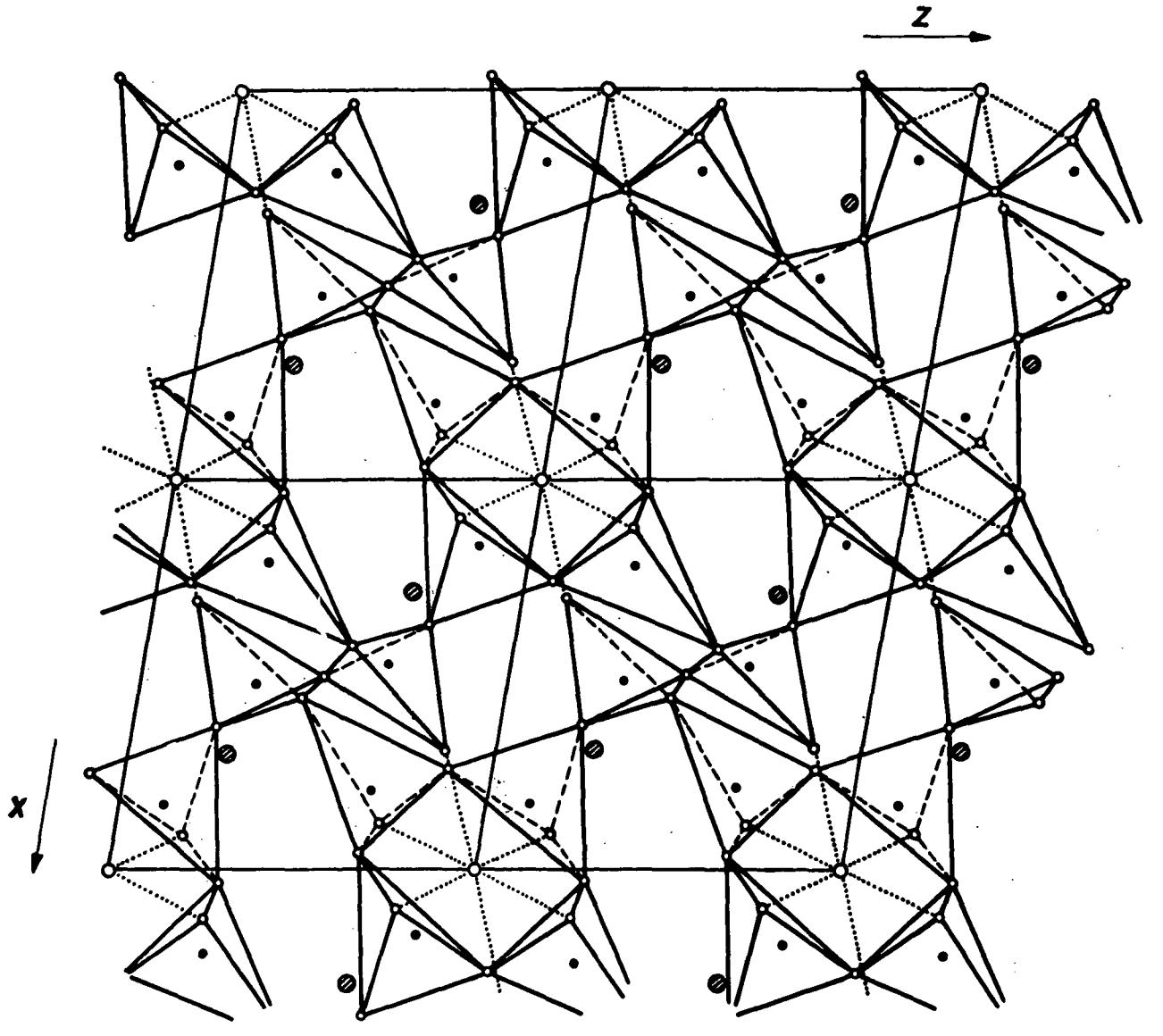

Fig. 33 The dalyite structure (ideally $K_2ZrSi_6O_{15}$): ● = Si; o = 0; ○ = Zr; ◍ = K. After Ref. 27.

made up of SiO_4 tetrahedra sharing corners to give four, six and 8-membered rings, as illustrated in Fig. 33. These silica sheets are held together in the third dimension by ZrO_6 octahedra, giving rise to a three-dimensional framework with interconnected channels, occupied by K^+ ions. Motion of the K^+ ions seems possible in this structure, particularly if we consider the large temperature factor for K^+ ($B = 3.8 Å^3$ in the a-direction). The K-O distances are also larger than average (2.83Å to 3.49Å) which may indicate a fairly loose K^+ ion.

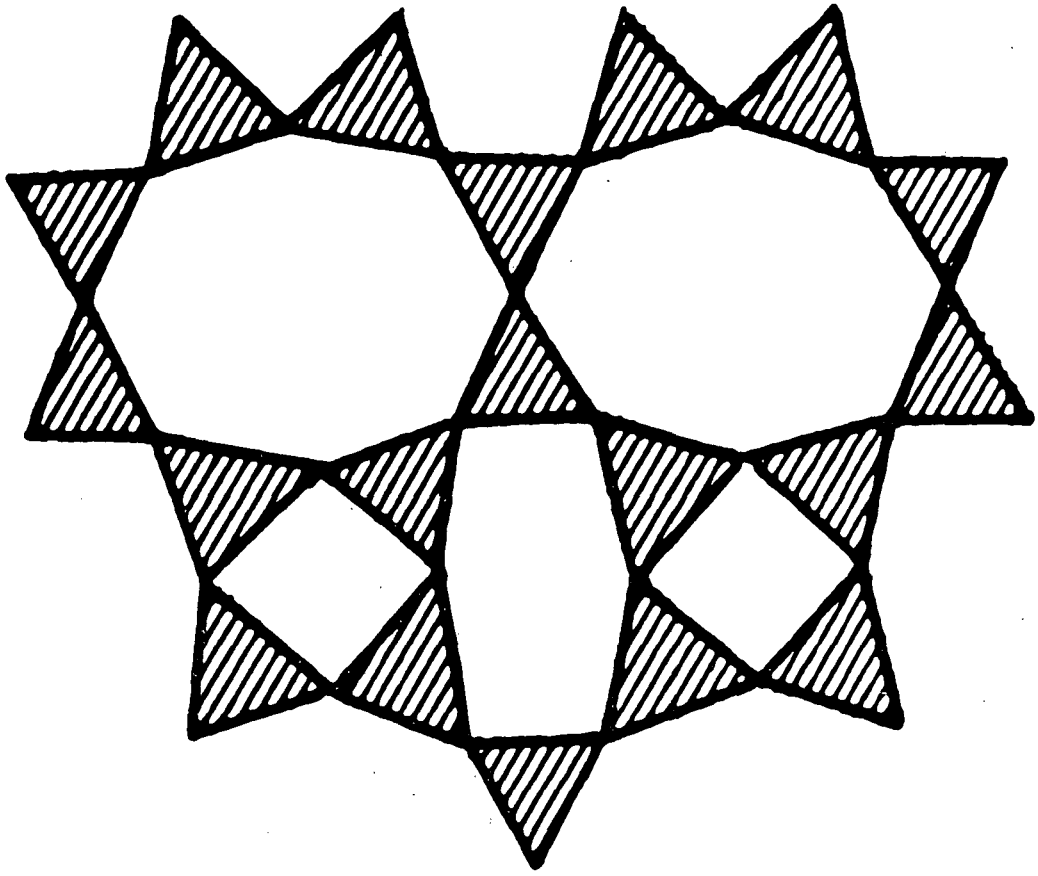

(III)

Fig. 34 Idealized dalyite sheets made up of SiO_4 tetrahedra sharing corners. After Ref. 27.

The structure would be even a more attractive candidate if nonstoichiometric variants could be made and if the K^+ ion could be exchanged with Na^+ or Ag^{1+}. To make the structure nonstoichiometric, one could substitute Zr^{4+} with Ta^{5+}, i.e., $K^+ + Zr^{4+} = \square + Ta^{5+}$. It might also be possible to exchange K^+ with Na^+ or Ag^{1+} in a nitrate melt. It is well known that, in the mineral dalyite, significant amounts of Na^+ (~15%) can replace the K^{1+} ions,[27, 28] and the smaller Na^+ or Ag^+ ions might be very loose and mobile in the structure.

2. Synthesis of Dalyite-Type Phases

So far, synthetic dalyite has been prepared only under hydrothermal conditions at low temperatures and efforts to make the phase by more conventional sintering techniques have been unsuccessful.[29, 30] It was felt that an effort should be made to synthesize $K_2ZrSi_6O_{15}$ by a more easily accessible method.

Reagent grade K_2CO_3, $ZrOSO_4 \cdot H_2SO_4 \cdot 3H_2O$, and silicic acid ($SiO_2 \cdot xH_2O$) were intimately mixed, pelletized, and heated gradually up to 1200°C in a platinum container. At this stage the resulting product did not contain any dalyite-like phase but was a mixture of at least four different products, as observed by optical and x-ray methods: a glassy phase, a cristobalite-like crystalline material, ZrO_2, and an unidentified crystalline product.

This mixture was now heated for 20 minutes at 1700°C in a platinum boat, and cooled in air. The resulting product was a homogeneous glass. (Attempts to prepare such glasses at lower temperatures were unsuccessful.) When this glass was heated for one day at 1200°C, the resulting product had completely crystallized. The x-ray pattern of this crystallized product is not identical to the published dalyite patterns,[28, 29] but it nevertheless bears a resemblance to these published patterns. It is possible to interpret these data as indicating the presence of a dalyite-related phase, not identical to the mineral dalyite, but similar to it.

Since the dalyite work was initiated two weeks before the termination of the contract, no further synthesis could be carried out.

3. Evaluation

The "dalyite" samples could not be synthesized in time for evaluation before the expiration of the contract.

V. CONCLUSIONS AND RECOMMENDATIONS

A large number of structure types and many compounds have now been evaluated as possible solid electrolytes for high-energy and power-density batteries to operate at ambient temperature. A compilation of the results obtained this year is given in Table XII. The crystal-chemical basis for predicting potential conductors has been validated in many cases. We have obtained evidence for ionic conductivity in one-dimensional and three-dimensional channel structures. No new solid electrolyte has yet been discovered with the requisite properties of high cation conductivity and chemical stability for application in a practical low-temperature battery, but we believe further work as outlined below is warranted and has a high probability for success. We have obtained new information which allows us to make the crystal-chemical criteria for high ionic conductivity more restrictive. In addition, we have developed significant new methods for evaluation of ion transport. In this section we have summarized the conclusions which result from the present study and make recommendations for future work.

TABLE XII

Summary of Materials and Screening Results

	Structure	Substitutions and Phase	Screened by NMR	Screened by Dielectric Loss	Screened by AC	Screened by Pulse	Estimated Conductivity at Room Temp ($ohm^{-1} cm^{-1}$ at 10^6 Hz) 10^{-8}	10^{-6}	10^{-4}
1-Dimensional	$LiNb_6O_{15}F$	Mo, W, Ti	●	●	●	●			—
	Hollandite	$K_2[MgTi]_8O_{16}$		●	●	●			—
	Cordierite	Na, K	●	●	●				—
2-Dimensional	$NaNbO_2F_2$	Ca, Sr, Pb Y, Nd, Mo, W	●	●	●				
3-Dimensional	Perovskite	Li, Na-La, Nd, Y							
	Tungsten Bronze	Na				●			
	$NaLiGe_4O_9$	glass, crystal Ta, Nb, Sb, V	●	●	●	●	—	—	—
	$Li_2Ge_7O_{15}$	glass, crystal Ta, Nb, Sb, V	●	●	●		—	—	—
	H-$NaLnF_4$	Pr, Nd, Y	●	●	●			—	—

A. Conclusions

The principal conclusions resulting from this study are as follows:

1. Crystal chemistry has been used successfully to predict and identify many structures in which cations are loosely bound and capable of at least short-range motion at low temperature.

2. Compounds with this degree of ionic mobility can be screened by NMR and dielectric loss.

3. Short-range motion is a necessary although not sufficient condition for ion transport. In the compounds that have been evaluated thus far the long-range ionic motion or transport has been small at room temperature.

4. Our investigation of channel structures has led to an important refinement of the crystal chemical criteria for the selection of candidate cation conductors:

(a) The channels through which ion migration is expected to occur should be interconnected in at least two dimensions, and preferably in three dimensions.

(b) Each potentially mobile ion should have available a minimum of three vacant sites into which it can move in a single elementary jump.

5. We have developed and validated a new fast pulse technique for the measurement of ion transport in very small solid specimens. This method is extremely promising and we believe it probably will prove to be a major breakthrough in evaluating ion transport in solids. The method will be particularly useful for measuring materials that are difficult to prepare as large single crystals or as pure dense polycrystalline solids.

6. Microwave measurements can be used to measure the conductivity of powders.

B. Recommendations

We believe that work in the future should be restricted to three- and two-dimensional interconnected channel structures, and that evaluation should be made principally by the fast pulse technique. Dielectric loss and/or microwave conductivity on powders are useful adjunct measurements.

A broad family of anhydrous zeolitic*-like structures related to analcite ($NaAlSi_2O_6$) has been selected for a focused search. The following considerations were used to arrive at this class of compounds:

(1) The channels should be interconnected in three-dimensions to avoid blocking;

(2) The channel diameter should be slightly larger than the dimensions of nonhydrated ions;

(3) It should be possible to modify the materials in a relatively continuous manner over a broad range of composition and structure;

(4) It should be possible to fabricate the materials into dense nonporous membranes for battery applications; and

(5) There should be x-ray or other evidence of ion mobility in at least some of the compositions.

The starting points chosen for our zeolite system are the anhydrous compositions $NaAlSi_2O_6$ (analcite), $KAlSi_2O_6$ (high leucite), and $CsAlSi_2O_6$ (pollucite). These are well-known minerals and their structures have been described.[34-39]

All three of these minerals are cubic with space group O_h^{10}-Ia3d and with cell constants around 13.7Å. The zeolitic, three-dimensional aluminosilicate network is the same for all three minerals, but only high-leucite and pollucite are truly isotypic. The AlO_4 and SiO_4 tetrahedra are randomly interlinked at all four corners to form an open three-dimensional framework.

---

*It is appropriate to comment on two objections usually encountered when zeolites are considered as potential solid electrolytes. The first of these involves the fact that it is well known that removal of water from the zeolite structure results in disappointingly low conductivities and diffusion rates.[31] This is a valid concern, but there have not been intensive studies of ion transport in nonstoichiometric, anhydrous, small channel zeolites of the type considered for this study. In fact, the channels in the proposed compounds are so small it may be somewhat inaccurate to refer to them as zeolites. A second objection is that since most zeolites are porous and composed of extremely small crystallites, it may be difficult to fabricate into dense non-porous membranes for practical applications. We believe this is not necessarily a valid objection since some anhydrous zeolites can be made by devitrifying glasses of the same composition. For example, $KAlSi_2O_6$ (leucite), and $CsBSi_2O_6$ (pollucite structure) can be made by devitrifying the appropriate glasses.[32, 33] We feel that if glasses can be used as precursors to the crystalline materials, it may be possible to fabricate dense membranes.

This leaves large channels, which in high leucite and pollucite, are occupied by potassium and cesium ions, respectively. The potassium and cesium ions are surrounded loosely by 12 oxygens at K-O distances of 3.35Å to 3.54Å and Cs-O distances of 3.40Å to 3.57Å. In hydrated specimens, water can partly occupy these 12-coordinated sites (or adjacent sites in pollucite).

The analcite structure differs from that of pollucite and high-leucite in that sodium ions occupy the " windows" that connect the large cavities. The Na-O distances are approximately 2.4Å. These smaller window sites are more suited for the smaller sodium ions than are the larger cavities.

We believe high ionic conductivity might be obtained in nonstoichiometric zeolites by the creation of additional vacancies (by adjustment of the Si/Al ratio) and by the simultaneous substitution of potassium ions for sodium or cesium ions. These intermediate-size ions may be small enough to move through the " windows, " yet small enough to be only loosely bonded inside the large cavity.

Such loose bonding has been observed in high temperature leucite, $KAlSi_2O_6$.[36] Here, the ion inside the large cavity is bonded to six oxygens at 3.37Å and to six oxygens at 3.57Å, with the potassium ions having the large isotropic temperature factor of 15.4$Å^{-1}$. In such an environment, potassium ion mobility appears possible, since K-O distances normally average about 2.7Å to 2.9Å. Unfortunately, the high form of $KAlSi_2O_6$ cannot be quenched and reverts to a distorted low temperature from at about 605°C. By crystal-chemical substitutions, it may be possible to lower this transition temperature.

VI. REFERENCES

1. Lundberg, M., Acta Chem. Scand. 19, 2274 (1965).

2. Roth, W.L., Mitoff, S.P., and King, R.N., Final Report, " Study, Selection and Preparation of Solid, Cationic Conductors, " Sept. 1972, Contract NAS3-15692, NASA-Lewis Research Center, Cleveland, Ohio.

2a. Rice, M.J. and Roth, W.L., J. Solid State Chem. 4, 294 (1972).

2b. Kautz, H.E., Singer, J., Fielder, W.L., and Fordyce, J.S., NASA TN D-7146, " Electrical Screening Procedure for Solid Ionic Conductors, " March (1973).

2c. Roberts, S. and von Hippel, A., J. Appl. Phys. 17, 610 (1946).

3. Byström, A. and Byström, A.M., Acta Cryst. 3, 146 (1950) and Acta Cryst. 4, 469 (1951).

4. Bayer, G. and Hoffman, W., Am. Mineralogist 51, 511 (1966).

5. Kinomura, N., J. Am. Ceram. Soc. 56, 344 (1973).

6. Byström, A., Arkiv Kemi Min. Geol. 15B [12], 1 (1942).

7. Gibbs, G. V., Am. Mineralogist 51, 1068 (1966).

8. Smith, J. V. and Schreyer, W., Min. Mag. 33, 226 (1962).

9. Schreyer, W. and Schairer, J. F., J. Petrology 2, 324 (1961).

10. Provondra, P. and Langer, K., Neues Jahrbuch für Mineralogie, Abhandlungen 116, 1 (1971).

11. Anderson, S. and Galy, J., Acta Cryst. B25, 847 (1969).

12. Chaminade, J.-P., Pouchard, M., and Hagenmuller, P., Compt. Rend. 273C, 984 (1971).

13. Brous, J., Fankuchen, I., and Banks, E., Acta Cryst. 6, 67 (1953).

14. Kestigian, M. and Ward, R., J. Am. Chem. Soc. 77, 6199 (1955).

15. Johnston, W. D. and Sestrich, D., J. Inorg. Nucl. Chem. 20, 32 (1961).

16. Tien, T. Y. and Hummel, F. A., Trans. Brit. Ceram. Soc. 66, 233 (1967).

17. Lejus, A. M. and Queyroux, F., Compt. Rend. 271C, 56 (1970).

18. MacChesney, J. B. and Sauer, H. A., J. Am. Ceram. Soc. 45, 419 (1962).

19. Studer, F., Montfort, Y., and Raveau, B., J. Solid State Chem. 7, 269 (1973).

20. Völlenkle, H., Wittmann, A., and Nowotny, H., Mh. Chem. 100, 79 (1969).

21. Krishna Murthy, M. and Ip, J., J. Am. Ceram. Soc. 47, 328 (1964).

22. Wittmann, A. and Modern, E., Mh. Chem. 96, 581 (1965).

23. Völlenkle, H., Wittmann, A., and Nowotny, H., Mh. Chem. 101, 46 (1970).

24. Burns, J.H., Inorg. Chem. 4, 881 (1965).

25. Thoma, R.E., Hebert, G.M., Insley, H., and Weaver, C.F., Inorg. Chem. 2, 1005 (1963).

26. Thoma, R.E., Insley, H., and Hebert, G.M., Inorg. Chem. 5, 1222 (1966).

27. Fleet, S.G., Zeit. Krist. 121, 349 (1965).

28. Van Tassel, R., Min. Mag. 29, 850 (1954).

29. Caruba, R., Baumer, A., and Turco, G., Compt. Rend. 270D, 2741 (1970).

30. Thibaut, G., Caruba, R., and Turco, G., Compt. Rend 274D, 792 (1972).

31. Beattie, I.R., Trans. Faraday Soc. 50, 581 (1954).

32. Schairer, J.F. and Bowen, N.L., Am. J. Sci. 253, 681 (1955).

33. Richerson, D.R., and Hummel, F.A., J. Am. Ceram. Soc. 55, 269 (1972).

34. Taylor, W.H., Z. Krist. 74, 1 (1930).

35. Knowles, C.R., Rinaldi, F.F., and Smith, J.V., Indian Mineralogist 6, 127 (1965).

36. Peacor, D.R., Zeit. Krist. 127, 213 (1968).

37. St. v. Náray-Szabó, Zeit. Krist. 99, 277 (1938).

38. Newnham, R.E., Am. Mineralogist 52, 1515 (1967).

39. Beger, R.M. and Buerger, M.J., Proc. Nat. Acad. Sci. U.S. 58, 853 (1967).

OFFICIAL DISTRIBUTION LIST

NASA

NASA-Lewis Research Center (40)
Attn: Mr. A. C. Antoine (M. S. 309-1)
21000 Brookpark Road
Cleveland, OH 44135

NASA-Lewis Research Center
Attn: L. W. Schopen (M. S. 500-206)
21000 Brookpark Road
Cleveland, OH 44135

NASA-Lewis Research Center
Attn: N. T. Musial (M. S. 500-113)
21000 Brookpark Road
Cleveland, OH 44135

NASA-Lewis Research Center (2)
Attn: Library (M. S. 60-3)
21000 Brookpark Road
Cleveland, OH 44135

National Aeronautics and Space Administration
Scientific and Technical Information Facility
Attn: Acquisitions Branch
P. O. Box 33
College Park, MD 20740
(12 copies and 1 reproducible)

Mr. Simon Manson, Code ES
National Aeronautics and Space Administration
Washington, DC 20546

Mr. Floyd Ford, Code 761. Z
Goddard Space Flight Center
National Aeronautics and Space Administration
Greenbelt, MD 20771

Mr. Gerald Halpert, Code 761. Z
Goddard Space Flight Center
National Aeronautics and Space Administration
Greenbelt, MD 20771

Mr. Thomas Hennigan, Code 761
Goddard Space Flight Center
National Aeronautics and Space Administration
Greenbelt, MD 20771

Dr. Louis Rosenblum, MS 302-1
Lewis Research Center
National Aeronautics and Space Administration
21000 Brookpark Road
Cleveland, OH 44135

Mr. Harvey Schwartz, MS 309-1
Lewis Research Center
National Aeronautics and Space Administration
21000 Brookpark Road
Cleveland, OH 44135

Dr. J. Stuart Fordyce, MS 309-1
Lewis Research Center
National Aeronautics and Space Administration
21000 Brookpark Road
Cleveland, OH 44135

Mr. Charles B. Graff, S&E-ASTR-EP
George C. Marshall Space Flight Center
National Aeronautics and Space Administration
Huntsville, AL 35812

Mr. Hoyt McBryar, EP5
Johnson Space Center
National Aeronautics and Space Administration
Houston, TX 77058

JPL

Mr. Daniel Runkle, MS 198-220
Jet Propulsion Laboratory
4800 Oak Grove Drive
Pasadena, CA 91103

Dr. R. Lutwack, MS 198-220
Jet Propulsion Laboratory
4800 Oak Grove Drive
Pasadena, CA 91103

Mr. Aiji A. Uchiyama
MS 198-220
Jet Propulsion Laboratory
4800 Oak Grove Drive
Pasadena, CA 91103

ARMY

Harry Diamond Laboratories
Room 300, Building 92
Connecticut Ave. & Van Ness St., N. W.
Washington, DC 20438

U. S. Army Electronics Command
Attn: AMSEL-TL-P
Port Monmouth, NJ 07703

Commanding Officer
U. S. Army Mobility Equip. Research &
Development Center
Electrotechnology Department
Electrochemical Division
Attn: SMEFB-EE
Fort Belvoir, VA 22061

NAVY

Director, Power Program, Code 473
Office of Naval Research
Arlington, VA 22217

Dr. George A. Neece
Code 472
800 N. Quincy St.
Office of Naval Research
Arlington, VA 22217

Mr. S. Schuldiner, Code 6160
Naval Research Laboratory
4555 Overlook Avenue, S. W.
Washington, DC 20375

Mr. J.H. Harrison, Code 2724
Naval Ship R&D Center
Annapolis, MD 21402

Commanding Officer
Naval Ammunition Depot
(305, Mr. D. G. Miley)
Crane, Indiana 47522

Mr. Phillip B. Cole, Code 232
Naval Ordnance Laboratory
Silver Spring, MD 20910

Mr. Albert Himy, 6157D
Naval Ship Engineering Center
Center Bldg., Prince Georges Center
Hyattsville, MD 20782

Dr. H. E. Ruskie, NISC-4321
4301 Suitland Road
Suitland, MD 20390

AIR FORCE

AFAPL/ POE-1/ D. R. Warnock
Wright-Patterson AFB, OH 45433

Air Force Aero Propulsion Laboratory
POE-1/ W. S. Bishop
WPAFB, OH 45433

Mr. Edward Raskind, LCC, Wing F
U. S. AF Cambridge Research Laboratory
L. G. Hanscom Field
Bedford, MA 01731

Rome Air Development Center
Attn: TUGG/ F. J. Mollura
Griffiss AFB, NY 13441

SAMSO/ DYAE
P. O. Box 92960
Worldway Postal Center
Los Angeles, CA 90009

OTHER GOVERNMENT ORGANIZATIONS

Dr. Leonard Topper
NSF, RANN
Washington, DC 20550

PRIVATE ORGANIZATIONS

Dr. E. A. Heintz
Technical Department
Airco Speer Carbon-Graphite
P. O. Box 828
Niagara Falls, NY 14302

Dr. R. T. Foley
Chemistry Department
American University
Massachusetts & Nebraska Aves., N. W.
Washington, DC 20016

Mr. R. A. Knight
Research Division
AMF Inc.
689 Hope Street
Stamford, CT 06907

Dr. H. Shalit
ARCO Chemical Co.
Division of Atlantic Richfield Co.
500 South Ridgeway Avenue
Glenolden, PA 19036

Dr. James D. Birkett
Arthur D. Little, Inc.
Acorn Park
Cambridge, MA 02140

Dr. H. L. Recht
Atomics International Division
International Corp.
P. O. Box 309
Canoga Park, CA 91304

Mr. R. F. Fogle, GA 28
North American Rockwell
Autonetics Division, NAR
P. O. Box 4192
Anaheim, CA 92803

Mr. J. E. Clifford, Technical Representative
Electrochemical Eng. Technical Division
Battelle
Columbus Laboratories
505 King Avenue
Columbus, OH 43201

Mr. D. O. Feder
Bell Telephone Laboratories, Inc.
Murray Hill, NJ 07974

Dr. Carl Berger
13401 Kootenay Drive
Santa Ana, CA 92705

Mr. Sidney Gross
MS 8+-37
The Boeing Company
P. O. Box 3999
Seattle, WA 98124

Professor T. P. Dirkse
Calvin College
3175 Burton Street, S. E.
Grand Rapids, MI 49506

Professor Ernest Yeager
Department of Chemistry
Case Western Reserve Univ.
Cleveland, OH 44106

Mr. C. E. Thomas
Chrysler Corporation
Space Division
Dept. 2730
P. O. Box 29200
New Orleans, LA 70189

Mr. E. P. Broglio
Eagle-Picher Industries, Inc.
P. O. Box 47, Couples Dept.
Joplin, MO 64801

Dr. J. M. Williams
Experimental Station, Bldg. 304
Engineering Technology Lab.
E. I. du Pont de Nemours & Co.
Wilmington, Delaware 19898

Mr. R. P. Mikkelson
Electrical Systems Dept. 623-2
General Dynamics/ Convair Aerospace Division
P. O. Box 80847
San Diego, CA 92138

Xerox Corporation
Electro-Optical Systems
300 North Halstead Street
Pasadena, CA 91107

Mr. Martin Klein
Energy Research Corporation
15 Durant Avenue
Bethel, CT 06801

Dr. J. G. Cohn
Engelhard Industries
Menlo Park
Edison, NJ 08817

Mr. L. Berkowitz
Government Research Lab.
Esso Research and Engineering Co.
P. O. Box 8
Linden, NJ 07036

Dr. Arthur Fleischer
466 South Center Street
Orange, NJ 07050

The Garrett Corporation
Suite 515, Cafritz Building
1625 Eye Street, N. W.
Washington, DC 20006

Dr. J. B. Bush, Jr.
Research and Development Center
General Electric Company
Bldg. K-1, Room 4A28
P. O. Box 8
Schenectady, NY 12301

Mr. Kenneth Hanson
General Electric Company
Valley Forge Space Technology Center
P. O. Box 8555
Philadelphia, PA 19101

Mr. J. A. Keralla
Delco Remy Division
General Motors Corporation
2401 Columbus Avenue
Anderson, IN 46011

Dr. John McCallum
President
Invention Talents, Incorporated
1149 Chesepeake Avenue
Columbus, OH 43212

Mr. L. G. Nuttall
General Electric Company
930 Western Avenue, 274A4
Lynn, MA 01910

Mr. F. T. O'Brien
Direct Energy Conversion Programs
General Electric Company
930 Western Avenue
Lynn, MA 01910

Dr. E. L. Simons
Environmental Protection Operation - Building 36
General Electric Company
Schenectady, NY 12345

Dr. G. Goodman
Globe-Union, Inc.
P. O. Box 591
Milwaukee, WI 53201

Dr. J. E. Oxley
Dr. B. B. Owens
Gould Inc., Gould Lab.
P. O. Box 3140
St. Paul, Minnesota 55165

Grumman Aerospace Corp.
S. J. Gaston, Plant 35,
Dept. 553
Bethpage, Long Island
New York 11714

Gulton Battery Corporation
212 Durham Ave., Middlesex County
Metuchen, NJ 08840

Dr. P. L. Howard
Millington, MD 21651

Dr. M. E. Ellion, Manager
Propulsion & Power Systems Lab.
Building 366, MS 524
Hughes Aircraft Company
El Segundo, CA 90245

Mr. R. Hamilton
Institute for Defense Analyses
400 Army-Navy Drive
Arlington, VA 22202

Mr. James R. Hunt
International Nickel Company
1000-16th Street, N. W.
Washington, DC 20036

Dr. A. Moos
Leesona Corporation
Warwick, RI 02887

Dr. R. A. Wynveen, President
Life Systems, Inc.
23715 Mercantile Road
Cleveland, OH 44122

Mr. Robert E. Corbett
Department 62-25, Building 151/1
Lockheed Aircraft Corporation
P. O. Box 504

Sunnyvale, CA 94088
Mr. S. J. Angelovich
Chief Engineer
Mallory Battery Company
South Broadway
Tarrytown, NY 10591

Mr. A. D. Tonelli
Dept. A3-833, MS 22-2
McDonnell Douglas Astronautics Co.
5301 Bolsa Avenue
Huntington Beach, CA 92647

Dr. Robert C. Shair
4921 Sanayer Dr.
Hollywood, FL 33021

Rocketdyne Division
North American Rockwell Corp.
Attn: Library
6633 Canoga Avenue
Canoga Park, CA 91304

National Center for Energy Management & Power
113 Towne Building
University of Pennsylvania
Phil., PA 19104

Dr. C. Bocciarelli
112 E. 2nd Street
Moorestown, NJ 08057

Mr. D. C. Briggs
WDL Division
Philco-Ford Corporation
3939 Fabian Way
Palo Alto, CA 94303

Dr. Per Bro
P. R. Mallory & Company, Inc.
Northwest Industrial Park
Third Avenue
Burlington, MA 01801

P. R. Mallory & Company, Inc.
Library
P. O. Box 706
Indianapolis, IN 46206

Mr. V. D'Agostino
RAI Research Corporation
225 Marcus Blvd.
Hauppauge, L. I., NY 11787

Southwest Research Institute
Attn: Library
P. O. Drawer 28510
San Antonio, TX 78284

Library
Standord Research Institute
333 Ravenswood Avenue
Menlo Park, CA 94025

Dr. W. R. Scott (M1-1208)
TRW Systems, Inc.
One Space Park
Redondo Beach, CA 90278

Dr. Herbert P. Silverman
(R-1/2094)
TRW Systems, Inc.
One Space Park
Redondo Beach, CA 90278

Union Carbide Corporation
Battery Products Division
Development Laboratory Library
P. O. Box 6056
Cleveland, OH 44101

Dr. Robert Powers
Consumer Products Division
Union Carbide Corporation
P. O. Box 6116
Cleveland, OH 44010

United Aircraft Corporation
Attn: Library
400 Main Street
East Hartford, CT 06108

Power Information Center
University City Science Institute
3401 Market Street, Room 2210
Philadelphia, PA 19104

Dr. Frederick Morse
Department of Mechanical Engineering
University of Maryland
College Park, MD 20742

Yardney Electric Corporation
Power Sources Division
3850 Olive Street
Denver, CO 80207

Yardney Electric Division
82 Mechanic Street
Pawcatuck, CT 02891

Dr. Eugene Y. Weissman, Director
Inorganic-Electrolytic R&D
BASF Wyandotte Corporation
Wyandotte, MI 48192

Dr. Charles Levine
Dow Chemical U. S. A.
Walnut Creek Research Center
2800 Mitchell Drive
Walnut Creek, CA 94598

Prof. Donald M. Smyth
Materials Research Center
Lehigh University
Bethlehem, PA 18015

Prof. John W. Patterson
Dept. of Metallurgy
Iowa State University
Ames, IA 50010

Prof. Rustum Roy
Materials Science Dept.
Pennsylvania State University
University Park, PA 16802

Prof. John H. Kennedy
Univ. of Calif. at Santa Barbara
Santa Barbara, CA 93106

Dr. Paul Jorgensen
Stanford Research Institute
Menlo Park, CA 94025

Dr. L. Topper
Div. of Advanced Technology Applications
National Science Foundation
Washington, DC 20550

Mr. L. R. Rothrock
Union Carbide Corp.
8888 Balboa Ave.
San Diego, CA 92123

Prof. K. E. Cox
Dept. of Chem. & Nucl. Eng.
Tech. Appl. Center
University of New Mexico
Albuquerque, N. M. 87131

Dr. Robert A. Huggins
Dept. of Materials Science and Engineering
Stanford University
Stanford, CA 94305

Dr. M. Stanley Whittingham
Esso Research and Engineering Co.
Linden, NJ 07036

Dr. Neill T. Weber
Ford Motor Co. Research Lab.
Dearborn, MI 48121

Prof. James I. Mueller
Ceramic Engineering Div.
University of Washington
Seattle, WA 98195

Dr. Douglas O. Raleigh
North American Rockwell Science Center
Thousand Oaks, CA 91360

Dr. R. H. Doremus
Rensselaer Polytechnic Institute
Materials Division
Troy, NY 12181

Dr. Robert S. Roth
National Bureau of Standards
U. S. Department of Commerce
Washington, DC 20234

Prof. Alexander F. Wells
Dept. of Chemistry
University of Connecticut
Storrs, CT 06268

Dr. Elton J. Cairns
Electrochemistry Dept.
General Motors Research Lab.
12 Mile and Mound Roads
Warren, Michigan 48090

Dr. John B. Goodenough
Massachusetts Institute of Technology
Lincoln Laboratory
Lexington, Mass. 02173